

Magneto-Electric coupling in the multiferroic composite $(1-x)\text{Ba}_5\text{RTi}_3\text{V}_7\text{O}_{30}-x\text{BiFeO}_3$

Thesis submitted to National Institute of Technology,
in fulfillment of the requirements for the award of
Doctor of Philosophy in Physics

by

Hage Doley
Roll no. Ph.D(PHY)/2017/02
(Registration No. 00075/B/2017)

Under the supervision
of

Dr. Pratap Kumar Swain
Assistant Professor
Department of Basic and Applied Science
NIT Arunachal Pradesh, Yupia

And

Dr. Pinaki Chakraborty
Associate Professor
Department of Physics
Raiganj University, West Bengal




National Institute of Technology, Arunachal Pradesh
Yupia -791 112, Arunachal Pradesh
2020

DECLARATION

I certify that

- a. The work contained in this thesis is original and has been done by me under the guidance of my supervisor(s).
- b. The work has not been submitted to any other Institute for any degree or diploma.
- c. I have followed the guidelines provided by the Institute in preparing the thesis.
- d. I have conformed to the norms and guidelines given in the Ethical Code of Conduct of the Institute.
- e. Whenever I have used materials (data, theoretical analysis, figures, and text) from other sources, I have given due credit to them by citing them in the text of the thesis and giving their details in the references. Further, I have taken permission from the copyright owners of the sources, whenever necessary.

 06/01/2021
Signature of the Student

APPROVAL OF THE VIVA VOICE BOARD

Date: 06/01/2021

Certified that the thesis entitled **Magneto-Electric coupling in the multiferroic composite $(1-x)\text{Ba}_5\text{RTi}_3\text{V}_7\text{O}_{90}-x\text{BiFeO}_3$** submitted by **HAGE DOLEY** to the National Institute of Technology, Arunachal Pradesh, for the award of the degree of Doctor of Philosophy has been accepted by the external examiners and that the student has successfully defended the thesis in the viva-voice examination held today.

Signature

(Member of the RAC)

Signature

(Member of the RAC)

Signature

(Member of the RAC)

Signature

(External Examiner)

Signature

(Supervisor)

Signature

(Dean (acad))



NATIONAL INSTITUTE OF TECHNOLOGY, ARUNACHAL PRADESH
(Established by MHRD, Govt. of India)
YUPIA, ARUNACHAL PRADESH -791112, INDIA

Dr. Pratap Kumar Swain
Asst. Professor, Physics

Website : www.nitap.ac.in
E-Mail : pratap@nitap.ac.in
Fax No. : 0360- 2284972
Mob. No.: 9436828864

Date: 06/01/2021

This is to certify that the thesis entitled “**Magneto-Electric coupling in the multiferroic composite $(1-x)\text{Ba}_5\text{RTi}_3\text{V}_7\text{O}_{30} -x\text{BiFeO}_3$** ” being submitted by Hage Doley for the award of the degree of ‘**Doctor of Philosophy**’ is a record of the original bonafide experimental work carried out by him. He has worked under my supervision and guidance and has fulfilled the requirement for the submission of thesis. The results presented in this thesis have not been submitted to any other university or institute for any degree or diploma.

Prswain
06/01/2021

Dr. Pratap Kumar Swain
(Supervisor)

Dr. P. Chakraborty
(Co-supervisor)

Acknowledgement

I'm extremely grateful to my research supervisors, Dr. Pratap Kumar Swain, National Institute of Technology, Arunachal Pradesh for giving me the opportunity to do research and providing invaluable guidance throughout this research. I would also like to thank him for his sincerity, empathy and bearing the patience with me that cannot be underestimated. It was great privilege and honor to work and study under his guidance.

My success would not have been possible without the support and nurturing of Dr. Anuradha Panigrahi. She has taught me the methodology to carry out the research and the present the research works as clearly as possible. I am highly indebted for her profound belief in my abilities, unparalleled support, unwavering guidance and motivation.

My warm thanks to Dr. Pinaki Chakraborty for his unrelenting support and ingenious suggestions through my research work.

I would like to extend my gratitude to Dr. S. R. Shanigrahi (IMRE, Singapore) for his invaluable contribution in carrying out magnetization study and providing insightful suggestions and encouragement.

My special thanks to Mr. Gyati Tachang Tado for extending his help in various ways during my experimental work. I would also thank him for his friendship, helpful contributions, relentless support and helpful advice.

I would like to extend my sincere thanks to Department of Physics, NERIST to permit me to carry out research work in their institute (Physics Research lab).

I am also thankful to the TEQUIP-III, Arunachal Pradesh for the financial assistance for the procurement of consumable items for my research work.

Finally, I thank to all those, whose names I cannot remember at this moment but have contributed in their own way to the completion of the present work.

(Hage Doley)

FIGURE CAPTIONS:

1. Fig. 1.1. Dependency of Temperature to order parameter (η) and physical parameters (like polarization and dielectric constant) 7
2. Fig. 1.2. Dependency of Temperature on order parameter (a) first order and (b) second order phase transition 8
3. Fig. 1.3. Unit cell atomic arrangement of a tungsten-bronze type structure. 13
4. Fig. 1.4. Multiferroics interactions: Ferroic orderings, ferromagnetism (M), ferroelasticity (ϵ), and Ferroelectricity (P), can be switched by their conjugate magnetic (H), stress (σ) and electric (E). Coexistence of at least two ferroic ordering results in additional interactions. 15
5. Fig. 1.5. Unit cell crystal structure of hexagonal ($R3c$) BiFeO₃ 17
6. Fig. 2.1. Flow chart for the preparation of ceramics samples by a solid-state reaction technique. 35
7. Fig. 2.2(a) Schematic diagram of SEM 43
8. Fig. 2.2(b) Schematic diagram of SEM setup 43
9. Fig. 2.3. Vector resolution of ac current in a capacitor 47
10. Fig. 2.4(a) High Temp Furnace (MI-F800C) with Sample Holder (VESPL-S1000) 48
11. Fig. 2.4(b) HIOKI-IM3536 LCR meter 49
12. Fig. 2.5. Block diagram of PPMS SQUID VSM system 51
13. Fig. 3.1. XRD pattern for (1-x)Ba₅TbTi₃V₇O₃₀-xBiFeO₃ 61
14. Fig. 3.2. XRD pattern for (1-x)Ba₅PrTi₃V₇O₃₀-xBiFeO₃ 64
15. Fig. 3.3: SEM micrographs of (1-x)Ba₅TbTi₃V₇O₃₀-xBiFeO₃ (a) $x = 0$ (b) $x=0.3$ (c) $x= 0.5$ (d) $x= 0.7$ (d) $x= 1$. 70
16. Fig. 3.4: SEM micrographs of (1-x)Ba₅PrTi₃V₇O₃₀-xBiFeO₃ (a) $x = 0$ (b) $x=0.3$ (c) $x= 0.5$ (d) $x= 0.7$ 73
17. Fig. 4.1. : Testing procedure flow chart for an impedance meter 80
18. Fig. 4.2. Frequency variation of ϵ_r for (1-x)Ba₅TbTi₃V₇O₃₀-xBiFeO₃ at room temp. 82

19.	Fig. 4.3. Frequency variation of $\tan\delta$ for $(1-x)\text{Ba}_5\text{TbTi}_3\text{V}_7\text{O}_{30-x}\text{BiFeO}_3$ at room temp.	83
20.	Fig. 4.4. Frequency variation of ϵ_r for $(1-x)\text{Ba}_5\text{PrTi}_3\text{V}_7\text{O}_{30-x}\text{BiFeO}_3$ at room temp.	84
21.	Fig. 4.5. Frequency variation of $\tan\delta$ for $(1-x)\text{Ba}_5\text{PrTi}_3\text{V}_7\text{O}_{30-x}\text{BiFeO}_3$ at room temp.	85
22.	Fig. 4.6. Variation of ϵ_r with temperature for $(1-x)\text{Ba}_5\text{TbTi}_3\text{V}_7\text{O}_{30-x}\text{BiFeO}_3$ at 1kHz.	86
23.	Fig. 4.7. Tangent loss with temperature for $(1-x)\text{Ba}_5\text{TbTi}_3\text{V}_7\text{O}_{30-x}\text{BiFeO}_3$ at 1kHz.	87
24.	Fig. 4.8. Variation of ϵ_r with temperature for $(1-x)\text{Ba}_5\text{PrTi}_3\text{V}_7\text{O}_{30-x}\text{BiFeO}_3$ at 1kHz.	89
25.	Fig. 4.9. Variation of $\tan\delta$ with temperature for $(1-x)\text{Ba}_5\text{PrTi}_3\text{V}_7\text{O}_{30-x}\text{BiFeO}_3$ at 1kHz.	90
26.	Fig. 5.3.1. Variation of $\ln\sigma_{ac}$ with $10^3/T$ for $(1-x)\text{Ba}_5\text{TbTi}_3\text{V}_7\text{O}_{30-x}\text{BiFeO}_3$ ($x= 0, 0.3, 0.5, 0.7$) at 1kHz.	97
27.	Fig. 5.3.2. Variation of $\ln\sigma_{ac}$ with $10^3/T$ for $(1-x)\text{Ba}_5\text{PrTi}_3\text{V}_7\text{O}_{30-x}\text{BiFeO}_3$ ($x= 0, 0.3, 0.5, 0.7$) at 1kHz.	99
28.	Fig. 6.3.1. Variation of Magnetization, M (emu/g) w.r.t. Temp for $(1-x)\text{Ba}_5\text{TbTi}_3\text{V}_7\text{O}_{30-x}\text{BiFeO}_3$.	105
29.	Fig. 6.3.2. Variation of Susceptibility with Temperature for $(1-x)\text{Ba}_5\text{TbTi}_3\text{V}_7\text{O}_{30-x}\text{BiFeO}_3$.	106
30.	Fig. 6.3.3. M-H hysteresis loops for BiFeO_3 at 300 K.	107
31.	Fig. 6.3.4. M-H hysteresis loops for $(1-x)\text{Ba}_5\text{TbTi}_3\text{V}_7\text{O}_{30-x}\text{BiFeO}_3$ at 300 K.	108
32.	Fig. 6.3.5 M-H hysteresis loops for $(1-x)\text{Ba}_5\text{PrTi}_3\text{V}_7\text{O}_{30-x}\text{BiFeO}_3$ at 300 K.	109

TABLE CAPTIONS:

1. Table 3.1 Comparison of observed (obs.) and calculated (cal.) d values of $(1-x)\text{Ba}_5\text{TbTi}_3\text{V}_7\text{O}_{30-x}\text{BiFeO}_3$ ($x= 0, 0.3$) 62
2. Table 3.2 Comparison of observed (obs.) and calculated (cal.) d values of $(1-x)\text{Ba}_5\text{TbTi}_3\text{V}_7\text{O}_{30-x}\text{BiFeO}_3$ ($x= 0.5, 0.7$). 63
3. Table 3.3 Comparison of observed (obs.) and calculated (cal.) d values of $(1-x)\text{Ba}_5\text{PrTi}_3\text{V}_7\text{O}_{30-x}\text{BiFeO}_3$ ($x= 0, 0.3$) 65
4. Table 3.4 Comparison of observed (obs.) and calculated (cal.) d values of $(1-x)\text{Ba}_5\text{PrTi}_3\text{V}_7\text{O}_{30-x}\text{BiFeO}_3$ ($x= 0.5, 0.7$) 66
5. Table 3.5 Comparison of lattice parameters (\AA), particle size (P) (in \AA) and volume (\AA^3) of $(1-x)\text{Ba}_5\text{RTi}_3\text{V}_7\text{O}_{30-x}\text{BiFeO}_3$ ($x= 0,0.3,0.5,0.7$; R = Pr, Tb). 75
6. Table 4.1 Dielectric properties such as dielectric constant and dielectric loss are analysed for $(1-x)\text{Ba}_5\text{TbTi}_3\text{V}_7\text{O}_{30-x}\text{BiFeO}_3$ at 1 kHz. 88
7. Table 4.2 Dielectric properties such as dielectric constant and dielectric loss for $(1-x)\text{Ba}_5\text{PrTi}_3\text{V}_7\text{O}_{30-x}\text{BiFeO}_3$ at 1 kHz. 90
8. Table 5.1 Comparison of Activation energy E_a (eV) for $(1-x)\text{Ba}_5\text{RTi}_3\text{V}_7\text{O}_{30-x}\text{BiFeO}_3$ multiferroics at 1 kHz, where $x = 0,0.3,0.5,0.7$ and R= Tb, Pr calculated from $\ln\sigma_{ac}$ vs. $1/T$ graphs. 100
9. Table 6.1 Values of the parameters obtained for $(1-x)\text{Ba}_5\text{RTi}_3\text{V}_7\text{O}_{30-x}\text{BiFeO}_3$ at 300 K. 110

CONTENTS

Content Details	Page No.
Preface	i
Abstract	iii
List of Symbols	iv
Figure captions	vi
Table captions	viii
Contents	ix
Chapter I Introduction	1-27
1.1 General Introduction to Ferroelectrics	
1.2 Applications of Ferroelectrics materials	
1.3 Phase transition in ferroelectrics	
1.4 Thermodynamics of ferroelectric phase transition	
1.5 Phase Transition of Diffuse nature	
1.6 Classification of representative ferroelectrics	
1.7 Multiferroic and its technological applications.	
1.8 Literature Survey	
1.9 Selection of material for the present work	
1.10 Materials under present investigation	
1.11 Aim and Objectives of the work	
Chapter II Methodology	28-53
2.1 Introduction	
2.2 Section-I: Material Synthesis	
2.2.1 Introduction	
2.2.2 General method of preparation of ceramics	
2.2.3 Mixed Oxide Process	
2.2.4 Preparation of the compounds	

- 2.3 Section-II: Characterization
 - 2.3.1 Introduction
 - 2.3.2 Structural characterisation
 - 2.3.2 (a) X-ray Diffraction Study (XRD)
 - 2.3.2 (b) Scanning electron microscope (SEM)
 - 2.3.3 Dielectric study
 - 2.3.4 AC conductivity study
 - 2.3.5 Magnetization study using Vibrating Sample Magnetometer(VSM)

Chapter III Structural and microstructural analysis 54-76

- 3.1 Introduction
- 3.2 Structural study
 - 3.2.1 X-ray Powder Diffraction
 - 3.2.1.1 Experimental
 - 3.2.1.2 Calculation
 - 3.2.2 Results and discussion
- 3.3 Scanning electron micrographs (SEM)
 - 3.3.1 Introduction
 - 3.3.2 Results and discussion
- 3.4 Conclusions

Chapter IV Dielectric Study 77-92

- 4.1 Introduction
- 4.2 Principles
- 4.3 Experimental
- 4.4 Results and discussion
- 4.5 Conclusions

Chapter V Electrical conductivity study 93-101

- 5.1 Introduction
- 5.2 Experimental

- 5.3 Results and discussion
- 5.4 Conclusions

Chapter VI Magnetic Study 102-110

- 6.1 Introduction
- 6.2 Experimental
- 6.3 Magnetization study
- 6.4 Conclusions

Chapter VII Summary, conclusions and future scopes 111-115

- 7.1 Summary
- 7.2 Conclusions
- 7.3 Future scopes

References 116-126

Chapter I
INTRODUCTION

1.1. General Introduction to Ferroelectrics

The properties of ferroelectricity was first observed in 1920 [1] by Joseph Valasek in Sodium Potassium tartrate salt ($\text{NaKC}_2\text{H}_4\text{O}_6 \cdot 4\text{H}_2\text{O}$) also commonly known as Rochelle salt. He found that by applying an electric field to the Rochelle salt the polarisation could be switched on, which gets reversed on the reversal of electric field leading to the discovery of whole new properties of materials called Ferroelectricity (E. Schrodinger first coined the term). However, the term ferroelectric does not have any relation to the element Iron (Ferrite). The derivation of the name is due to the reason that electrical properties of ferroelectric materials are similar to the magnetic properties of ferromagnetic materials. Since the discovery of ferroelectricity in Rochelle salt, a wide range of materials such as water-soluble crystals, liquid crystals, and ceramics have also shown the property of ferroelectricity. The discovery of ceramic BaTiO_3 (Barium Titanate) by B. Wull and I.M. Goldman, having ferroelectrics properties led to further search for more materials in ceramic form with similar properties [2].

Ferroelectrics materials are type of dielectrics which have the following typical properties:

- i. Spontaneous polarization (domains formation)
- ii. Polarisation reversal (showing hysteresis)
- iii. Ferroelectric transition (temperature dependent) at Curie temperature.

In these types of materials, crystal structures are non-centrosymmetric (lacks a centre of symmetry) or *acentric* (crystal structure which lacks point of inversion). They exhibit the phenomenon of piezoelectricity [3](*a*. Direct piezoelectric effect – on application of stress there is a separation of charge on the face of crystal. *b*. Converse Piezoelectric effect – on application of electric field, mechanical strain develops) e.g. α -quartz mineral, which is used as resonators for filtering frequency and electronic clocks.

Acentric crystals which possess a unique axis of symmetry is called a *polar crystal*. All the polar crystals are piezoelectric in nature and in addition to that they also possess pyroelectric properties [4] (charge separation on the surface is sensitive to the change in temperature). In the polar structure, dielectric polarisation is *built in*. Hence, this is also known as a *spontaneous polarisation*.

A Change in stress or temperature results in a change of dipole moment. On application of an external electric field the direction and magnitude of spontaneous polarisation changes, and returns back to its zero field value on taking away the electric field. On application of an external field in some polar dielectric materials, there is shifting of spontaneous polarization in some more stable direction. However, removal of the field doesn't result in the return of polarization spontaneously to its original magnitude and direction.

The lattice structure of Ferroelectric material shows that it has crystal symmetry (i.e. the crystal can be grouped into microscopic symmetry types). The types of symmetry effects the crystal properties have been discussed by Nye [5] and Bhagavan [6]. There are seven types of crystal systems i.e. Triclinic, Monoclinic, Orthorhombic, Tetragonal, Rhombohedral (trigonal), Hexagonal, Cubic (in ascending symmetry order). According to the point group symmetry they possess, these are again divided into point groups, there are 32 point groups. The prerequisite condition for the materials to be ferroelectricity is the absence of a centre of symmetry i.e. non-centrosymmetric or *acentric*. Based on rotational symmetry, there are 21 classes of crystal which are acentric, out of which 20 are piezoelectric. By determining the crystal structure it can be predicted whether the particular material will have piezoelectric property or not. Out of 20 piezoelectric classes, in 10 of them, polarization occurs along a particular axis due to application of thermal energy i.e. pyroelectric materials (Ferroelectrics are a subsection of pyroelectrics). The properties of the reversal of polarization or if a material will show ferroelectricity cannot be determined solely by the crystal structure and other indirect methods such as dielectric experiment*.

We can say that all the ferroelectrics are pyroelectrics, all the pyroelectrics are piezoelectric, and all the Piezoelectrics are dielectrics. But vice-versa is not true.

*Unlike ferroelectricity, piezoelectric property can be determined solely by crystal structure.

The properties of switchable spontaneous polarisation of ferroelectrics results into ferroelectric hysteresis [7-10]. With the increase of electric field (E) from zero, the whole polarisation (P) in the crystal also increases but the increase is non-linear in nature. Eventually, reaching a saturation point beyond which the further increase in P is owing to the relative permittivity. (For linear dielectric, permittivity is gradient of P/E curve). Further extrapolation gives the saturation spontaneous polarisation (P_s) value in abscissa. When the field (E) is reduced to zero, it gives a *remanent polarisation* (P_r), the value of which is lesser than P_s . When field is applied in the opposite direction (i.e. $-E$), the polarisation reduces further, the field at which polarisation is zero is *coercive field* ($-E_c$). The further decrease in field, eventually leads to a reverse saturation of polarisation ($-P_s$). And when the field is increased to zero, the polarisation measured is remnant polarisation ($-P_r$) of negative direction. Further increase of field leads to increase in polarisation from $-P_r$ to zero at E_c , and then back again to $+P_s$, in total completing a whole loop, called a ferroelectric hysteresis loop. Inside the different regions of the crystal; polarisation can have a different direction within the same region, resulting in the existence of *ferroelectric domains*.

1.2. Applications of Ferroelectric materials

Ferroelectric materials are extensively used in many areas of science and technology because of its properties. A hysteresis property of ferroelectric materials is used to make non-volatile memory devices such as RAM and RFID cards. Due to high relative permittivity it is ideal for capacitors, the non linear property of ferroelectric material can be utilised to change the capacitance through tuning to make tunable capacitors. The direct piezoelectric effect phenomenon of ferroelectrics is used in hydrophones, microphones, accelerometers etc. Whereas, the converse piezoelectric effect phenomenon of ferroelectrics is used in resonators, filters, ultrasonic generators, actuators etc. The pyroelectric effect of ferroelectric materials is used in heat seeking infra-red detectors. The electro-optic effect has utility in photonic devices, optical shutters and Q-switches. The nonlinear optical effects are applied in the development of optical mixing and frequency doubling. The ferroelectric material is also used inside in waveguide.

1.3. Phase transition in ferroelectrics

The structural change and physical properties of dielectric/ferroelectric crystals with temperature without affecting its chemical composition is called phase transition. The point at which phase transition occurs by altering the physical quantities such as temperature and pressure is called transition point. The polar state of most ferroelectrics exists in a certain temperature range. With the increase of temperature, a transition point is reached where the ferroelectric and polar phase changes to non-ferroelectric and non-polar phase (*paraelectric* phase). Spontaneous polarization is connected with spontaneous electro-strictive strains of the crystals, because of which the ferroelectric phase has a low symmetry in comparison to the paraelectric phase. The temperature at which ferroelectric properties disappear i.e. ferroelectric phase changes to paraelectric phase is called as *Curie temperature* (T_c). Some ferroelectric material such as polyvinylidene fluoride (PVDF), a polymeric ferroelectric melts before T_c is reached. In certain types of ferroelectrics material known as *proper ferroelectrics*, where as the temperature approaches near Curie temperature, there is an increase in relative permittivity, reaching peak at T_c and then it decreases below T_c . In other types of ferroelectrics, called as *extrinsic* or *improper ferroelectrics*, no particular peak in permittivity is observed, but only an anomaly.

The phase transition at Curie temperature (T_c) could be of first order (discontinuous) or of second order (continuous). The permittivity (or dielectric constant) is non-constant and is dependent on the field strength. Above T_c , dielectric constant (ϵ_r) obeys the relation : $\epsilon = C/(T - T_0) + \epsilon_0$. C is temperature independent constant called as *Curie-Weiss constant*, ϵ_0 is a constant, which is contributed by an electronic phenomena and is independent of polarization, T_0 is called *Curie-Weiss temperature*, and the value of which is equal to T_c of phase transition of second-order.

Bueger (1961) broadly classified the phase transition into of two types:

- a) Reconstructive transition: In such a type of transition there is a major restructuring of the crystal system, a bond might break and form a new bond. Example is the transition of diamond to graphite and vice-versa. Diamond has a four coordinated three dimensional framework of carbon atoms whereas

graphite has three coordinated two dimensional hexagonal sheets of carbon atoms.

- b) In displacive phase transitions, only the distortion of bonds takes place and no or very small breaking and the structural changes occur. It has small activation energy. A symmetry relation exists between the two polymorphs, the symmetry of low temperature polymorph is lower than, and belongs to a subgroup of, that of the high temperature polymorph. Examples are the three main polymorphs of silica: quartz, tridymite and cristobalite, all of which undergo displacive, low-high transitions. These transitions involve small distortions or rotations of the SiO_4 tetrahedra, without breaking any primary Si-O bonds.

1.4. Thermodynamics of ferroelectric phase transition

The independency of thermodynamic theory to any particular model of atom results into a general conclusion. Even though the theory doesn't provide any physical mechanism, it points towards certain characteristics of the atomic models.

Ehrenfest classified phase transitions into *first order* and *second order* by taking into consideration the thermodynamic quantities such as entropy, heat, capacity and volume while transiting from one polymorph to another. Gibbs free energy of two polymorphs at equilibrium condition is equal i.e. $\Delta G = \Delta H - T\Delta S = 0$. Hence, there is no discontinuity in free energy while transiting from one polymorph to the other.

In *first order* transition when the first derivative is taken w.r.t. pressure and temperature (i.e. volume ($dG/dP = V$ and entropy ($dG/dT = -S$)*, there is the discontinuity in the slope.

First order transitions are relatively easier to detect, it can be determined by looking at discontinuity in first order derivatives such as volume and entropy corresponding to a change in crystal structure two polymorphs.

*from relation $G=H-TS$ and $H=U+PV$

The transitions of *Second-order* nature are characterized by break of slope when the derivative of second order of the free energy is taken such as thermal expansion ($\partial^2 G/\partial P_T \partial T = \partial V/\partial T_P = -V\alpha$), compressibility ($\partial^2 G/\partial P_T^2 = \partial V/\partial P_T = -V\beta$), and Heat capacity ($\partial^2 G/\partial T^2 = \partial S/\partial T_P = -C_p/T$). However, detection of *second-order* transitions is not as easy as for *first-order* ones since the changes involved are smaller. One method to detect *second-order transition* is to measure the heat capacities by Calorimetry. Heat capacities increase as transition temperature (T_c) approaches and show a discontinuity at T_c .

In the vicinity of ferroelectrics transition temperature T_c ; Devonshire [11] discussed the essentials of thermodynamic theory. Landau [12] tried to explain the phase transition of ferroelectric by thermo-dynamical theory. It explains the behaviour of ferroelectric crystal by considering Helmholtz free energy F ; in one dimension it could be represented by the relation formally as:

$$F(P,T,E) = -EP + c_0 + (1/2)c_2P^2 + (1/4)c_4P^4 + (1/6)c_6P^6 + \dots$$

Where the coefficients c_n , are functions of temperature. It can be observed that the series does not have any odd powers of P since on the reversal of polarization the free energy doesn't change.

In an applied electric field E , equilibrium polarization satisfies the condition:

$$\partial F/\partial P = 0 = -E + c_2P + c_4P^3 + c_6P^5 + \dots$$

$$\partial F/\partial P = E = c_2P + c_4P^3 + c_6P^5 + \dots$$

And $1/\chi = dE/dP$, where χ is susceptibility.

However, for $T > T_c$, the susceptibility (χ) is specified by Curie Weiss law:

$$\chi = C/(T-T_0)$$

For the polarized state of the ferroelectrics to be steady, the coefficient of the terms P^2 should be negative, whereas for paraelectric state the coefficient should be positive and having value zero at some particular temperature, T_0 (Curie-Weiss temperature):

$$c_2 = (T - T_0) / \epsilon_0 C$$

Where, C is a known as Curie-Weiss constant (positive constant magnitude) and $T_0 \leq T_c$

The first order or second order phase transition could also be expressed by the order parameter (η). For phase transition of first order, at the transition temperature there is an abrupt transform of η values from some finite to zero. In second order, it is in a small range of temperature about T_c , where η move towards zero from some finite value. The schematic representations of temperature dependence of order parameters, physical properties (polarization and dielectric constant) are shown in Fig.1.1 and dependence of Temperature to order parameters for the first and second order phase transitions are shown in Fig. 1.2.

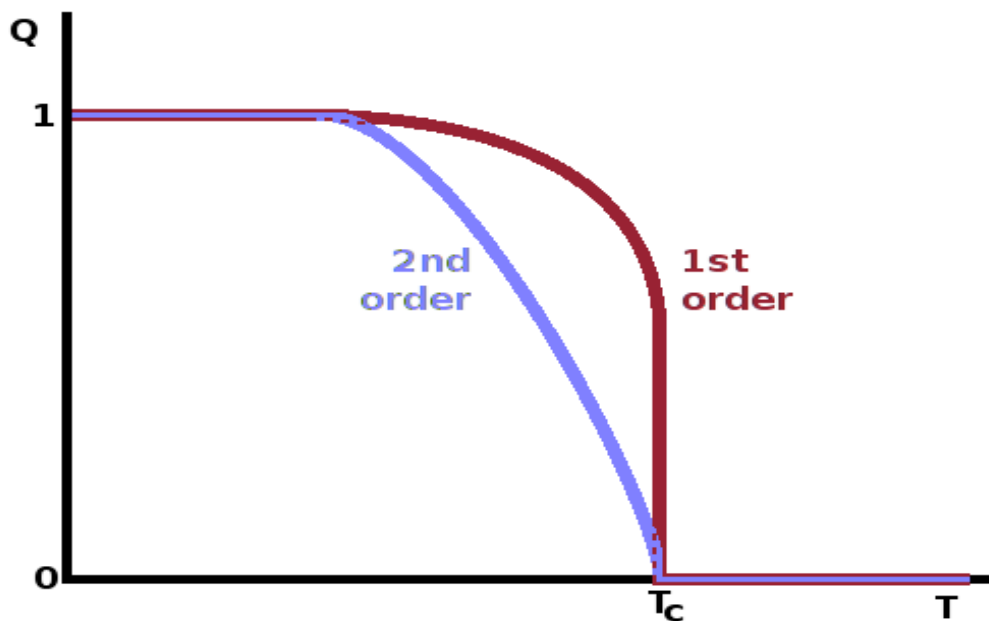


Fig. 1.1. Dependency of Temperature to order parameter (η) and physical parameters (like polarization and dielectric constant)

Broadly ferroelectrics materials can be divided into two major groups, depending upon the temperature variation with Curie constant or dielectric constant:-

- (a) Soft (KH_2PO_4 -type) or order-disorder type transition: The phase transition is soft (H-bonded) ferroelectrics. In the paraelectric phase, the electric dipole exists but is thermally disordered; hence the average polarisation is zero. It involves ordering disordered hydrogen atoms and deformation of atomic groups like PO_4^{3-} , SO_4^{2-} , SeO_4^{2-} and NO_2^- . It has Curie constant of the order 10^3 .
- (b) Hard (BaTiO_3 -type) or displacive type transition: Even though it has no dipoles moments in the crystal structure above transition temperature T_c , yet there exist net dipole which is due to cooperative motion phenomena of its ions (a small atomic displacement in some perovskites) which results in phase transition. It has a Curie constant of the order of 10^5 .

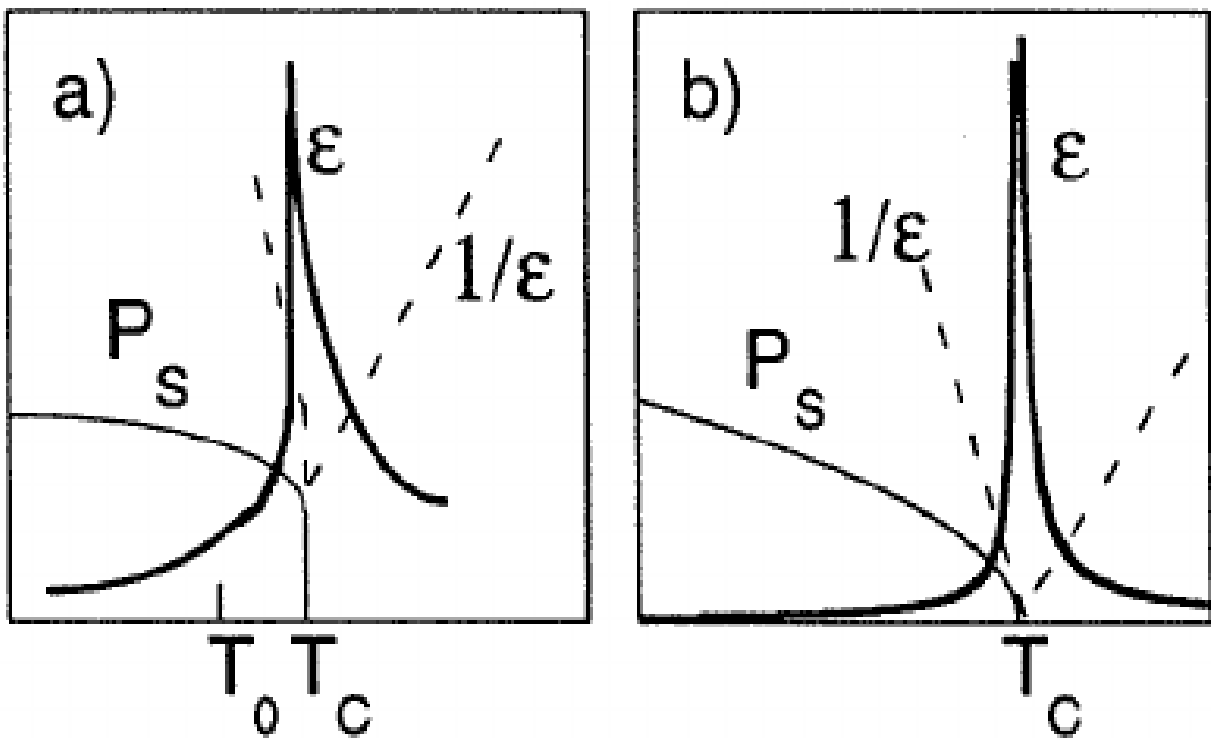


Fig 1.2. Dependency of Temperature on order parameter (a) first order and (b) second order phase transition

However, the distinction between order-disorder and displacive type of transition is not so clear, where the division of appropriate disorder turn out to be comparable to the mean thermal amplitude value of the atoms. The nature of ferroelectrics is expressed by the dynamics of phase transition.

1.5. Phase Transition of Diffuse nature

It has been observed that in some ferroelectrics materials [13] the physical property around the transition temperature is not sharp but gradual, such kind of phase transition is known as diffuse phase transition (DPT). The transition temperature is not sharply defined rather we get a temperature region. The gradual change of physical properties is due to smearing of transition in the given temperature region. Although this type of phenomenon is also being observed in other types of materials but it is more prominent in ferroelectric materials. In the early 1950 [14], for the first time ferroelectric materials with diffuse phase transitions were discussed in the literature. Some salient features of Diffuse Phase Transition are:

- In ($\epsilon \sim T$) curve, the maxima are broadened.
- Remanent and Spontaneous polarisation gradually decreases with increase in temperature,
- Transition temperatures attained through diverse techniques does not coincide,
- Dielectrics has relaxor characteristic, and
- Curie-Weiss behaviour is absent above transition temperature (T_c).

The occurrence of phase transition diffuseness may be because of the reason that around the transition region there is a large fluctuation of temperatures. There are two types of fluctuations:

- a) Compositional fluctuations: it is common in ferroelectric solid solution.
- b) Structural (polarization) fluctuations: it is may be because of the difference in the energy between low and high temperature phases around the transition point.

Even a minute difference in entropy between ferroelectric and paraelectric phases will have significant probability of fluctuations.

From X-ray diffraction study, Kanzing [15] observed that in a wide temperature range just about the transition, BaTiO₃ (single crystal) splits into micro ferroelectric and micro paraelectric regions. As per Fritsberg [16] substance having more diffuse transition is expected to be less stable. Width of the transition region has many practical applications. Based on Gaussian distribution concept, Smolensky [17] and Rolov [18] introduced a model to calculate the polarisation and compositional fluctuation, where from the diffuseness parameter (δ_g) is being calculated. The ferroelectric material of Complex perovskite structure which has distorted arrangements of cation shows DPT, characterised by a broad maximum of dielectric constant (ϵ) and dielectric dispersion in the region of transition [17-19]. For DPT; ϵ follows the relation: $\{(1/\epsilon) - (1/\epsilon_m)\} = \{(T - T_c)^Y / C\}$; where T_c is the transition temperature at which the value of ϵ is maximum (ϵ_m), C is the modified Curie Weiss constant and Y is a critical exponent (which give explanation about the diffusivity and the values lies in the region $1 < Y < 2$) [20]. The smearing of ϵ vs T response is ascribed [17, 21, 22] to the existence of micro regions having average local compositions varying from 100 to 1000 Å. In a range called Curie range of a macroscopic sample, different micro regions are assumed [23] to transfer at different temperature results into compositional fluctuations DPT.

1.6. Classification of representative ferroelectrics

Based on crystal structure and their chemistry, ferroelectrics can broadly be categorized into four groups:

1. **Tartrate Group:** In 1672, pharmacist Seignette prepared Rochelle salt, sodium potassium salt of tartaric acid ($NaKC_4H_4O_6 \cdot 4H_2O$) salt [1] (also known as Seignette salt). It has two transition temperatures. i.e. -18 °C and 23 °C. In the region above 23 °C and below -18 °C the structure is orthorhombic and in the ferroelectric phase it has monoclinic structure.
2. **KDP (KH₂PO₄):** In 1935, it was discovered by Busch and Scherrer that potassium dihydrophosphate KH₂PO₄, groups [24] (consisting of arsenates of the alkali metals and dihydrogen phosphates) has a ferroelectric properties. It has only one Curie temperature $T_c = 123$ °C. Below the T_c the structure of the crystal is orthorhombic and above the transition temp it's tetragonal in structure. From

analysis of the structure it shows that it is the PO_4 groups which form tetrahedrons with Phosphorus at the centre and having four oxygen at the corners. And it is the hydrogen bonds which bind these phosphate groups together. Hydrogen bonds are crucial in the polarization of this kind of ferroelectrics.

3. **Oxygen Octahedron group** : The ferroelectric oxides with oxygen octahedral have four different types of structure:
- Perovskite-type [25-27],
 - Tungsten Bronze (TB) type [28].
 - Bismuth Oxide layer structured ferroelectrics [29].
 - Lithium Niobate and Tantalate [30].

In 1942 Wainer and Salomon observed a number of anomalous dielectric properties in Barium Titanate (BaTiO_3). It is of perovskites type having common formula ABO_3 (where A is a mono- or divalent element and B is a tetra- or pentavalent element). BaTiO_3 in a nonpolarized phase has cubic symmetry with Ba^{2+} ions occupying the corners of the cube, the oxygen ions are located at the centre of faces and Ti^{4+} ions is at the centre. It has an arrangement of the highly polarisable oxygen ions in the form of an octahedron having small metallic ions at the centre. Barium titanate has a transition temperature of 120°C ; above this temp it is non ferroelectric and has the cubic structure. In this region it obeys the Curie-Weiss law

4. **Guanidine aluminium sulphate hexahydrate, $\text{NHC}(\text{NH}_2)_2\text{AlH}(\text{SO}_4)_2 \cdot 6\text{H}_2\text{O}$** [16]: The structure of this compound is currently unidentified. It seems they decompose even before a Curie temp is reached.

Our work is concerns with the TB type of compounds hence details has been given below:

Among numerous groups of ferroelectrics, the family of oxygen octahedral is one of the most important crystals groups. The structure of this group is a combination of oxygen octahedral forming the centres and voids of which other ions are located.

A huge class of ferroelectric crystals is prepared by mixed oxides which have octahedral of O^{2-} ions sharing its corner. And inside each octahedron has a B^{b+} cation (where 'b' has

value from 3 to 6). The space in between the octahedral is taken by A^{a+} ions (where 'a' has value from 1 to 3). In basic forms, the geometric centres of A^{a+} , B^{b+} , and O^{2-} ions coincide, resulting in a lattice of non-polar nature. On polarization, the A and B ions are moved from its geometric centres w.r.t. the O^{2-} ions, giving rise to a net polarity. The occurrence of displacement is due to the transform in the structure of the lattice, during the phase transitions. The formation of dipoles due to the displacement of ions need not result in spontaneous polarization, if the compensation patterns of dipoles have a zero net dipole moment.

The component oxides in the oxygen octahedral play an important part in ferroelectrics. Materials having these types of structure have BO_6 oxygen octahedral, although they may have dissimilar crystal structures, T_c polarization, mechanical and electrical properties, [31]. Magneli [32] described a ferroelectrics family of the largest crystal with oxygen octahedral structure, associated with tetragonal tungsten bronze K_xWO_3 and Na_xWO_3 . The basic octahedral framework of TB structure is shown in Fig. 1.3.

The unit cell of tetragonal structure has 10 BO_6 octahedra connected at the corners resulting into three diverse types of tunnels in a row parallel to the c -axis. Typically, unit cell has a height of one octahedron (~ 4 nm) along the c -axis and having length dimension, $a = b$ of about $\sqrt{10} c$ (~ 1.25 nm). Along the c -axis there is a long chain of oxygen octahedral resembling that of perovskite, while at the normal to this axis it contains somewhat wrinkled sheets of oxygen atoms. The TB- structure has a skeletal frame of BO_6 octahedra involving corners to have three different kinds of tunnels (A, B, C) along the c -axis having general formula $[A_1A_2A_4C_4][B_1B_2B_8]O_{30}$. In the interstitials A1, A2 and C, an A-type cations (mono or divalent) can be accommodated, whereas at octahedral site of B1 and B2, cations (tri or pentavalent) of B-type can be substituted [33]. The particular composition determines how the A-type cations will interact with the structure of the interstitial tunnels sites. Such types of arrangement provides in 9 coordinated trigonal A2 sites a space for up to four cations, in smaller 12 coordinated A1 sites a space for two cations, and in the smaller planar C sites a space for four cations. Also, there are two B-cation sites, which are branded as B1 and B2.

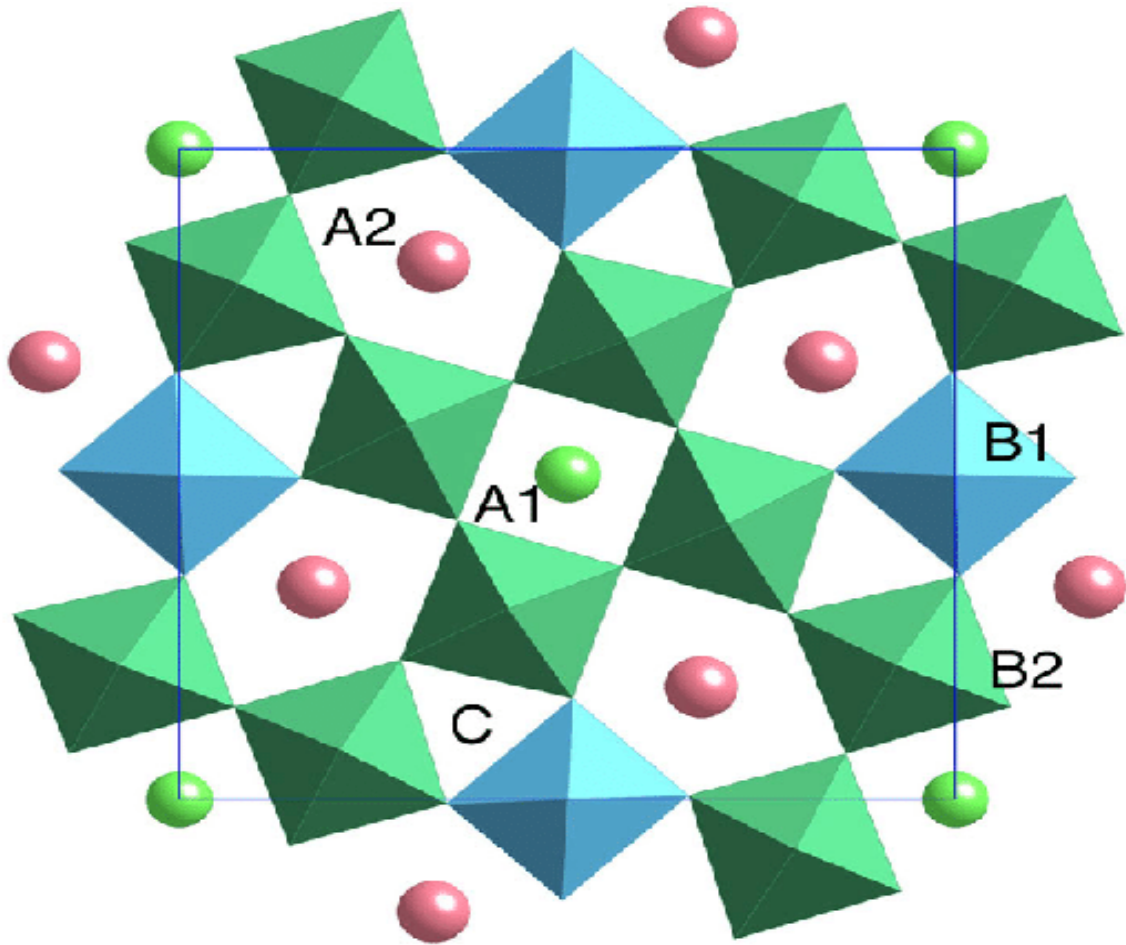


Fig. 1.3. Unit cell atomic arrangement of a tungsten-bronze type structure.

There are large numbers of ferroelectric tungsten bronzes, showing nonstoichiometry. In the paraelectric phase all are tetragonal, which can transform into tetragonal ferroelectric phase or into an orthorhombic phase (which in general is more common). Lead metaniobate (PbNb_2O_6) [34, 35] having structure of tungsten bronze type is one of the first crystals to show ferroelectric properties. Nb^{5+} ions occupy the B_1 and B_2 sites, whereas Pb^{2+} ions occupy the five out of available six A- sites. Lead metaniobate ceramic is not easy to make, yet are used for piezoelectric devices because of its high Curie point ($T_c = 560^\circ\text{C}$). The crystals of ferroelectric developed by forming composites of alkaline and alkali earth niobates material have a potential for being used as pyroelectric detectors, laser modulation, ultrasonic, and hydrophones applications.

The structure of tungsten bronze type is more open in nature as compared to the perovskite structure, due to which a wide range of cation and anion substitutions can be made with improved ferroelectric properties.

1.7. Multiferroic and its technological applications

Multiferroics are the class of materials called smart material which do possess various ferroic ordering [36] such as ferro -magnetism, -electricity, and -elasticity in the same phase by adoption of spontaneous, switchable internal alignment [37]. In ferromagnetic, a magnetic field can switch the electron spins alignment; in ferroelectrics, an electric field can switch alignment of electric dipole moment; and in ferroelasticity, stress field can switch the strain alignment (see Fig. 1.4). Due to its multifunctional properties it has wide application in various fields such as piezoelectric transducers which exploit the combination of ferroelectric and ferroelastic nature of certain materials [38,39].

Materials which exhibit ordering of both electrical and magnetic in the same phase are commonly known as *magnetoelectric multiferroics*. The existence of spontaneous electric and magnetic ordering has potential for wide application on sensors [40] and actuators, spintronic devices (magnetic spins controlled by electric field), data storage media, dual storage devices (Random Access Memories (RAMs) where both the electric and magnetic polarisation are used for data storage) and multiple state memories. The magnetically ordered state is good for storing information, but in application magnetic fields are more complicated to control those states. However, electric voltage is relatively easy to apply at microscopic level; therefore an electrically controlled magnetic state is very useful. Electrical control can be achieved because the electric voltages can switch the ferroelectric state which interacts with the magnetic state and thus causing it to switch too.

Majority of “multiferroic” deals with perovskite-related materials [41,42], due to which it has two limitations. First, that in ABO_3 multiferroics, A and B cations have electronic structure which is not companionable with its magnetic order at high temperatures [43]. Second, the electric and magnetic order may couple only when the material has a non standard magnetic structure [44], toroidal, or a spiral order [45].

In ferroelectric materials, non-centro symmetry or uneven displacement between negative and positive charges gives rise to the electric dipole moment i.e. the polarization arises due to shifting of nonmagnetic cations from the centre of their surrounding anions. Whereas, in case of magnetic materials, there is no dipole moment due to centrosymmetric position, the magnetic cations sit exactly at the centre of surrounding atoms. The difference in nonmagnetic behaviour and magnetic cations is due to contest between Coulombic repulsion which raises the electronic energy (cations with d shell electrons) and of the formation of covalent bond which lowers the energy level (large for d^0 cations having empty d shells). Such balance results in off-centering of d^0 ions as in the case of Ti^{4+} ions in BaTiO_3 (ferroelectric material). In magnetic material however, magnetism occurs due to presence of partially filled d orbital (unpaired localized electrons) of transition metal.

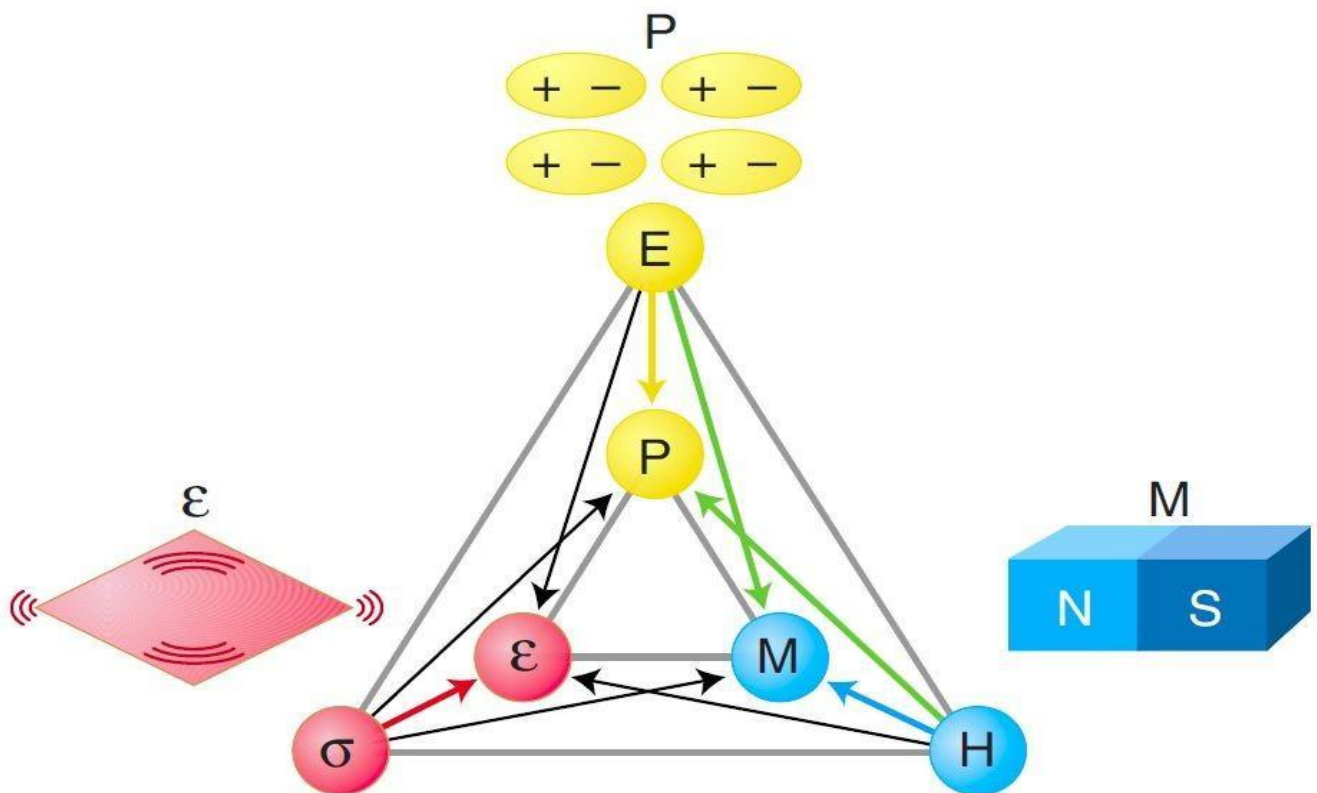


Fig.1.4. Multiferroics interactions: Ferroic orderings, ferromagnetism (**M**), ferroelasticity (**ε**), and Ferroelectricity (**P**), can be switched by their conjugate magnetic (**H**), stress (**σ**) and electric (**E**). Coexistence of at least two ferroic ordering results in additional interactions.

So far, the availability of single phase multiferroics at room-temperature is few. It is because for ferroelectrics materials to have a polarization, it must be an insulator but most of the magnetic materials are conducting in nature. Moreover, the presence of any kind of leakage like inexact proportion of atoms and impurities weakens the ferroelectric properties, even if the material is formally insulating.

Single phase multiferroics are usually Fe- or Mn- based oxides. Among all the multiferroic, Bismuth Ferrite (BiFeO_3) is the most popular one, because it can be easily manufactured in bulk and thin-film forms and also it is the only material which demonstrates the multiferroic behaviour at room temperature. It shows both ferroelectric and (anti-)ferromagnetism coupling (coupling effect between electric and magnetization polarization might results into presence of ferroelectric and ferromagnetic in a single material to generate coupling characteristics) between the two order parameters i.e. charge and spin respectively. It has Neel temperature (~ 643 K) [46-48] and Curie temperature (~ 1100 K) [49] which is above the room temperature. BiFeO_3 is a rhombohedral ferroelectric, ferroelastic in nature in the temperature range from low temperature to 810°C and has a remunerated antiferromagnet having cycloidal spin with Neel temperature of 370°C . However, its complex antiferromagnetic ordering yields small remnant magnetization.

Bismuth ferrite (BiFeO_3) is ferroelectric in nature with Fe^{3+} ions having magnetic properties and its Bi ion with lone pair electrons in the $6s$ orbital which moves away from the center-symmetric location (surrounded by oxygens). BiFeO_3 has a non-centrosymmetric rhombohedrally distorted perovskite structure [50, 51] having space group $R3c$ [52] (see fig. 1.5). The mechanism is stereochemical activity of the Bi^{3+} $6s^2$ lone pair; there is a transfer of a charge from $6s^2$ to properly empty $6p$ orbitals. The presence of weak ferromagnetic is may be because of the residual moment of the canted Fe^{3+} spin structure. Electric and magnetic coupling arises because of lattice distortion of BiFeO_3 .

The structural study of ferroelectric phase of BiFeO_3 shows the shifts of Bi^{3+} and Fe^{3+} ions, also the counter rotation of oxygen octahedrons along $\langle 111 \rangle$ direction from the non ferroelectric centrosymmetric cubic structure, resulting to $R3c$ space group and spontaneous polarization (P_s). The magnetic structure is of G type [54] having cycloidal

spiral arrangement of magnetic moments of Fe^{3+} ions [55], and the canted spins due to Dzyaloshinskii-Moriya (D-M) [56,57] interaction results into weak ferromagnetism [58].

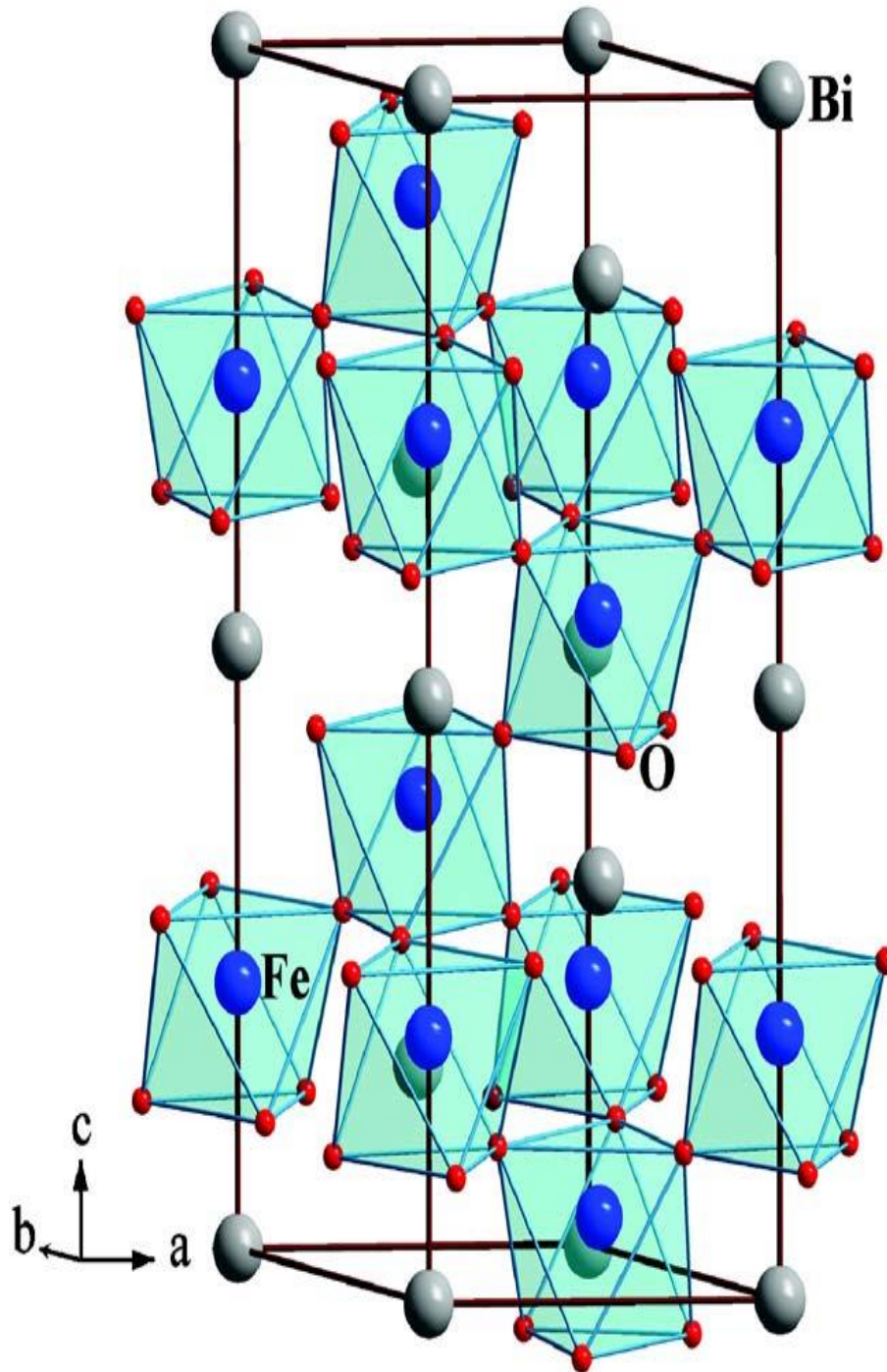


Figure 1.5 Unit cell crystal structure of hexagonal ($R3c$) BiFeO_3

However when P_s was measured for single crystal BiFeO_3 at liquid nitrogen temperature it was found to be only $6.1 \mu\text{C}/\text{cm}^2$ along the $\langle 111 \rangle$ polar direction. High value of P_s ($\sim 50 \mu\text{C}/\text{cm}^2$) [59] was reported for thin films in comparison to bulk BiFeO_3 . The high value of P_s for thin films was initially attributed to its tetragonal ($P4mm$) structure, while the bulk BiFeO_3 is of rhombohedral ($R3c$) structure. The Berry phase calculation shows that for tetragonal BiFeO_3 ($P4mm$) the P_s is of $110 \mu\text{C}/\text{cm}^2$ along $\langle 111 \rangle$ directions, whereas for rhombohedral BiFeO_3 ($R3c$) [59] is only $6.6 \mu\text{C}/\text{cm}^2$ along $\langle 111 \rangle$ directions. In later improved first-principal calculation, it was shown that P_s of rhombohedral BiFeO_3 ($R3c$) can reach upto $90\text{-}100 \mu\text{C}/\text{cm}^2$ [60].

To improve the properties of BiFeO_3 , materials of other perovskite structure are introduced to form the solid solutions with BiFeO_3 . The introduction of PbTiO_3 introduces a difference in crystal systems which stabilize the perovskite phase and also forms morphotropic phase boundary (MBP). The addition cause change in the electric properties of BiFeO_3 (there is decrease in the electric conductivity and display of ferroelectric hysteresis loop with P_r of $17 \mu\text{C}/\text{cm}^2$ [61], making it a good ferroelectric material) and also it affects the magnetic properties of material, the introduction of diamagnetic Ti^{4+} ions onto the B site of perovskite structure changes the crystallographic structure, which dilutes the concentration of paramagnetic Fe^{3+} ions, resulting into the decrease of magnetic ordering strength causing decrease in T_N .

1.8. Literature Survey

The materials which have more than one ferroic order coexist in one phase i.e. ferroelectricity, (anti)ferromagnetism, ferrotoroidicity, and ferroelasticity, is called 'multiferroic' [62]. As per expectation, multiferroics with ferroelectricity and ferromagnetism ordering should have a coupling between dielectric and magnetic properties which can be controlled by applying electric and/or magnetic fields [63]. However, most of the oxides of ferroelectric consist of transition metal ions without active d - electrons (source of magnetism) and oxides of ferromagnetic contain centre of symmetry (which do not allow an electric polarization). Therefore, there are only few multiferroics reported so far [64] even though, in 1958, Smolenskii and co-workers [65, 66] started work on ferro electromagnets.

In the 1960s-1970s [67-77], wide studies were done on BiFeO_3 but very little were reported on its ferroelectric properties. The bulk BiFeO_3 in spite of its good ferroelectric and multiferroic properties has several drawbacks. Firstly, the macroscopic magnetization which arises from D-M interaction [78] gets cancelled by spiral spin, which severely restrains the linear magnetoelectric effect [79]. Secondly, the presence of high electric coercive fields (E_c) limits the ferroelectric applications of bulk material.

Preparation of pure and dense bulk material of BiFeO_3 (free from electronic and chemical defects such as Fe^{2+} ions and oxygen vacancies, which results in increase of electrical resistivity) possess technical problems [80]. Firstly, during synthesis process, it is difficult to maintain the stoichiometry ratio (its phase stabilization has narrow temperature range) of precursor materials Fe_2O_3 and Bi_2O_3 due to evaporation of Bi_2O_3 giving rise to impurities such as $\text{Bi}_2\text{Fe}_4\text{O}_9$ phase [81]. Such impurity phases cause high leakage current in BiFeO_3 resulting in a poor ferroelectric behaviour (thus inappropriate for any practical applications). Secondly, BiFeO_3 is an incongruent-melting compound i.e. kinetic cooling result in local deviation from its stoichiometry. Different techniques have been developed to form phase-pure BiFeO_3 with better properties such as: (a) formation of solid solution of BiFeO_3 with similar perovskites structure of ABO_3 type like PbTiO_3 , [82, 83] (b) calcination of a Stoichiometric combination of Fe_2O_3 and Bi_2O_3 pursued by leaching through nitric acid, and (c) sintering of rapid liquid phase of BiFeO_3 [84], it's also known as Rapid thermal process

(RTP) where a high heating rate is introduced to lessen the evaporation of unstable compound [59]. In this framework, doping of BiFeO_3 with elements of lanthanide series has been established to be reasonably successful.

Earlier it was assumed that BiFeO_3 has an antiferroelectric nature since it has a superstructure and value of dielectric constant is low. Tabares-Munoz *et al.* [85] using polarized light microscopy observed ferroelectric/ferroelastic single domain in BiFeO_3 proving ferroelectric nature of it. It was found to be not easy to detect at room temperature a ferroelectric loop due to the low resistivity nature of the materials. To enhance the resistivity Teague *et al.* [86] took the measurements at 80 K and observed a hysteresis loop. It is classified as ferroelectric with ferroelastic at T_C of around 850 °C. It also has an antiferromagnet property (T_N at 310 °C). The presence of both magnetic and ferroelectric ordering makes it a magnetoelectric material. It has also been reported that BiFeO_3 also shows a weak ferro/ferri magnetic characteristic. Because of the semiconducting nature of BiFeO_3 proper electrical poling is not possible at room temperature, which results in high dielectric loss [87]. Hence, the resolution of dielectric anomaly becomes difficult. To overcome the problem of high dielectric loss at elevated temperatures, Krainik *et al.* [88] measured the dielectric constant (ϵ) of BiFeO_3 at microwave frequencies. Smith *et al.* [89] adopted another way, by doping BiFeO_3 with other perovskites to make it an insulator. They synthesize a solid solution of BiFeO_3 - PbTiO_3 with high values of resistivity, which enables to measure maxima of dielectric with small losses in the BiFeO_3 rich phases of the solid solution. By extrapolating the curve of T_C by varying the composition, it is possible to pinpoint the transition of the pure sample. BiFeO_3 may form composites with other perovskites of ABO_3 type. It has been reported that during the formation of solid solutions, BiFeO_3 demonstrates a changed transformation of structure, with rising content of the second phase. Khomskii [53] has emphasized that magnetism and ferroelectricity in multiferroics materials could be combined in different ways.

Most of the multiferroics are antiferromagnetic in nature with exception to few compounds such as magnetite [90] and boracites [91]. James *et al.* [92] studied magnetic and magnetoelectric studies of polycrystalline $\text{LaBi}_4\text{FeTi}_3\text{O}_{15}$ and summarized that the compound is 4-layered belonging to a family of BLSF's. The magnetic studies at room temperature indicate the compound is antiferromagnetic in nature and the

further studies indicate the material has “canted antiferromagnetic” ordering. The magnetoelectric effect was also being observed. They studied the dielectric and electrical properties [93] of $\text{LaBi}_4\text{FeTi}_3\text{O}_{15}$ of orthorhombic symmetry to have a dielectric peak at 773K and of diffusive type. The same team also investigated the dielectric and magnetic nature of $\text{Bi}_7\text{Fe}_3\text{Ti}_3\text{O}_{21}$ [94] and concluded that the values of lattice parameters lies between five-layered and eight-layered compound, the compound is ferroelectrics exhibiting two dielectrics anomaly and it also has an antiferromagnetic nature showing weak ferromagnetism at room temperature. Thus, the material exhibits both electric and magnetic order at room temperature. Mahesh *et al.* [95] developed an experimental set up for measurement of dynamic magnetoelectric effect. They also performed impedance and dielectric studies on $\text{BiFeO}_3\text{-BaTiO}_3$ solid solutions [96]. They concluded that the lattice parameters of the system increases due to addition of tetragonal BaTiO_3 , the conductivity of the sample increases with increase in temperature, the transition temperature of the solid solutions is less than BiFeO_3 , the sample indicates a Debye like behaviour. The similar team also measured spontaneous magnetization in $\text{BiFeO}_3\text{-BaTiO}_3$ solid solutions at low temperature [97] and found that the solid solution in bulk form behaves similar to amorphous thin films, exhibiting spontaneous magnetic moment even at low temperature, not like those of pure BiFeO_3 compound which doesn't show any magnetic moment at low temperature even if the magnetic field is very high. Thus, though the material is antiferromagnetic in character they display a ferromagnetic order. The study about the structural character relations in $\text{BiFeO}_3\text{-BaTiO}_3$ solid solutions [98] conclude that the BiFeO_3 has ferromagnetic properties, making it one of few ferromagnetic insulator; the $\text{BiFeO}_3\text{-BaTiO}_3$ undergoes structural transition with the increase of BaTiO_3 content; at cubic phase no ferroelectric phase was observed; T_c decreases with increase in the content of BaTiO_3 , BiFeO_3 belongs to displacive type ferroelectrics, the structure determine the grain and grain boundary effect; the antiferromagnetic order is due to Fe-O-Fe interactions and in distorted perovskite structure due to canting of the spin, a weak ferromagnetism is observed; the structure become simpler with the increase in concentration of BaTiO_3 and paramagnetism sets in. A team was also able to prepare a ceramic of phase pure BiFeO_3 having ferroelectric transition temperature of 1109K [99]. Zhu [100] chemically modified and studied the electrical properties of $0.67\text{BiFeO}_3\text{-}0.33\text{PbTiO}_3$ ferroelectric ceramics and summarised that chemical modification effectively improve the dielectric

properties and it has potential applications in magneto-electric and in high temperature piezoelectric appliances. Later on, they also studied about the structural and magnetic characteristics of $(\text{BiFeO}_3)_{1-x}(\text{PbTiO}_3)_x$ solid solution multiferroic [101] and found that the system has morphotropic phase boundary region having three region i.e. tetragonal, rhombohedral, and orthorhombic exist simultaneously and shows three anomalies corresponding to antiferromagnetic order in the respective phases. Jong *et al.* [102] prepared multiferroic BiFeO_3 by sol-gel technique and were able to attain high purity BiFeO_3 R-Phase powders having particle size of ~ 200 nm; A reversible phase transformation pair of exothermic and endothermic 1094 K during cooling and at 1109 K during heating respectively was observed; the dielectric constant of ~ 15 at the frequency range of $10^4 \sim 10^6$ Hz at room temperature was observed. Wang *et al.* [103] doped the multiferroic BiFeO_3 with Ba at room temperature and studied the ferroelectric, magnetic, and magnetoelectric properties. They concluded that their dielectric constant varies when magnetic field is applied which suggests that the compound has magnetoelectric coupling. Manoj [104] studied the Ti substituted $\text{BiFe}_{0.75}\text{Ti}_{0.25}\text{O}_{30}$ bulk ceramic; the electrical resistivity was found to be $\sim 5.5 \times 10^{10} \Omega \text{ cm}$ and an enhance dielectric constant with reduced dielectric loss; ME effect was observed at room temperature; near Neel temperature, an anomaly was observed in dielectric constant and $\tan\delta$. Nalwa *et al.* [105] studied the effect of Sm doped BiFeO_3 and concluded that solid state reaction of Bi_2O_3 and Fe_2O_3 powders cannot eliminate the Bi-rich impurity phase(s); with Sm doping it is feasible to obtain Sm-doped BiFeO_3 of single phase by calcined at temperature above 1073 K; there is also enhancement of magnetization by two orders in magnitude in room temperature; the antiferromagnetic transition is at ~ 603 K; thus the Sm doping increases the remnant polarization of BiFeO_3 sample but accompanied by higher conductivity. Simões *et al.* [106] prepared lanthanum modified BiFeO_3 thin films fabricated on Pt substrate via soft chemical method and studied about strain behaviour, it was found that the Raman modes were not affected strongly by lanthanum substitution; the strain behaviour of the BiFeO_3 films also reduced due to addition of lanthanum; substitution of La^{+3} in place of Bi^{+3} reduces the Bismuth vacancies which comes with Oxygen vacancies thus reducing the film conductivity; the outcome strongly suggesting that $\text{La}_x\text{Bi}_{1-x}\text{FeO}_3$ thin film is suitable for storage elements in non volatile FeRAM. S. Chandarak *et al.* [107] also studied about dielectric properties of $x\text{BaTiO}_3-(1-x)\text{BiFeO}_3$ ceramics and concluded that the dielectric

properties improves with increase of BaTiO₃ content; the large dielectric properties is due to giant-dielectric like behaviour which is the effect of Fe multivalent states, with the increase of BaTiO₃ content in ceramic density of grain packing also gets better; it also reveals that BaTiO₃-BiFeO₃ ceramics have giant-dielectric like behaviour similar to the pure BiFeO₃. A. Huang [108] studied about electrical and structural properties of BiFeO₃ thin films developed using chemical solution deposition method and microwave annealing and summarised that microwave improves the ferroelectric properties of BiFeO₃ films; also established that superior electrical properties and morphology can be accomplished in BiFeO₃ films by microwave in short period of time. Chaudhari *et al.* [109] prepared multiferroic BiFe_{1-x}Zn_xO₃ ceramics by solution combustion method and concluded that material exhibits a weak ferromagnetism at room temperature and elucidates a super paramagnetic behaviour at 5 K; the room temperature ferroelectric hysteresis loop does not really saturate indicating ferroelectric behaviour. J. Rout *et al.* [110] did the structural, electrical, and magnetic properties of *x*BaMnO₃-(1-*x*)BiFeO₃ multiferroic system and summarised that in the FTIR spectra there are two vibrational modes at 550 cm⁻¹ and 442 cm⁻¹ which corresponds to the stretching and bending of Fe-O and Bi-O bonds, respectively; the increase in the BMnO₃ content results in decrease of grain size of the system; the dielectric constant increases with increase in BMnO₃ content and it may be suitable for energy storage devices; the electrical properties of the system is robustly dependent on frequency and temperature; there is simultaneous occurrence of Ferroelectrics and Antiferromagnetism which confirms the system is multiferroic in nature.

At the crystal chemistry level, Tetragonal Tungsten Bronze (TTB) structure has two main advantages. Firstly, the number of cation sites is more than that of perovskites i.e. 5 sites instead of 2 sites, which extend substitution prospects to advance magnetic interactions. Finally, TTB compounds exhibit a disproportionate polar state [111, 112], which might support a coupling between ferroelectric and magnetic order.

Among the TB type structure family, Niobates have a lot of utility because of its various applications such as in acoustic optics, nonlinear optics, electro-optics etc. Some examples of such types of ferroelectrics are PbNb₂O₆ and its related system [113, 114], (Pb-Ba)Nb₂O₆, (Ba-Sr)Nb₂O₆, etc. Ballman *et al.* [115] were able to obtain a large

dielectric constant in a single crystal of (Ba-Sr)Nb₂O₆ was obtained [116] by varying Ba:Sr ratio also the transition temperature shifted toward room temperature.

Of the many materials studied Ba₂NaNb₅O₁₅, Barium Sodium Niobate (BNN) was found to be one of the best ferroelectric materials with TB structure having many useful properties.[117-119]. Ferroelectricity in BNN was first established by J. J. Rubin *et al.* [120] in 1967 by observing transition temperature at 328 K. Subsequently another transition temperature of 833 K was reported by Burgreat and Toledano [121]. The first transition is due to dielectric anomaly whereas the second corresponds to elastic anomaly. Sati et al [122] reported a detailed structural study and the effect of doping of rare-earth ions in the properties of BNN. Umakantham et al [123] confirmed orthorhombic symmetry for the lead strontium niobate (TB structure family). Bu *et al.* [124] studied the space charge effect on (K_{0.5}Na_{0.5})₂(Sr_{0.75}Ba_{0.25})₄Nb₁₀O₃₀ ferroelectric ceramics. Wakiya *et al.* [125] studied Ba_{1-x}R_{2x/3}Nb₂O₆ (R=rare earth ions) for the intended FeRAM application in place of PZT. They concluded that it is a better replacement for PZT i.e. replacing Pb by Ba, in the path towards Pb free environment. Panigrahi et al [126,127] studied the structural and electrical properties of Ba₅RTi₃Nb₇O₃₀ (R= rare earth elements). They came to the conclusion that at room temperature, structures of the compounds are orthorhombic and they undergo phase transition of diffuse type, and it also shows relaxor properties and negative temperature coefficient of resistance. When Ti⁴⁺ is replaced by Zr⁴⁺, transition temperature and permittivity decreases with increase of Zr⁴⁺ contents. In Ba₅RTi₃Nb₇O₃₀ by changing R we get a wide range of Curie Temperature T_c [128].

However, the problem with Ba₅RTi₃Nb₇O₃₀ compound is that it has a high sintering temperature (~1473 K) [129]. It was found that when Niobium (Nb) is replaced by Vanadium (V) the calcination and sintering temperature reduces considerably [130-133]. The drastic reduction in sintering temperature may be due to lower atomic radius of Vanadium (V) in comparison to Niobium (Nb) and there is no compromise in its ferroelectrics properties [134].

It has been reported that the ferroelectric properties of the ferroelectric compound could be increased by addition of multiferroics such as BiFeO₃ by making a solid

solution with ferroelectrics [135]. The magnetic order of BiFeO₃ can be improved by employing solid solution technique reaction [136] with pure ferroelectrics.

1.9. Selection of material for the present work (Aim of the work)

BiFeO₃ (Bismuth Ferrite) [137] is a multiferroic material having both ferromagnetism and ferroelectricity in a single phase. An electric polarization can be induced by an external magnetic field and magnetization by change in an electric field [138]. This material has a wide application in ferroelectric and magnetic devices [139]. However, due to its semiconducting nature it has a high dielectric loss and low dielectric constant [140]. The complex magnetic properties also yield a very small remnant magnetization [141]. Smith *et al.* adopted a technique by which BiFeO₃ is made insulator by doping it with other perovskites with good ferroelectrics properties [142, 143]. It has been observed that T_N and T_C changes considerably by addition of Sodium Potassium Niobate. The magnetic order parameter also improves when BiFeO₃ is mixed with ferroelectric compounds.

As per literature survey it's been seen that both the magnetic and dielectric properties of BiFeO₃ can be improved by making solid solutions with different ferroelectrics.

Among different types of TB structure ferroelectrics, Niobates are of great significance due to its diverse applications in a range of fields as in nonlinear optic, acoustic-optic, electro-optic, etc. Some lead containing ferroelectrics such as PbNb₂O₆, (Pb-Ba)Nb₂O₆, etc though has wide application such as in pyroelectric, piezoelectric and capacitor, but its lead oxides are health hazardous. So the expedition is to minimize lead content or make the compound completely lead free. (Ba-Sr)Nb₂O₆ (BNN) became more appealing for it is not only Lead free but also showed better electro-optic coefficient and also diffused phase transitions. This particular area became a breeding ground for lots of research and hordes of new material are being unearthed. One of such kinds is Niobate-Titanate (of TB structure) of Rare Earth doped; Ba₅RTi₃Nb₇O₃₀ [144], by different Rare earth element (R) substitution; it gives the scope to obtain diverse types of Ferroelectrics. However, Niobate-Titanate has a high calcination and sintering temperature. It has

been reported that when in $\text{Ba}_5\text{RTi}_3\text{Nb}_7\text{O}_{30}$, Nb(Niobium) is substituted by V(Vanadium) element, the calcination and sintering temperature reduces considerably [145] with enhance thermal stability, low leakage current [146] and improved dielectric and ferroelectric properties [147, 148].

Though various literatures shows mixing of BiFeO_3 of perovskite structure with different ferroelectrics with same structural family [149, 150] but in our present work we have decided to mix BiFeO_3 with $\text{Ba}_5\text{RTi}_3\text{V}_7\text{O}_{30}$ of different structural family (TB-structure). The motivation behind the selection of TB structure is its more open structure as compared to perovskite, which might allow a wide range of cation and anion substitution resulting in improved ferroelectric properties consequently, improved magnetic properties and finally, a better multiferroic.

1.10. Materials under present investigation

For detailed studies the ten samples to be studied can be represented by a general formula $(1-x)\text{Ba}_5\text{RTi}_3\text{V}_7\text{O}_{30}-x\text{BiFeO}_3$; where $x = 0-1$; $R = \text{Tb, Pr}$. (Rare earth elements)

These compounds can be again classified into two groups, i.e.

Group A: $(1-x)\text{Ba}_5\text{TbTi}_3\text{V}_7\text{O}_{30}-x\text{BiFeO}_3$

Group B: $(1-x)\text{Ba}_5\text{PrTi}_3\text{V}_7\text{O}_{30}-x\text{BiFeO}_3$

1.11. Aim and Objectives of the work

The followings are the main objectives of the current work:

- Preparation of Solid Solution using high temperature solid-state reaction method.
- To study the structural and micro-structural properties of the samples for better perceptive of their structural parameters.
- To study the dielectric responses as a function of temperature and frequency to uncover the phase transition in them.
- To study the AC electrical conductivity as a function of temperature for better understanding the conduction process of the sample.
- To study the effect of rare-earth substitution in the $\text{Ba}_5\text{RTi}_3\text{V}_7\text{O}_{30}$ (R = Tb, Pr) in the ferroelectrics properties.
- To study the solid solution $(1-x)\text{Ba}_5\text{RTi}_3\text{V}_7\text{O}_{30}-x\text{BiFeO}_3$; for different R (i.e. Tb, Pr) in different values of $x = 0, 0.3, 0.5, 0.7, 1.0$. And to see for what value of x , the ferroelectrics and magnetic properties are improved.

Our aim is to find a better magnetic-electric coupling in the composite system to have better multiferroic materials.

CHAPTER II
METHODOLOGY

2.1. Introduction

In order to understand the physics and chemistry of materials, various characteristics of materials like microstructure, structure, surface morphology, mechanical, thermal, optical, electrical etc is needed to be considered in detail. In condensed matter physics and material research, the detailed analysis of synthesis and characterization of material is an important aspect during the experimental research. How the materials are fabricated to a large extent determines the quality and properties of materials. There are various ways to fabricate a particular material and the proper selection of fabrication parameters is important to acquire the desired characteristic of the desired potential, which not only depends on the overall composition and structure but also in the preceding steps. The Composition, Structure and process of fabrication of material determine the Surface Morphology, Structure, transport of electrons, Grain growth, and also the magnetic properties. The addition of impurities which might be inherent or dopants modifies the properties of the synthesised ceramic materials. The properties of material are related to the synthesis process that is the way it has been prepared.

Material research is mostly an experimental research. Its methodology is based on different experimental techniques, different instruments used for this purpose. In order to develop new materials for device application, its characteristics are to be studied (electrical, magnetic, optical, etc.). Properties of material also depend on the method of preparation. So, the methodology has two aspects i.e. (i) Material Synthesis and (ii) Characterisation. In the following section we have discussed in detail about the two aspects.

2.2. Section-I: MATERIAL SYNTHESIS

2.2.1. Introduction

Fabrication technique determines the properties of ceramic materials and their suitability to be used as devices.

Through study of physical properties of materials is possible because of the minimum effect of surface and imperfections in their single crystals.

Works on ferroelectric and associated compounds are mostly carried out by growing crystals via diverse methods like melt growth, solution growth, etc [1, 2]. To make single

crystal suitable for device applications particular care is needed in their preparation, cutting and polishing [3, 4]

Single crystal could be replaced by Ceramics for device applications since it is easier and economised in fabrication; it has greater durability, higher mechanical strength and is less sensitive to temperature and humidity variations [5]. Moreover, it's cheaper and has an easier fabrication process [6].

Ceramics may be considered as substitutes for single crystal due to:

- (i) It is easier to construct ceramics into diverse sizes and shapes. Ceramic materials are predominantly inorganic oxides. They are produced from unreacted, partially reacted or fully reacted powders which are sintered to a low porosity state by heat treatment. The advantages of ceramic processing are that it can be shaped accordingly as per the requirement.
- (ii) Ceramics have supplementary structural features, the microstructure (i.e., grain shape, size, porosity etc.). The microstructure character can be exploited to design and fabricate a particular device. Presence of grain boundaries gives rise to an extra effect, which is absent in single crystals, and plays an essential role in applications of electroceramics.
- (iii) Ceramics have the benefits of chemical, mechanical and thermal stability. Ferroelectric ceramics plays an important role in electrical and electronics applications. In many cases the ferroelectric properties approach near to those of single crystals. It is also possible to prepare a wide range and varieties of ceramic materials, and to adjust the characteristics of materials for different applications.

Despite the ceramics being brittle and non-ductile characteristics it may be justified to use ceramics due to above given advantages.

2.2.2. General Methods of Preparation of Ceramics

Due to vast applications of ceramics, there is growing interest in multidisciplinary approach in their synthesis. The composition of the materials, structure and the arrangement of phases determine the properties of the ceramics materials [7]. The

fabrication technique and the raw materials determine the microstructure or phase distribution of the materials.

For studying the various properties of materials the synthesis of material and characterization plays an important role.

Synthesis of materials is the steps of operations which purposely and methodically modify the physical properties of the system. The aim of the synthesis is to change the characteristics purposefully to enhance the quality. It is to understand the effect of processing variables and to identify the important characteristics.

The various techniques for the synthesis of materials:

➤ **Mechanical Methods**

1. High temperature solid state reaction or Mixed Oxide Process (MOP)
2. High Energy Ball Milling
3. Vibratory Milling
4. Attrition Milling
5. Roll Crushing
6. Hammer Milling
7. Turbo Milling
8. Fluid energy Milling

➤ **Chemical methods**

1. Co-precipitation method
2. Sol-gel process
3. Decomposition
4. Plasma
5. Laser
6. Molten salt
7. Hydrothermal techniques
8. Liquid-phase and gas-phase reaction etc.
9. Cyrochemical processing
10. Polymer pyrolysis

The Mechanical Methods and Chemical Methods have their own advantages and disadvantages. However, in our present work, we are employing Mechanical Method and High temperature solid state reaction in particular. The solid state reaction is particularly suitable for large scale bulk ceramic powder production due to its easy adaptability and low cost. However, it also has several restrictions in the fabrication of fine ceramics [8]. Generally, Solid does not react at normal temperature and normal time period. High temperature for large timescale is required for reaction to occur at a significant rate, which in turn makes the particle coarse, which in turn requires high energy breakdown force to obtain fine powders [9]. For mixing the constituent solid gradients temperature as high as 1500°C may be required. Fabrication and the properties of ceramics prepared by Mixed Oxide Process have been studied by various authors [10-12]. The thermal schedule, homogeneity of the mixture, particle size, and atmosphere all through calcinations determine the completion of the uniformity and reaction of the product.

2.2.3. Mixed Oxide Process

For the preparation of polycrystalline samples the conventional Mixed Oxide Process or high temperature solid-state reaction is being employed due to its convenient, easy preparation and reliability. The starting chemical chosen has to meet certain specifications such as the grain purity and the grain distribution. The main steps of the Mixed Oxide Process are given in a flow chart form (Fig. 2.1). In the processing the following steps are involved:

- **Raw Materials**

On the base of the particle size and purity the raw materials are being selected. It is essential for the size of the particle to be small preferably in nano size, for the size determines how effectively the chemical equilibrium is being attained, especially for the development of a solid solution. The occurrence of impurity in the fired ceramics might have an effect on the reactivity and the electrical properties of the system. Hence, it is important to have knowledge about the magnitude of volatile ingredients or impurities in the raw materials. Many materials can endure certain digression from stoichiometry,

although at the cost of substitution modification of their characteristics. In order to maintain stoichiometry therefore, the ignition losses must be established.

- **Weighting and Mixing**

In the ceramic technology, it is very important to weigh the ingredient material precisely. The ingredient is to be taken in required Stoichiometric. The necessary quantity of diverse chemicals such as metallic carbonates/oxides for the synthesis of ceramics is calculated is as follow below:

Weight requisite for a^{th} metallic oxides is specified by

$$m_a = \frac{M_a m Z}{M} \quad (2.1)$$

Where,

M = Molecular weight of the sample

m = material amount to be prepared (in gram)

M_a = Molecular weight of a^{th} metallic oxide/carbonates

Z = fraction of metallic ion

It may be noted that the ingredients of the ceramics may be thoroughly mixed and the obtained mixture is called a solid solution. The lack of homogeneity in the solid solution may result in variation of physical properties such as dielectrics, ferroelectrics etc. Therefore, for enhanced homogeneity it is necessary to mix the ingredients in dry and wet medium (i.e. in solvent like ethanol and acetone) for an extended period of time. The wet mixture is then kept in an open atmosphere for some time to let it parched by deliberate evaporation. Normally, the dried residue is kept below 100°C and then ground for a few hours in an agate mortar.

- **Calcination or Pre-sintering**

Calcination or Pre-sintering is a route in which the powder is heated to about $\frac{2}{3}$ of its melting point for several hours. According to Swallow and Jordan [13] the calcination is carried out for the subsequent reasons.

- i) It disintegrates the oxides or higher carbonates present in the mixture, hence reducing the unwanted gases in the concluding sintering.
- ii) It induces the thermo-chemical reaction amongst the component oxides to form the required solid solutions.
- iii) It helps in controlling the contraction occurring during the final sintering.
- iv) It helps in controlling the size of particles in Pre-sintered products on grinding.

The powder is engaged in an alumina crucible in a high temperature muffle furnace. The calcined powder is ground and re-calcined under the identical condition. The procedure is repetitive till compound is formed which is established by various techniques like X-ray analysis, SEM etc.

- **Grinding and Pelletization**

Through various means Grinding can be accomplished such as Pestle and Agate Mortar, Ball milling etc. Grinding assists in assimilation of the ingredient materials and homogenizes the compositional variant which could crop up at some stage in calcination. The coarse grain can have large intra granular voids with lower density and too fine a grain size may have colloidal properties which may well hamper ensuing forming operations. After the calcined powder is for a second time ground to a fine powder, a small amount of Poly-vinyl alcohol (PVA) is added to the sample powder acting as a binder. The addition of binder solution also reduces the fragility of the pellets and helps in improved firmness among the granules of the materials. The binder solution gets scorched out during the sintering process. Using a die punch in a hydraulic press, then the powder is put under cold high pressure to form a cylindrical pellet.

- **Testing of formation of the compound**

The calcined powder is then taken to get the x-ray diffraction profile of the materials using a powder diffractometer. By comparing the XRD profile of these materials with those of their ingredients the formation of the desired compound is confirmed.

- **Sintering**

It is a process by which the assortment of fine grains powders is transformed to a strong and dense poly-crystalline product past heating in an apt temperature (lower than melting point of the grains). Sintering process is a whole lot an intricate process where grain development, modification of the pore contour and size takes place by evaporating the gaseous materials of the samples which is accompanied by purging of inter granular voids (pores) which lead to contraction of the whole system. There is also shrinking in volume fraction which may be due to crystalline development and reorganization of the grains in the powder. The grains become more closely packed. Subsequently, pores are wholly eradicated by the advance of grain centres and enlarge in the region of contact linking the grains owing to mass transportation of the grain contact en route for the pores. The binder gets scorched all through the whole process.

- **Electroding**

To analyse the electrical properties of the sintered samples, the samples are being electrode by means of some apposite conducting materials such as Silver, Gold, Platinum, Graphite paste etc. The paste should stick to the sample and ought to have nearly zero contact resistance. It should be pasted in a thin film/layer. It should be noted that between the flat faces pellet and electrode, there should not be any fissure or else this gap would have an effect on the electrical properties. That's why; the sintered pellets should be polished at first with fine emery paper to craft the both sides of the faces parallel and flat. In our present work we are using conducting silver paste of high purity for electroding.

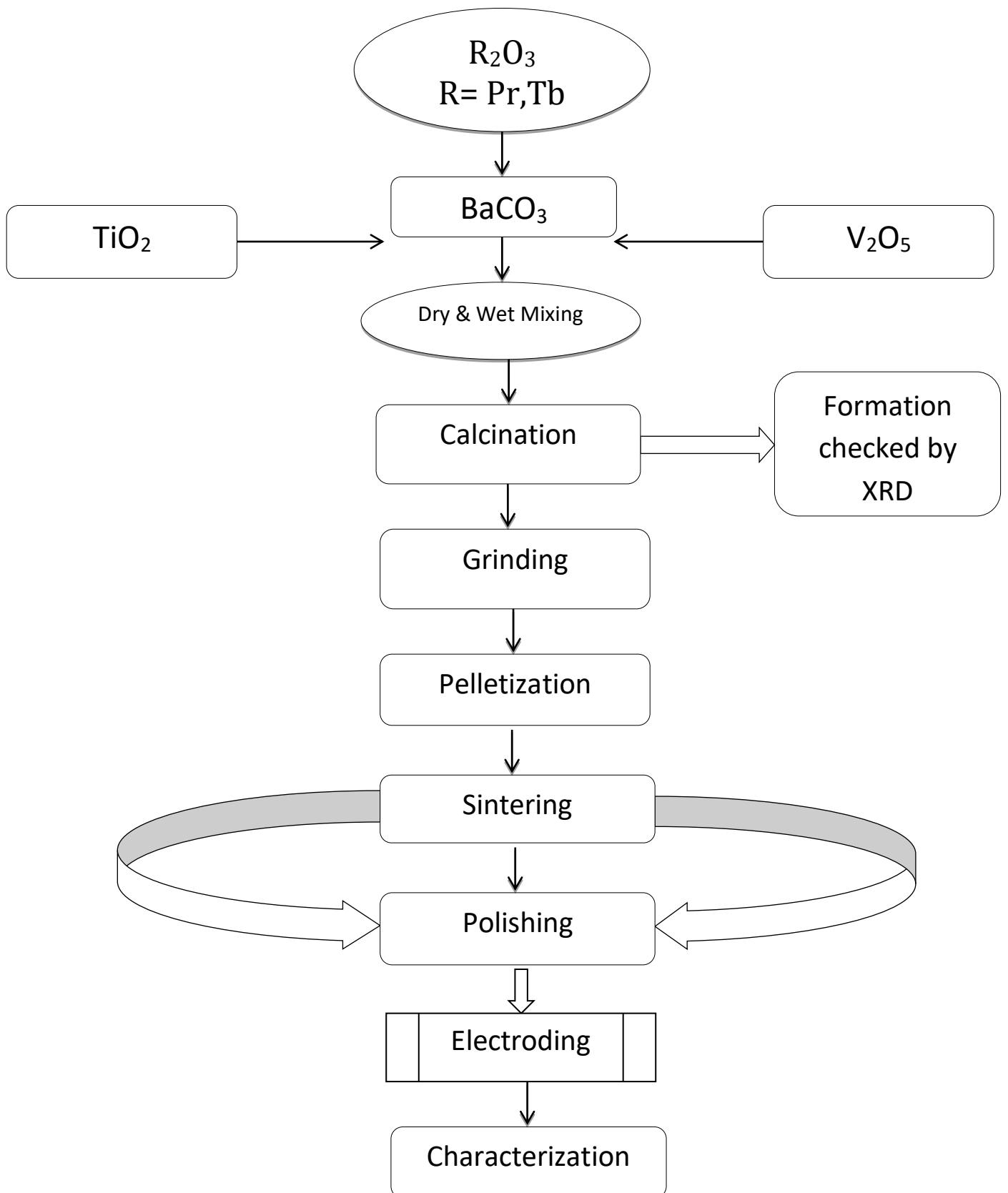
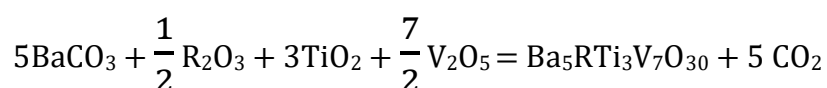


Figure 2.1 Flow chart for the ceramics samples preparation using solid-state reaction technique.

2.2.4. Preparation of the compounds

In our current research we are employing high temperature solid state reaction techniques for the production of ceramic samples using primarily the component materials of oxides and carbonates as reagents. The flow chart of solid state reaction (i.e. mixed oxide method) is shown in Fig 2.1

Polycrystalline samples of $\text{Ba}_5\text{TbTi}_3\text{V}_7\text{O}_{30}$ and $\text{Ba}_5\text{PrTi}_3\text{V}_7\text{O}_{30}$ were prepared using high temperature Solid-state reaction technique using high purity ($\geq 99.9\%$) oxides and carbonates raw materials; BaCO_3 , Pr_2O_3 , Tb_2O_3 , TiO_2 , V_2O_5 (all from Loba Chemie). The essential weight of the individual components required for synthesis of the considered necessary compounds is calculated from the reaction equation given below:



Where R = Tb, Pr.

The constituent compounds are weighed in electronic balance maintaining an appropriate Stoichiometric ratio and homogeneity. These components are mixed and thoroughly grinded in agate mortar for about 8-9 hours in wet medium by adding methyl acetate for uniform mixing. The wet mixture is let dry by slow evaporation. The thoroughly ground dry powder is then calcined in an alumina crucible boat and the formation of the compound is confirmed by the XRD profile of the fine powder of the sample. The grinding and calcination process is repeated several times with time and temperature for calcination is selected after optimizing parameters. The development of the desired compound is established at 1023 K heating for 12 hours. The obtained powder after the calcination contains pebbles, and for this reason it is crushed again using agate mortar and pestle for 5 hours by mixing with PVB as binder (to lessen the brittleness). The powder is then die pressed with hydraulic press to compress the powder into cylindrical pellets form having size 10 mm width and 1-2 mm depth by applying a uniaxial pressure of about ~ 7 tons. Finally, the cold pressed pellet is being sintered at 1073 K for 12 hours. The binder solution gets burned out on the process of the high temperature sintering process. The sample is then let cooled to room

temperature within the furnace. A course of action is being adopted for the preparation of the composite discussed later.

Preparation of BiFeO₃

Fe₂O₃ and Bi₂O₃ (both from Loba chemie having purity ($\geq 99.9\%$) oxides) are varied in a ratio maintaining stoichiometric and calcined at 973 K for 4 h to form BiFeO₃.

Preparation of Solid Solution (1-x)Ba₅RTi₃V₇O₃₀-xBiFeO₃

The calcined powder of BiFeO₃ and Ba₅RTi₃V₇O₃₀ are mixed at different proportions. In the composition as a binder a small quantity of polyvinyl butyral (PVB) is added then it is die pressed by hydraulic pressure at pressure of about ~7 tons to a pallet form having size of about ~10 mm in width and thickness of about ~2 mm. Then the pallet is sintered at 1073 K for 6 h followed by cooling at 2 °C/min. The sintered powder is used to make magnetic measurement and also the pallet is painted with silver paste on plane surface for making it conducting. The silver paste is dried for 5-10 min at 100-150°C and then fired at 700-875 °C for 5-10 min then the electrical analysis is done using impedance analyser.

2.3. Section-II: CHARACTERISATION

2.3.1. Introduction

The probable applications of the particular material can be predicted by knowing the range of physical properties of the solid such as mechanical, thermal, electrical, structural, magnetic etc. in variable circumstances. The characterization is an essential aspect of ceramic technology. Different techniques are employed to characterise the properties and mechanism of the materials. The technique used in current examination is given in the subsequent sections:

2.3.2 Structural Characterisation

The properties of material are extremely sensitive to the structure. Structure is dependent on composition, heat treatment, and dispensation. As a consequence it is

essential to differentiate both microstructure and composition at the utmost levels of resolution achievable so as to comprehend material behaviour, and to assist in the creation of novel or better materials. Such categorizations involve sophisticated equipment based on microscope, spectrographic and diffraction techniques.

2.3.2. (a) X-ray Diffraction Study (XRD)

It is essential to identify the ceramic materials in order to describe the characteristics of the composition and structure (including defect) of the synthesized materials. The X-ray diffraction technique [14] could be used for identifying the existence of different crystalline phases in the synthesized materials and it can also distinguish secondary phases, if they exist. It is also used to find out the lattice parameters and particle size.

The XRD pattern is extensively used since the interplanar d-spacing of diffraction patterns have order of X-ray wavelength. When the crystal is made up of tiny fragments, then it is known as polycrystalline materials. Despite the fact that the x-ray technique is used for single crystal specimens, it is also reasonably effective with polycrystalline specimens as well. X-ray on interaction with a crystal gives the maximum diffraction in accordance with Bragg equation; $2d\sin\theta = n\lambda$. The precise determination of interplanar spacing (d), lattice parameters, etc. is vital. In the midst of several X-ray experimental techniques, X-ray powder diffraction technique is among the simple one to provide structural information. Details of the XRD profile is described later in chapter-III.

Factors' which affects intensity of X-ray diffraction lines

Factors which control the intensities of X-ray diffraction lines are:

- (i) Polarization of X-rays,
- (ii) Temperature,
- (iii) Structure factor,
- (iv) Scanning rate,
- (v) Instrumentation limitations,
- (vi) Sensitiveness, etc.

The intensity of the ray beam diffracted from a crystal depends on the distribution, category and number of the unit cell atoms. To determine the intensity of a particular reflection and the relative intensities of various reflections, the contribution of the

entire atoms in the unit cell to the scattered amplitude of x-rays in a particular direction has to be taken into account. The relative x-ray intensities is given by

$$I = IFJ^2 \frac{(1+\cos^2\theta)}{\sin^2\theta\cos\theta} e^{-2M}, \text{ Where}$$

$$\frac{(1+\cos^2\theta)}{\sin^2\theta\cos\theta} = \text{Lorentz-polarization factor,}$$

$$e^{-2M} = \text{temperature factor,}$$

F = Structural factor and

J = Scale factor.

(a) Polarization factor :

Unpolarized rays of x-ray when scattered from electrons, get polarized. The Extent of polarization is a function of the scattered beam angle. The angle of scatter determines the intensity of scattered beam and is given by the equation:

$$I = I_o \frac{k}{r^2} \frac{(1+\cos^2\theta)}{2}, \text{ Where}$$

I_o = Intensity of the incident beam and k is a constant

$$\frac{(1+\cos^2\theta)}{2} = \text{Polarization factor (P).}$$

(b) Lorentz-Polarization

In the path of x-ray when the single crystal is rotated, diverse planes are in succession accessible to the beam at their Bragg angles θ , in order that they reflect. The rate of the passing of the plane through Bragg condition is dependent on θ . Which leads to addition of a Lorentz factor (L_p), which is an expression of intensity for each individual reflection.

$$L_p = \frac{(1+\cos^2\theta)}{\sin^2\theta\cos\theta}$$

It has a minimum value at 45° and maximum value when θ move towards 0° and 90° . This factor is prominent in low and high angles. In the present work, in profile line analysis the effect of the stated factor is slight and doesn't change noticeably over the line profile.

(c) Structure factor:

The modulus of structure, $|F|$ is related to intensity I^2 , by the relation: $|F| \propto I^2$. In theory, if the position of the atoms (i.e. x, y, z) in the unit cell is identified then:

$$F(hkl) = \sum_{j=1}^N f_j \exp 2\pi(hx_j + ky_j + lz_j),$$

Where x_j, y_j and z_j are the fractional atomic coordinates and f_j is the atomic scattering factor for the j^{th} atom in the unit cell, N is the total number of atoms in the unit cell and F is a complex number whose absolute value is defined as:

$$|F| = \frac{\text{amplitude of the wave scattered by all atoms of an unit cell}}{\text{amplitude of the wave scattered by an electron at origin}}$$

Structure factor is the materialization of the character of the component atoms and their arrangements in the unit cell.

(d) Scale factor:

The intensity of a line from a single plane is enhanced by the superposition of reflected beams. This amplified intensity, a factor J , is called scale factor is initiated to determine the comparative intensity. In X-ray powder diffraction technique, J depends on the symmetry of the crystalline matter.

(e) Temperature factor:

Crystal is a collection of atoms, positioned at a set position in the lattice. Even at absolute zero temperature atoms will have certain thermal vibration and when the temperature is increased the amplitude of the mean position of vibration also increases. Increase in thermal vibration has three major effects:

- The expansion of unit cell causes changes in the interplanar spacing d and for this reason 2θ positions of the diffraction lines.
- Decrease in an intensity of the diffraction line

- Increase in the intensity of the background scattering between lines. It is included as negative exponential of temperature.

(f) Instrumental factors:

The instrumental factors which persuade the enlargement of the profile are:

- Profile of X-ray source
- Beam Divergence
- Beam absorption by sample
- Receiving slits width
- Apparatus misalignment

The following structures parameters could be determined by XRD techniques

- Feature and conformation of the samples
- Reflection Intensities
- Crystallite size
- Interplanar d-spacing
- Unit cell dimensions and crystal system

With the structural information, XRD study also presents information as regards essential conditions for ferroelectricity (i.e. lack of centre of symmetry)[15,16].

2.3.2. (b) Scanning electron microscope (SEM)

This is a class of microscopes in which instead of visible light, electrons are rather used to generate magnified images, in particular to detect the objects having magnitudes smaller than the visible light wavelengths, the linear magnification may go beyond million (10^6) times. An image of a three dimension is formed on a cathode ray tube by moving a beam of focused electrons across an object and evaluating both the scattered electrons of the object and the secondary electrons formed from it. It creates an image by bombarding the crystal with a beam of electrons having high energy. The reflected electrons are then scanned to outline a magnified image which lets the assessment of the structure and morphology of crystals.

It is extensively used in material research. The advantage of SEM is that the focus is of large depth and there is no constraint in size and shape of the bulk crystal. The art of sintering has been considerably benefited by the utilisation of SEM. Incomplete sintered bodies are categorized by asymmetrical and an intricate surface, which necessitate depth visual interpretation about the field. SEM is able to produce the image of the particle/object with three-dimensional manifestation. It creates micrographs by scanning the plane of the crystal with an electron probe. The primary units of SEM are:

- i. Optical-electronic columns together with suitable electronics.
- ii. Vacuum system, with the specimen chamber and stages
- iii. Signal display and detection systems[17]

The electron column includes magnetic lenses whose role is to focus the beam of the electron. SEM contains sets of two scanning coils. The scanning coils are attached to the proper scan generator which deflects the beam over the surface of the specimen to form a pattern of like raster. The chamber for specimens is deliberated in such a way that specimens could be adjusted in any desired direction. A range of movement such as tilting, translation and rotation of the sample could be performed inside the chamber.

The systems used for detection in SEM depend on how the primary electron beam interacts with the specimen and also to some extent on the others like current of back or reflected scattered electron, secondary electron emission, cathode luminance, X-ray production, etc. Signals after detection are amplified then used for controlling the cathode ray tube (CRT) brightness. Scan generators establish the position of an electron beam by controlling the deflection of the electron beam in CRT. Hence, SEM is a great tool for scanning surface point to point of the micro-region such as grains and grains boundaries.

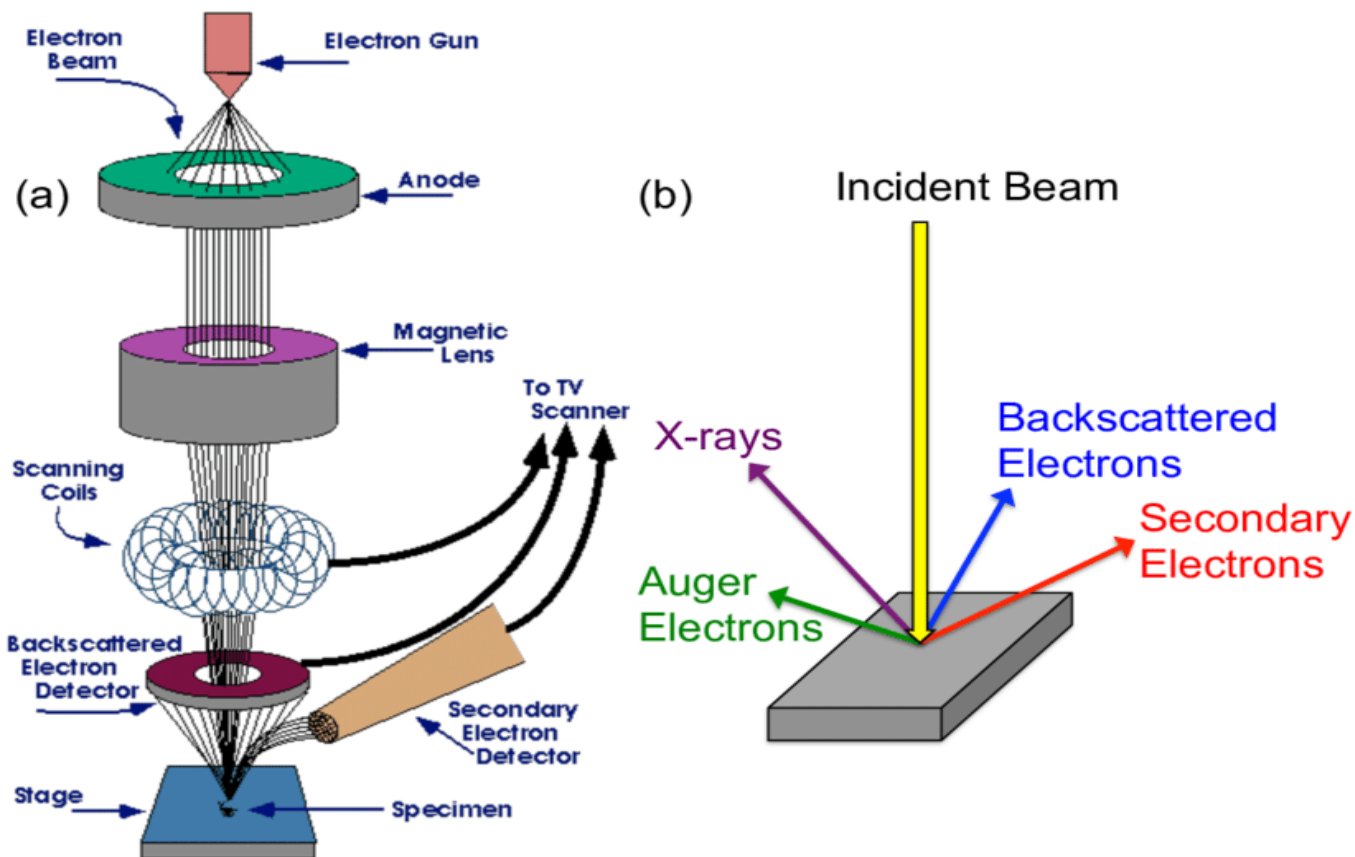


Fig.2.2(a) Schematic diagram of SEM

Fig2.2(b) Schematic diagram of SEM setup

In the present investigation, samples for microscopic study are prepared as follows:

- The surface of the cylindrical pellets was polished with the help of fine emery paper.
- Gold coating (thickness $\sim 40 \text{ \AA}$) was done on polished faces using sputtering technique.
- The micrographs of the samples of different magnifications have been taken using JEOL-IT300 Scanning Electron Microscope.
- Size of the grain is calculated by measuring the size of around 100 grains from different regions and taking the root mean square.

JOEL-IT300 SEM is a resourceful electron microscope having a magnetic deflection field just over the microscope objective. The final reducing lens lets the electron scan the plane of the surface of the object via two mutually perpendicular directions. The secondary electrons reflected by the surface represent the signal current. They are

collected by an electrode and amplified which modulates the viewing tube brightness, the screen of which is scanned by synchronizing with the sample. The image magnification is the ratio of the scanning region on the screen to that of the selected region of the sample. The contrast of the image is varied according to the composition and shape of the sample.

The main specifications of the instrument that are used in the current analysis are:

- Resolution : HV mode: 3.0 nm
LV mode: 4.0 nm
- Magnification: $\times 5 \sim \times 300,000$
- Accelerating voltage: 0.3kV to 30kV
- Specimen stage: 5-axis motor stage
X: 1.25cm Y: 1.00cm
Z: 0.5 to 0.80 cm
Tilt:- 10 to 90°
Rotation: 360° endless
- Maximum sample diameter: 200mm.

Detailed explanation of how a typical SEM works is schematically represented in Fig. 2.2(a,b)

2.3.3 Dielectric study:

The study of dielectric properties of materials is becoming very important in the present world as it plays a significant role in communication and electronic technology. To check the suitability in the device appliances such as in computer display and memory, microwave communication, IR sensors, etc., over a broad range of temperature, frequency and composition, the call for detail study of dielectric properties is becoming more pertinent. The ceramic dielectrics have core appliances as an electrical insulator and as capacitors in electronic circuits. It has essential characteristics such as; dielectric constant, tangent loss and dielectric strength, which is relevant in the application purpose.

Ceramics have many advantages like; enhanced electrical properties, deformation deficiency under stress, and larger resistance to any environmental changes.

Broadly the polarizations can be divided into three types based on their intrinsic physical mechanism and they are; orientational, electronic, and ionic. If the insulator is positioned in the vicinity of an external applied electric field, the cloud of electrons of the atom get slightly displaced with respect to the position of nuclei, because of which there is a development of an induced dipole moments which causes an electronic polarization. When the atoms in the molecule don't share their electrons equally, the electron cloud gets displaced in the direction of the stronger binding force, resulting in ions acquiring opposite polarity charges. The development of net charge modifies the position of equilibrium by causing displacement of ions or ions resulting in induced dipole moment, which represent the ionic polarization. On application of an external electric field the dipoles will experience a torque, which try to incline them along the direction of an external electric field. The existence of such polarization due to torque force is called an orientation polarization. The presence of three types of polarization mechanisms is due to the existence of charges which are locally bound to the atoms, molecules or to structure of the crystals. Apart from it, there are charge carriers which migrate certain space from side to side in dielectric. Usually, such carriers are impeding in motion for they are ensnared in the interface of the materials. Since, they cannot liberally discharge at the electrodes which results in space charges. The distortion emerges as an enlargement in the capacitance of the material and should be differentiated from that of the increase in dielectric constant. Such type of polarization is known as interfacial or space charge polarization. The total polarization is the sum of all the four discussed polarization [18]. In case of ionic and electronic polarizations, the consequence of frequency is negligible upto 10^6 Hz. In the optical range of frequency, electronic contribution is the sole contributor and the effect of temperature is negligible for both ionic and electronic polarization. However, at high temperatures due to presence of imperfect crystal and ionic mobility, the polarization increases. The combined effect of dipole and space charge effects produces sharp rise in the dielectric constant at high temperature. In dielectric material in an external alternating electric field there is a phase shift of temporary nature between the resulting polarization and the driving fields. Due to which there is a loss in current component, which results in an

increase in dielectric loss. The polarization \mathbf{P} changes cyclically with electric displacement \mathbf{D} also with time as well. Generally, \mathbf{P} and \mathbf{D} lag in phase with relative to the electric field \mathbf{E} , such that:

$$\mathbf{D} = D_0 \cos(\omega t - \delta) = \mathbf{D}_1 \cos(\omega t) + \mathbf{D}_2 \sin(\omega t)$$

Where δ is phase angle having a value little less than 90°

$$\mathbf{D}_1 = D_0 \cos(\delta) \text{ and } \mathbf{D}_2 = D_0 \sin(\delta)$$

The ratio of displacement vector to that of an electric field (D_0/E_0) is usually frequency dependent. To illustrate, thus establish two-frequency dependent dielectric constant:

$$\varepsilon'(\omega) = (D_0/E_0) \cos(\delta)$$

$$\varepsilon''(\omega) = (D_0/E_0) \sin(\delta)$$

Where $\varepsilon'(\omega)$ and $\varepsilon''(\omega)$ are real and imaginary complex dielectric constants respectively. The two dielectric constants can be expressed in terms of single complex dielectric constant such that:

$$\varepsilon = \varepsilon' - j\varepsilon''.$$

The applied voltage (V) varies at regular intervals with time as:

$$V = V_0 e^{j\omega t}$$

Then the total current can be expressed as,

$$I = \frac{dQ}{dt} = \frac{d(CV)}{dt} = jC\omega V = j\varepsilon C_0 \omega V$$

Where C and C_0 are the value of capacitance for the dielectric in medium and vacuum, respectively.

Therefore, $I = jC_0 \omega V (\varepsilon' - j\varepsilon'') = C_0 \varepsilon'' \omega V + jC_0 \varepsilon' \omega V = I_l + I_c$

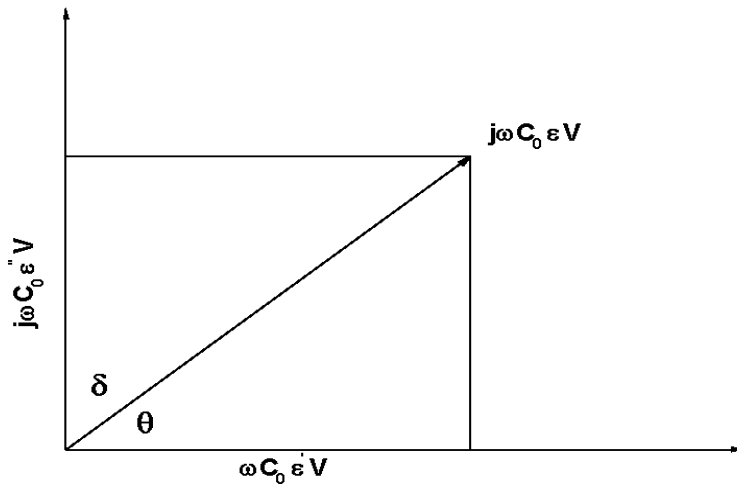


Fig. 2.3 Vector resolution of ac current of a capacitor

The dielectric or tangent loss is given as

$$\tan \delta = \frac{I_l}{I_c} = \frac{\epsilon''}{\epsilon'}$$

The current I passing in the capacitor could be resolved into two components i.e. conduction current (I_c) which is in phase with the voltage and charging current (I_l) which is in quadrature with voltage. For a parallel plate capacitor, the vector resolution of sinusoidal current is shown in Fig. 2.3, the charging current is specified as $I_c = jC_0\omega\epsilon'V$ and the loss current is given by $I_l = jC_0\omega\epsilon''V = \sigma V$, where $\sigma = \omega\epsilon\epsilon_0 \tan \delta$ is the dielectric conductivity. How an effective conductivity is defined is dependent on frequency and is for all time larger than that of dc conductivity. For the efficacy of a dielectric as an insulator material the loss factor is one of the key criterions. Applications in which high capacitance material is required, materials having high dielectric constant value and low dielectric loss ($\tan \delta$) should be used. The ferroelectrics' dielectric properties depend on the field strength at which it is measured; it is due to non-linear relation between electric field and polarization. Above the transition temperature the dielectric constant obeys Curie-Weiss law. Further, based on the thermodynamic model of ferroelectric ceramics by Yurkevich and Rolov [19], the following various special characteristics of TB-structural type of dielectrics can be drawn:

- In the transition region, the dielectric constant does not change sharply but shows a diffusive type (broad peak) over a wide range of temperature.
- The temperature at which the maximum dielectric constant is achieved strongly depends on the size of the grain of the materials.

Studies of the electrical properties as function and temperature provide valuable information as regards the existence of ferroelectricity and nature of phase transition.

Measurements of dielectric constant and loss

In the current investigation the dielectric analysis has been carried out using impedance analyser HIOKI- IM3536 with indigenously developed two terminal sample holders (Fig2.4 a,b). The system facilitates studies in the frequency range from 4Hz to 8MHz. The value of any four of the fourteen test parameters like capacitance (C), phase angle (θ), impedance (Z), dissipation factor or dielectric loss (D or $\tan \delta$), inductance (L), admittance (Y), conductance (G), etc. can be measured simultaneously at any frequency within the admissible range using the instruments.



Fig. 2.4(a) High Temp Furnace with Sample Holder



Fig. 2.4(b) HIOKI-IM3536

To study the temperature effect on the sample, the silver electrode pellet has been kept in between the two electrodes of the sample holder. Once the capacitance of the cell is known at any temperature, the dielectric constant at that temperature is calculated using the relation:

$$\epsilon = \frac{C}{C_0}, \text{ where } C \text{ is sample capacitance}$$

$$C_0 = \frac{\epsilon_0 A}{t} \text{ geometrical capacitance}$$

$$\epsilon_0 = 8.854 \times 10^{-14} \text{ f/cm, permittivity for free space}$$

$$A = \text{Area of the flat surface}$$

$$t = \text{thickness of the pellet}$$

2.3.4. AC conductivity study

On application of an alternating emf, V across the capacitor, an alternating current I flows having value; $I = j\omega\epsilon C_0V$, given that the dielectric is an ideal one [20]. However, an in- phase current appears which corresponds to resistive current in between the condenser plate. The current is owing to the dielectric medium and it's the

characteristic of it. The ac conductivity or dielectric conductivity can be figured out from the real component of density current passing through it. The activation energy (E_a) and ac conductivity (σ_{ac}) of the specimen in paraelectric phase (at high temperature) can be calculated using Arrhenius equation:

$$\sigma_{ac} = \omega \epsilon \epsilon_0 \tan \delta = \sigma_0 \exp\left(\frac{-E_a}{k_B T}\right), \text{ where}$$

ϵ_0 = the dielectric at vacuum

ω = the angular frequency and

k_B = the Boltzmann constant

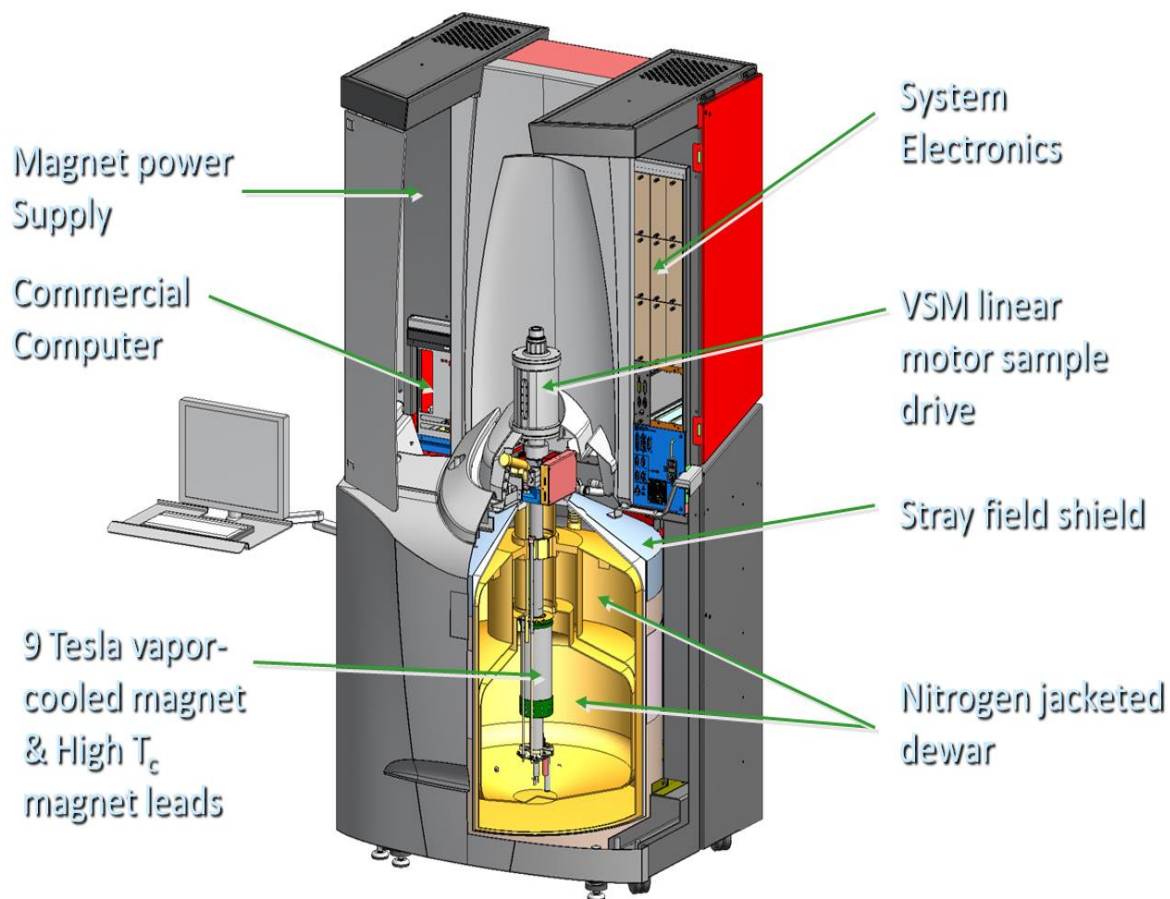


Figure 2.5 Block diagram of PPMS SQUID VSM system

2.3.5. Magnetization study using Vibrating Sample Magnetometer (VSM)

Vibrating Sample Magnetometer (VSM) is used to measure the magnetic behaviour of magnetic materials. It works on the principle of Faraday's law of induction i.e. change in magnetic field can generate an electric field. By measuring electric fields one can get information vis-à-vis magnetic fields. Sample placed in an external uniform magnetic field undergoes periodic motion (i.e. vibrate mechanically) which results into change in magnetic flux thus inducing a voltage or emf in the pick-up coils. The induced current is directly proportional to the magnetic moment in the specimen.

In our current research we are measuring the magnetic properties using a Physical Property Measurement System (PPMS: Quantum Design, San Diego, USA) VSM. The block diagram of a typical PPMS SQUID VSM setup is shown in Fig. 2.5. In VSM, specimens are placed in an external constant magnetic field. If the specimen is magnetic in nature then external constant magnetic fields magnetize the specimen by aligning the individual magnetic spins, or magnetic domains, along the direction of the field. When the intensity of the external constant magnetic field is high, then, magnetization will also be high. The dipole magnetic moment of the sample creates a magnetic field in the region of sample (also called as the magnetic stray field). While the sample vibrates the magnetic stray field also varies as a function of time and which is sensed by a set of pickup coils. According to Faraday's law of induction an alternating magnetic field will result in an electric field in the pick-up coils. This current is in proportion to the magnetization of the sample. Higher magnetization induces higher current in the sample.

The induce current is amplified by a lock-in amplifier. Computer interface is hooked by various components. Controlling and monitoring software gives the information regarding magnetization value and how the strength of magnetization is dependent on the external constant magnetic field. A characteristic measurement is done in subsequent steps:

- a. Set the external constant magnetic field strength.
- b. The sample is vibrated.
- c. The signal received from the probe is translated to the magnetic moment value.

- d. A new value is set to an external constant magnetic field. Data is not recorded in transition
- e. The constant magnetic field strength is set to a new value
- f. The probe signal is once more is converted into magnetization value of the specimen
- g. The external uniform magnetic field is varied and a plot of magnetization (M) versus magnetic field strength (H) curve is created.

The main specification of Magnetometry is:

- DC Magnetometry
- Torque Magnetometry SQUID Sensitivity, Small, anisotropic sample
- VSM: 2 - 400 K Oven
- Ultra-Low Field Capability

The main advantages of the Magnetometry are:

- It has inventive design to control temperature and cool the samples from RT to a stable 2 K in ~30 minutes
- It has capability to continuously and quickly incline field, acquire data and stabilize up to ± 9 T

CHAPTER III
STRUCTURAL AND MICROSTRURAL ANALYSIS

3.1 Introduction

Crystal structure analysis of materials is an essential tool of characterization. For molecular substances, identification is done by a combination of chemical analysis and spectroscopic methods. However, for crystalline and non-molecular substances, identification is done by X-ray diffraction method and supplement, facilitated by chemical study if possible. Crystalline solid has 'fingerprint' i.e. has distinctive X-ray diffraction pattern. By comparing the powder pattern of an unknown crystal with the obtained pattern of a known crystal, it is possible to identify an unknown sample. After identification, the structure of the crystal can be determined. For molecular material, further details for crystal structure can be obtained from spectroscopic measurement. Alternatively, for crystalline samples, X-ray crystallography is used for obtaining information about the way the molecules are packed together in the crystalline structure. Thus, identification and structural determination [1-3] completes the representation.

3.2 Structural study

A physical property of solid depends on the atomic arrangement in them. Solids can either exist as single crystal, polycrystalline or amorphous form. Polycrystalline material is a collection of a number of tiny single crystals known as grains and they are separated by the areas of disorder termed as grain boundaries. The distribution of grain along with shape, size, arrangement of grains together with the presence of porosity, different phases etc are called microstructure. Most of the physical properties are dependent on the microstructure. Therefore, study of microstructures' becomes an indispensable part for characterisation of the material. The information of chemical analysis of solid, atomic arrangement, particle size, stress factor and phase equilibrium is provided by structural characterization. It is vital to prepare material of single-phase; else the properties of one phase may be dissimilar from the other. So one must have an idea about the lowest temperature at which a single-phase compound might form. There are numerous techniques for characterisation of the crystal structure, but in our current work, preliminary structure (i.e., basic crystal system, particle size, lattice

parameters, etc.) and microstructural information of the compounds are obtained by the mentioned below experimental techniques:

- X-ray Powder Diffraction
- Scanning Electron Microscopy

3.2.1 X-ray Powder Diffraction

X-ray diffraction method is a powerful technique to not only study a single crystal but also be supportive in classifying the polycrystalline materials and thick/thin films. Earlier, XRD (X-Ray diffraction) technique was only applicable for single crystals for classification of materials and the study of their preliminary structure. The discovery of powder method by Debye and Scherrer has simplicity and advantages over X-ray diffraction method that it can be used for crystalline mixture. In the mixture each component produces a characteristic pattern independent of the others. It became feasible to classify the particular component from the observed XRD outline and estimate its fraction in the compound. The randomness of crystalline orientation in polycrystalline structure allows a portion of the material to be properly oriented with respect to the incident beam requisite to produce maximum diffraction pattern. For determining the inter-atomic spacing from the observed diffraction angle a monochromatic radiation is used. The ferroelectric materials from the structural point of view should have non-centro structure and space groups in the ferroelectric phase. Therefore, it becomes central to find the basic crystal structure and space group symmetry of the material in ferroelectric phase as well as in paraelectric phase. It is not easy to acquire the entire and precise information about the crystal structure but still the preliminary structure information can be obtained.

3.2.1.1 Experimental

In the present study X-ray powder diffractometer (Rigaku, Miniflex, Japan) is used to obtain the X-ray diffraction (XRD) pattern of the set specimen by mounting the specimen at the centre of diffractometer and rotating the angle θ around the axis in the specimen plane at 303K (Room Temperature) with X-ray source as $\text{CuK}\alpha$ radiation ($\lambda = 1.5405 \text{ \AA}$) at scan rate of $3^\circ/\text{minute}$ in broad range of Bragg angle 2θ ($20^\circ \leq 2\theta \leq 80^\circ$). The focusing circle diameter gets continuously lesser with increase in diffraction angle.

Only (hkl) planes which are parallel to the specimen plane contribute to the diffraction patterns of corresponding d -values (interplanar pairs) are compared. The diffractogram analysis is not only useful for structural determination but also in chemical analysis, stress management, phase equilibrium study, determination of particle size, etc. According to Klug and Alexander [4], crystalline size is of immense significance in X-ray analysis. They pointed out that the size of crystallite size must fall within the acceptable range or limit so that a smooth and sharp diffraction pattern could be obtained. If the coarsest portion of powder is less than $5\mu\text{m}$, the mean deviation of intensity is 1.2%, and if the coarsest portions range from 15 to $50\mu\text{m}$ then the mean deviation of intensity is around 18%. If the crystalline size does not exceed $5\mu\text{m}$, then the particle orientation effect and micro-absorption could be neglected. In our present work, the powders for X-ray analysis were 2- $5\mu\text{m}$, which were prepared by grinding the ceramic powder in an agate mortar and pestle. Using free fall technique as illustrated by NBS monograph [5] the powder is uniformly packed in a slotted-glass slide in order to evade favoured orientation and induced packing. The powder ought to be mounted in such a way that no alien substance is exposed to the X-ray beam. The operating current and voltage for the X-ray tube is 20mA and 40kV respectively. The Ar-filled proportional counter is fixed to the arm turning around an axis by an angle 2θ (twice as large as that of specimen rotation). The variance of X-ray tube is restricted to $3-5^\circ$ along the vertical direction. Soller slits are employed to craft the radiation monochromatic. The accuracy and calibration is checked with the aid of a standard powder sample before recording the intensity profiles (distribution). Diffraction pattern is made in a wide range of 2θ ($+20 \rightarrow 80^\circ$) with a continuous chart recording. After preliminary run, the line profiles are obtained by point counting of the small interval in 2θ . At the background and tail of the intensity distribution (where the counting rate is slow), counts are made high at every setting to maintain statistical fluctuations less than 1% all through the experiment.

3.2.1.2 . Calculation

XRD obtained is the diffraction/reflection of the X-ray beam from the family of parallel atomic planes with identical inter-planar spacing d obeying Bragg's law i.e. $2d\sin\theta = n\lambda$; where λ is the wavelength of the X-ray incident on the lattice planes having an angle θ . Profile of X-ray diffraction is used for establishing the atomic arrangement of the

structure of the sample, since the d of the diffraction planes is of X-ray wavelength order. The exact determination of d presents an imperative basis in appreciating the different properties of samples.

- 1) XRD profile is the distinctive of the material.
- 2) Each one of the stuffs in a mixture fabricates its own pattern independently.
- 3) It is proficient to provide qualitative and quantitative investigation of the substance.
- 4) It illustrates the condition of chemical arrangement of elements in the samples.

The d spacing of a particular plane can be calculated by using general formula [6] in terms of a, b, c, α , β , γ as lattice parameters and h, k, l as the Miller indices:

$$\frac{1}{d_{hkl}^2} = \frac{1}{V^2} [h^2b^2c^2\sin^2\alpha + k^2c^2a^2\sin^2\beta + l^2a^2b^2\sin^2\alpha + 2abc\{kla(\cos\beta\cos\gamma - \cos\alpha) + hlb(\cos\alpha\cos\gamma - \cos\beta) + khc(\cos\alpha\cos\beta - \cos\gamma)\}]$$

Where, V = volume of the unit cell

$$= abc (1 - \cos^2\alpha - \cos^2\beta - \cos^2\gamma + \cos\alpha\cos\beta\cos\gamma)^{1/2}$$

Crystal geometry equations for XRD Symmetry:

Cubic: $\frac{1}{d^2} = \frac{h^2+k^2+l^2}{a^2}$

Tetragonal: $\frac{1}{d^2} = \frac{h^2+k^2}{a^2} + \frac{l^2}{c^2}$

Hexagonal: $\frac{1}{d^2} = \frac{4}{3} \left(\frac{h^2+hk+k^2}{a^2} \right) + \frac{l^2}{c^2}$

Rhombohedral: $\frac{1}{d^2} = \frac{(h^2+k^2+l^2)\sin^2\alpha + 2(hk+kl+hl)(\cos^2\alpha - \cos\alpha)}{a^2(1-3\cos^2\alpha+2\cos^3\alpha)}$

Orthorhombic: $\frac{1}{d^2} = \frac{h^2}{a^2} + \frac{k^2}{b^2} + \frac{l^2}{c^2}$

Monoclinic:
$$\frac{1}{d^2} = \frac{1}{\sin^2\beta} \left(\frac{h^2}{a^2} + \frac{k^2 \sin^2\beta}{b^2} + \frac{l^2}{c^2} - \frac{2hlc\cos\beta}{ac} \right)$$

Triclinic:
$$\frac{1}{d^2} = \frac{1}{V^2} (S_{11}h^2 + S_{22}k^2 + S_{33}l^2 + 2S_{12}hk + 2S_{23}kl + 2S_{13}hl)$$

Where
$$S_{11} = b^2c^2\sin^2\alpha; S_{22} = a^2c^2\sin^2\beta; S_{33} = a^2b^2\sin^2\gamma$$

Unit cell Volume Symmetry:

Cubic:
$$V = a^3$$

Tetragonal:
$$V = a^2c$$

Hexagonal:
$$V = \frac{\sqrt{3}a^2c}{2}$$

Rhombohedral:
$$V = a^3\sqrt{1 - 3\cos^2\alpha + 2\cos^3\beta}$$

Orthorhombic:
$$V = abc$$

Monoclinic:
$$V = abc \sin\beta$$

Triclinic:
$$V = abc\sqrt{1 - \cos^2\alpha - \cos^2\beta - \cos^2\gamma + 2\cos\alpha\cos\beta\cos\gamma}$$

Above formula could be used for finding the lattice parameters for all the compositions. In the current case, calcined powder is categorized with respect to lattice parameter measurement, phase identification, etc. using CuK_α sourced XRD. For quantitative evaluation of phases, calcined powder is homogeneously mixed and ensuing mixture is analysed. The relative weight fraction is calculated from the ratio of peak areas. The phase which gives the maximum peak area at a given temperature is considered as the formation of complete phase at that particular temperature.

The powder profile is a feature of a material. It is the simplest interpretation for identification of pattern by evaluating it with the pattern of the standard material. Polycrystalline samples which consists of adequately large and strain free crystallites have a sharp line powder pattern but in practise such sharp lines are never observed for the reason that of the collective cause of numeral of physical and instrumental factors which widen the pure diffraction peaks.

The sharpness and broadening of profile are characterised by distribution of crystallite, crystallite size, and partial imperfection widespread in the crystal lattice. Considerably amount of experimental and theoretical works are being done on powder profile to determine the lattice strain and crystallite size. Theories proposed by Warren-Averbach [7], Wilson [8], and Scherrer [9] are among the most useful in our case. The Scherrer equation is used for calculating the apparent or mean effective crystallite dimensions P for a particular reflection (hkl)

$$P_{hkl} = \frac{k\lambda}{\beta_{1/2} \cos\theta}, \text{ where } k=0.89, \lambda = 1.5405 \text{ \AA}, \beta_{1/2} = \text{half width of peak (in radians)}.$$

Using powder profile, θ is measured from main peaks and the d values (inter-planar spacing) are analysed by the given formula

$$d_{\text{obs}} = \frac{\lambda}{2\sin\theta}$$

These d values are used in computer programming using different options of crystal systems. Cell parameters (a,b,c), d calculated, and hkl values of the composites are acquired and appropriate crystal system is chosen on the basis of the finest agreement linking d_{obs} and d_{cal} . For matching the unit cell parameters least- square refinement method is utilised.

3.2.2. Results and discussion

XRD profile of the calcined group A and group B is given in Fig. 3.1 and Fig. 3.2 respectively. The reflected peaks are indexed and the lattice parameters are determined in a variety of configurations using X'pert highscore software. On the basis of the best agreement involving calculated (cal) and observed (obs), an interplanar distance d (i.e., $\Sigma\Delta d = \Sigma(d_{\text{obs}} - d_{\text{cal}}) = \text{minimum}$), an appropriate unit cell is selected. The lattice parameters (a , b , c , α , β , and γ) are estimated from the peaks positions in the diffractograms.

3.2.2. (a) Group A: $(1-x)\text{Ba}_5\text{TbTi}_3\text{V}_7\text{O}_{30} - x\text{BiFeO}_3$

From table 3.1, it can be seen that there is a structural change in the crystal system by change in value of x . It may be due to the reason that the two systems are of two different structural families. BiFeO_3 is a structure of rhombohedrally distorted perovskite and $\text{Ba}_5\text{TbTi}_3\text{V}_7\text{O}_{30}$ is of Tungsten Bronze structure. The TB structure has a complex range of distorted BO_6 octahedra which share corners of three diverse kinds of interstices (A, B and C) for cation substitutions having a common formula of $(A_1)_2(A_2)_4(C_4)(B_1)_2(B_2)_8\text{O}_{30}$. Cations of mono or divalent can be accommodated at A_1 and A_2 sites, cations of tri or pentavalent at octahedral sites B_1 and B_2 [10], whereas the smallest interstice i.e. C site generally remains vacant; thus the common formula for tungsten bronze structure is also $A_6B_{10}\text{O}_{30}$. A variety of cations substitution at the A and B sites changes the electrical properties of material significantly [11]. So it is quite expected that there is significant distortion in the oxygen octahedron of both the structures producing mechanical stress giving rise to a structural change. It has been found when $x=0$ i.e. in case of pure $\text{Ba}_5\text{TbTi}_3\text{V}_7\text{O}_{30}$ it is most symmetric i.e. in Orthorhombic structure. The composite is most distorted (monoclinic structure) when $x= 0.5$ i.e. when the content of BiFeO_3 is 50% in the solid solution. This structural change is also well reflected in the dielectric properties. For $x=1$, it can be seen that there is a occurrence of a little quantity of impurity or secondary phases in BiFeO_3 which may be because of loss of Bi_2O_3 during high-energy reaction due to its high-temperature processing or synthesis. The amount and formation of secondary phase could be prevented or minimized using either the adding excess bismuth oxide in BiFeO_3 or high-purity ingredients (Bi_2O_3 and Fe_2O_3) [12, 13]. There are additional peaks

for $x= 0.3, 0.5,$ and 0.7 which may be due to presence of BiFeO_3 resulting in additional XRD peaks belonging to another phase. The secondary phase may be tungsten bronze phase corresponding to $\text{Ba}_5\text{TbTi}_3\text{V}_7\text{O}_{30}$ or solid solution formed with some Bi and/or Fe ions. The XRD result confirms the presence of composite structure of the prepared samples.

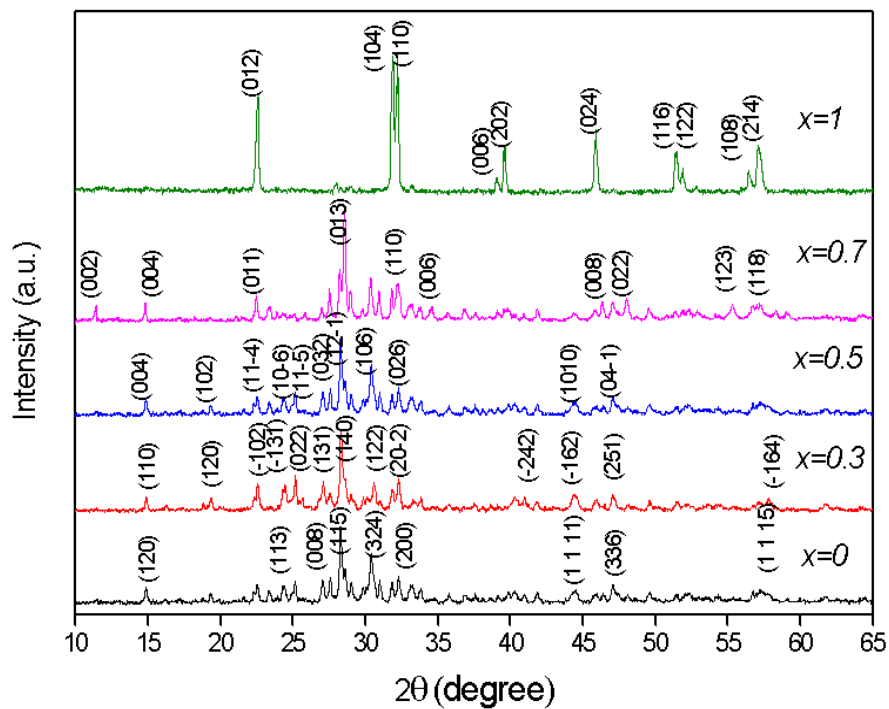
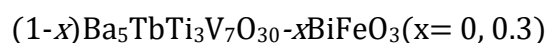


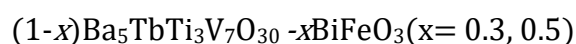
Fig. 3.1. XRD pattern for $(1-x)\text{Ba}_5\text{TbTi}_3\text{V}_7\text{O}_{30}-x\text{BiFeO}_3$

Table 3.1 Observed (obs.) and calculated (cal.) d values comparison of



Ba₅TbTi₃V₇O₃₀						0.7Ba₅TbTi₃V₇O₃₀-0.3BiFeO₃					
d_{obs}	d_{cal}	H	k	l	I/I₀	d_{obs}	d_{cal}	h	k	l	I/I₀
4.3625	4.3306	0	0	6	18.906	5.999	5.9303	1	0	0	14.312
3.592	3.5652	1	1	3	71.813	4.6145	4.5706	1	2	0	12.093
3.2833	3.248	0	0	8	48.02	4.0111	4.1428	0	3	1	9.677
3.1475	3.1254	1	1	5	100	3.9469	3.3984	-1	0	2	19.687
3.1114	3.0827	0	1	7	80.014	3.6817	4.0030	1	2	1	18.963
2.7901	2.7655	2	0	0	98.565	3.6188	3.3961	-1	3	1	8.096
2.3961	2.3786	2	1	3	15.2	3.1419	3.1330	0	3	2	38.381
2.2376	2.2336	2	1	5	35.485	3.089	3.0689	1	4	0	15.913
2.0333	2.0221	1	1	11	21.977	3.0633	3.3984	1	0	2	7.466
1.6645	1.6756	2	2	8	19.928	2.9974	3.3069	1	1	2	9.479
1.5841	1.5839	1	1	15	19.473	2.9694	2.9651	2	0	0	11.207
1.3934	1.4003	2	0	16	8.814	2.889	2.9037	2	1	0	6.89
1.2477	1.2469	1	2	18	4.308	2.8097	3.071	1	2	2	13.728
						2.78	2.6019	2	2	-1	33.384
						2.7691	2.4120	2	0	-2	10.539
						2.6538	2.466	-1	4	2	9.599
						2.2056	2.0540	-1	4	3	11.177
						1.9785	1.9767	3	0	0	10.833
						1.9348	2.0010	2	5	1	16.302
						1.93	1.6874	-2	1	4	11.184
						1.7788	1.5690	3	2	-3	8.299
						1.5973	1.4190	-2	2	5	11.073
						1.592	1.5145	-1	6	4	6.042

Table 3.2 Observed (obs.) and calculated (cal.) d values comparison of



0.5Ba ₅ TbTi ₃ V ₇ O ₃₀ -0.5BiFeO ₃						0.3 Ba ₅ TbTi ₃ V ₇ O ₃₀ -0.7BiFeO ₃					
d _{obs}	d _{cal}	h	k	l	I/I _o	d _{obs}	d _{cal}	h	k	l	I/I _o
11.99986	11.999	0	0	2	26.1	7.7855	7.7855	0	0	2	25.3
4.61091	4.992	1	0	2	18.1	3.8023	3.8023	0	1	1	12.9
4.6061	4.05030	1	0	-4	17.6	3.12861	3.12860	0	1	3	100
3.9606	4.19457	1	1	2	22.8	2.77257	2.77256	1	1	0	30.3
3.95755	3.58817	1	1	-4	23.7	2.61189	2.61188	1	1	2	6.3
3.68104	3.68116	0	2	-2	13.6	2.59517	2.59516	0	0	6	12
3.65682	4.05030	1	0	4	20.8	2.43862	2.43862	0	1	5	9.5
3.65282	3.2328	1	0	-6	21.1	2.25831	2.25831	1	1	4	7.4
3.553	3.55303	0	1	-6	26.3	1.9605	1.9605	0	2	0	15.5
3.30598	3.58817	1	1	4	30	1.90115	1.90115	0	2	2	3.7
3.30303	2.98284	1	1	-6	29	1.89467	1.89467	1	1	6	22.9
3.16121	3.05745	1	2	-2	100	1.74251	1.74251	1	2	1	3.9
2.93085	3.2328	1	0	6	30	1.66128	1.66127	1	2	3	24.7
2.92797	2.63256	1	0	-8	30	1.59303	1.59302	1	1	8	2.6
2.819	2.67586	2	0	-2	35.2	1.58287	1.58287	0	1	9	12.3
2.81687	2.94047	1	2	3	29.2	1.5643	1.56430	0	2	6	8.7
2.8154	2.64043	1	2	-5	22.8	1.52795	1.52795	1	2	5	3.8
2.78038	2.78044	0	2	6	29.3	1.38628	1.38628	2	2	0	3.5
2.23773	2.23849	2	2	0	16.3	1.26743	1.26743	0	3	3	4
2.2094	2.09728	2	2	-4	17.4	1.23993	1.23992	1	3	0	3.1
2.20729	2.37552	2	1	4	13.1	1.23157	1.23156	1	2	9	7.5
2.16713	1.95912	2	1	-8	12.7	1.22276	1.22276	2	2	6	3.3
2.04512	2.17626	1	2	8	17.4	1.17524	1.17524	1	1	12	3.2
1.9363	1.79408	2	2	-8	15.5	1.11879	1.1187	1	3	6	5.2
1.93503	2.01580	1	3	6	12						
1.93375	1.84206	1	3	-8	14.1						

3.2.3. (b) Group B: $(1-x)\text{Ba}_5\text{PrTi}_3\text{V}_7\text{O}_{30}-x\text{BiFeO}_3$

From table 3.2, it can be seen that the crystal structure of the system remains more or less constant i.e. orthorhombic. However, there is change in crystal structure for $x = 0.5$, i.e. when the system contains 50% of BiFeO_3 in the solid solution the crystal structure of the system is Tetragonal.

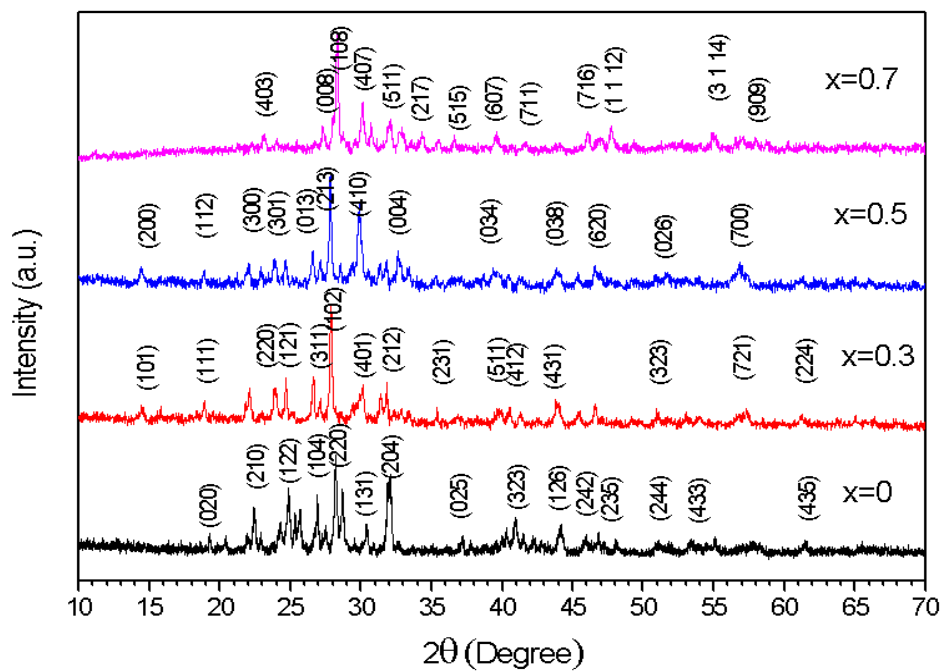
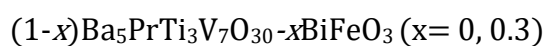
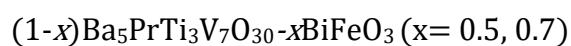


Fig. 3.2. XRD pattern for $(1-x)\text{Ba}_5\text{PrTi}_3\text{V}_7\text{O}_{30}-x\text{BiFeO}_3$

Table 3.3 Observed (obs.) and calculated (cal.) d values comparison of

Ba₅PrTi₃V₇O₃₀						0.7 Ba₅PrTi₃V₇O₃₀-0.3BiFeO₃					
d_{obs}	d_{cal}	h	k	l	I/I₀	d_{obs}	d_{cal}	h	k	l	I/I₀
3.8436	3.8277	3	0	5	13.673	3.8436	3.8277	3	0	5	13.673
3.3252	3.3117	4	0	5	9.545	3.3252	3.3117	4	0	5	9.545
3.263	3.2716	1	1	5	15.75	3.263	3.2716	1	1	5	15.75
3.1784	3.173	0	0	8	23.779	3.1784	3.173	0	0	8	23.779
3.1401	3.1226	1	0	8	100	3.1401	3.1226	1	0	8	100
3.0789	3.0790	3	0	7	10.512	3.0789	3.079	3	0	7	10.512
3.0027	3.0084	1	1	6	9.904	3.0027	3.0084	1	1	6	9.904
2.8967	2.8935	6	0	1	20.537	2.8967	2.8935	6	0	1	20.537
2.7964	2.7906	4	0	7	18.686	2.7964	2.7906	4	0	7	18.686
2.7266	2.7237	5	1	1	17.382	2.7266	2.7237	5	1	1	17.382
2.7041	2.7047	3	1	6	16.305	2.7041	2.7047	3	1	6	16.305
2.6592	2.6680	2	1	7	8.376	2.6592	2.6680	2	1	7	8.376
2.6061	2.6064	5	1	3	14.336	2.6061	2.6064	5	1	3	14.336
2.5262	2.5264	6	0	5	8.545	2.5262	2.5264	6	0	5	8.545
2.5156	2.5153	5	1	4	10.239	2.5156	2.5153	5	1	4	10.239
2.2731	2.2709	6	0	7	12.413	2.2731	2.2709	6	0	7	12.413
1.9661	1.9653	4	1	10	11.992	1.9661	1.9653	4	1	10	11.992
1.9318	1.9328	7	1	6	8.645	1.9318	1.9328	7	1	6	8.645
1.9212	1.9260	5	0	11	9.586	1.9212	1.9260	5	0	11	9.586
1.8982	1.8965	1	1	12	20.086	1.8982	1.8965	1	1	12	20.086
1.6666	1.6661	8	1	8	12.874	1.6666	1.6661	8	1	8	12.874
1.6611	1.6616	6	2	5	11.758	1.6611	1.6616	6	2	5	11.758
1.6122	1.6118	3	1	14	9.586	1.6122	1.6118	3	1	14	9.586

Table 3.4 Observed (obs.) and calculated (cal.) d values comparison of

0.5Ba ₅ PrTi ₃ V ₇ O ₃₀ -0.5BiFeO ₃						0.3 Ba ₅ PrTi ₃ V ₇ O ₃₀ -0.7BiFeO ₃					
d _{obs}	d _{cal}	h	k	l	I/I ₀	d _{obs}	d _{cal}	h	k	l	I/I ₀
4.4794	4.2804	2	2	0	8.85	4.6386	4.5413	2	0	1	12.43
3.8696	3.8741	2	1	2	14.787	3.6803	3.6639	2	2	0	27.93
3.742	3.7924	3	0	1	9.479	3.5679	3.5695	1	2	1	28.18
3.4799	3.6190	3	1	1	20.545	3.3177	3.29	0	0	2	33.17
3.2473	3.2630	3	0	2	22.356	3.2582	3.2873	3	1	1	13.35
3.1793	3.1551	0	2	3	18.715	3.1716	3.1846	1	0	2	100
3.1059	3.0531	2	1	3	100	3.0051	3.0032	1	1	2	10.06
3.0299	3.026	4	0	0	15.652	2.9629	2.9621	4	1	0	19.68
2.9535	2.9363	4	1	0	16.081	2.8243	2.8310	4	0	1	21.68
2.8385	2.8385	4	1	1	11.849	2.7827	2.7806	3	2	1	19.33
2.7719	2.7727	0	0	4	18.847	2.7509	2.7373	0	3	1	5.86
2.7371	2.7260	3	0	3	19.461	2.7025	2.70	4	1	1	8.42
2.6591	2.6594	3	1	3	23.674	2.519	2.5087	2	3	1	4.57
2.6172	2.6299	4	2	1	13.93	2.2623	2.2689	5	1	1	6.04
2.4768	2.4856	3	2	3	8.626	2.2051	2.2021	4	1	2	6.12
2.2734	2.2853	0	3	4	7.492	2.0481	2.0365	6	1	0	15.53
2.2419	2.2456	3	1	4	10.299	1.7776	1.773	0	3	3	6.91
2.2141	2.2190	5	0	2	10.697	1.6872	1.6780	2	5	1	5.29
2.0279	1.3111	0	3	8	8.047	1.5976	1.5923	2	0	4	11.51
2.0126	2.0160	4	1	4	9.416	1.5061	1.5016	2	2	4	6.23
1.9119	1.9142	6	2	0	15.165						
1.8974	1.8962	6	0	2	8.147						
1.5975	1.5929	7	2	2	13.871						
1.5909	1.5897	7	3	0	11.536						

3.3. Scanning electron micrographs (SEM)

3.3.1. Introduction

By great extent, the physical properties of the ceramics are controlled by the microstructure. The scanning electron microscope (SEM) is a powerful microscope which can be used for microstructure study. It is a tool which can be used for observing the grain, grain boundaries, and pores, which facilitates the morphological study of the sample. SEM is an exceptional diagnostic tool for micro-fabrication due to its high magnification attainable combined with large field depths. It employs a high energetic electrons beam to scan matter to a fine scale. SEM makes scanning point to point on the solid surface and yields a rich image of specimen, which is visible to a naked eye and provides information regarding the sizes which lies in the μm range.

The following information can be obtained from SEM micrographs:

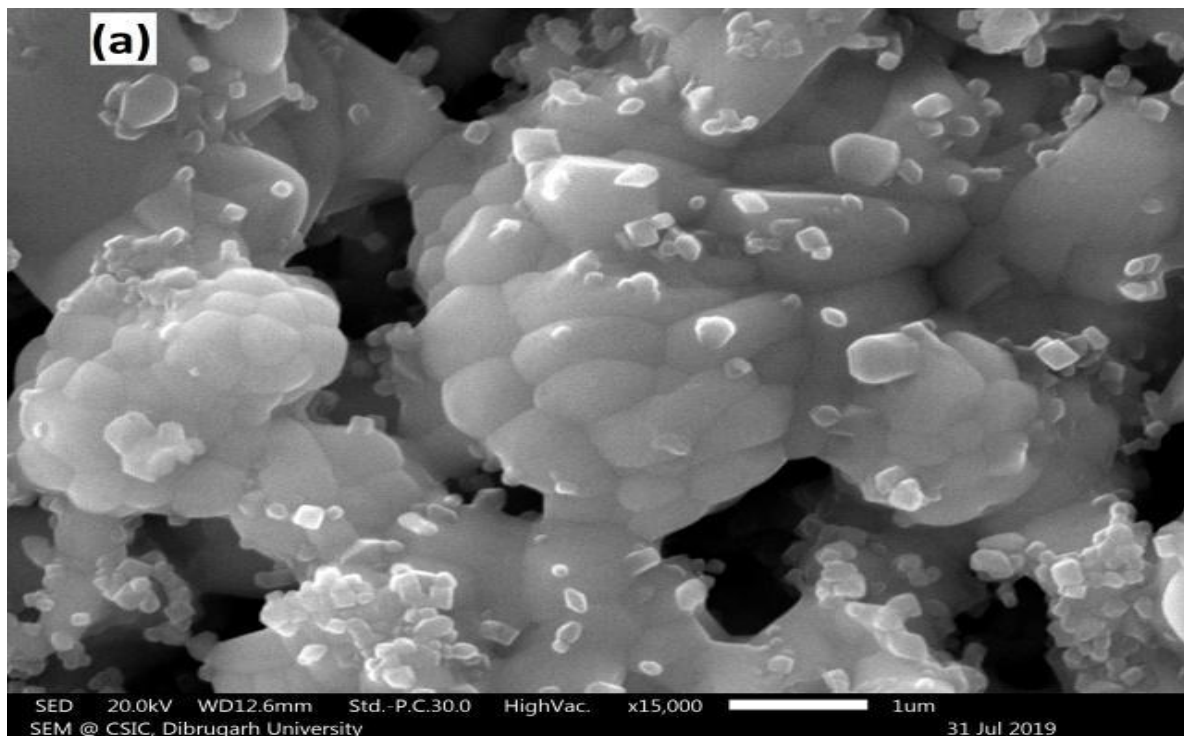
- a) **Topography:** The features of the surface of an object or “how it looks”, its texture; relation between the materials properties and features (reflectivity, hardness, etc.)
- b) **Morphology:** the shape and size of the particles of the object; relation between the materials properties and structure (strength, ductility, reactivity, etc.)
- c) **Composition:** the composition and relative amount of elements and the compounds in the object; direct relationship between materials properties and composition (reactivity, melting point, hardness, etc.)
- d) **Crystallographic information:** arrangements of atoms in the object, relation between these materials properties and arrangements (electrical properties, conductivity, strength, etc).

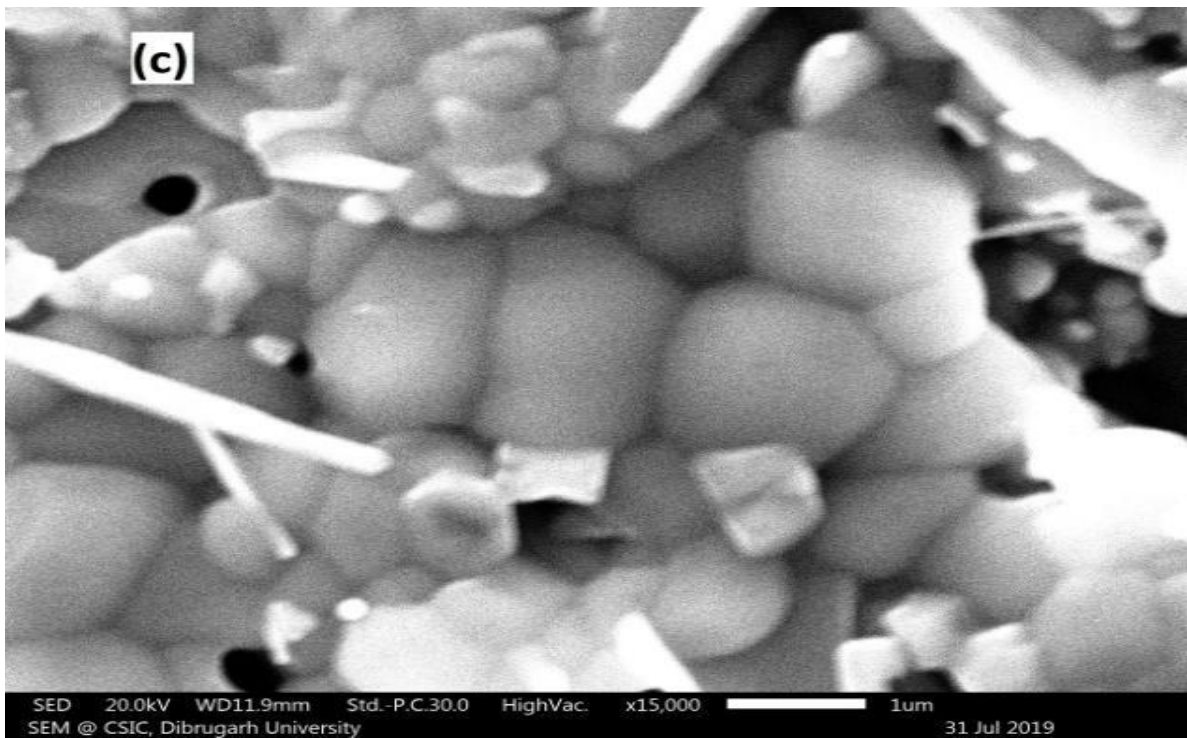
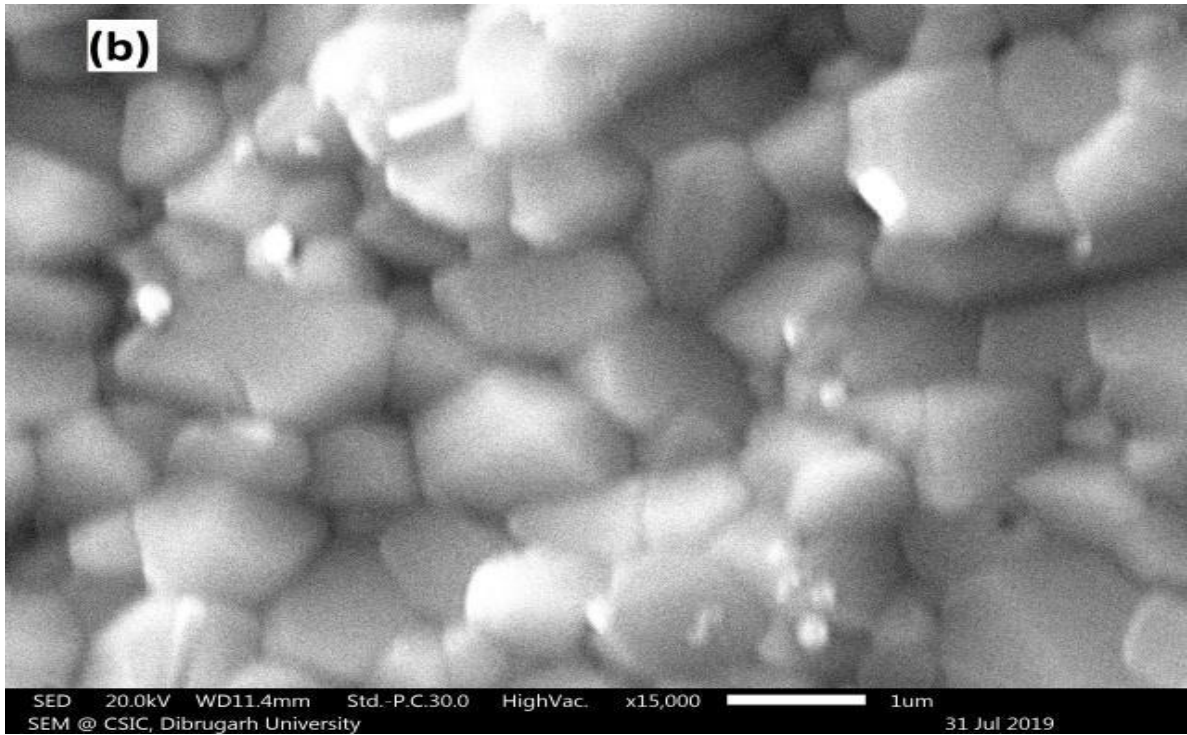
3.3.2. Result and discussion

The microstructure of the sintered pellets shows that the growth of the grain is more or less complete in sintering process and there is no secondary recrystallization.

3.3.2.1. Group A: $(1-x)\text{Ba}_5\text{TbTi}_3\text{V}_7\text{O}_{30}-x\text{BiFeO}_3$

Fig 3.3 (a-e) shows the SEM micrographs of which show for $x=0, 0.3, 0.5, 0.7$ and 1 and found that the growth of the grain is more or less complete. From fig 2(a-e) by linear intercept method the average grain size of all the materials are measured.





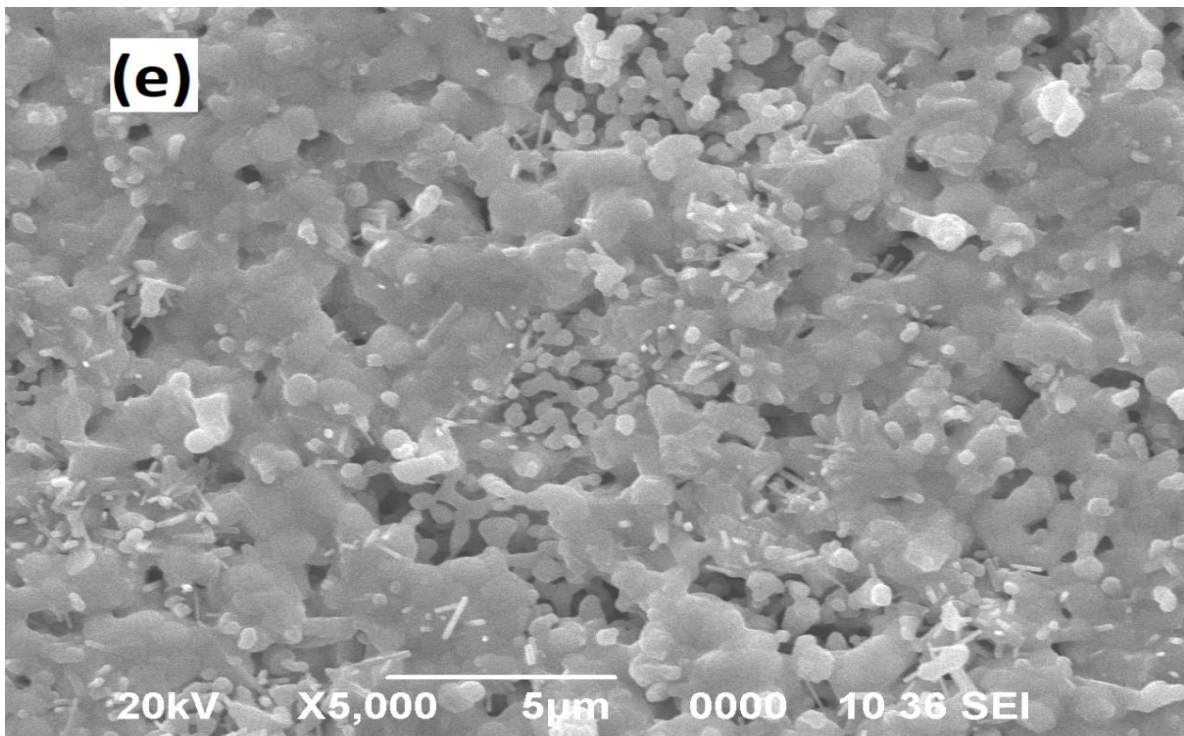
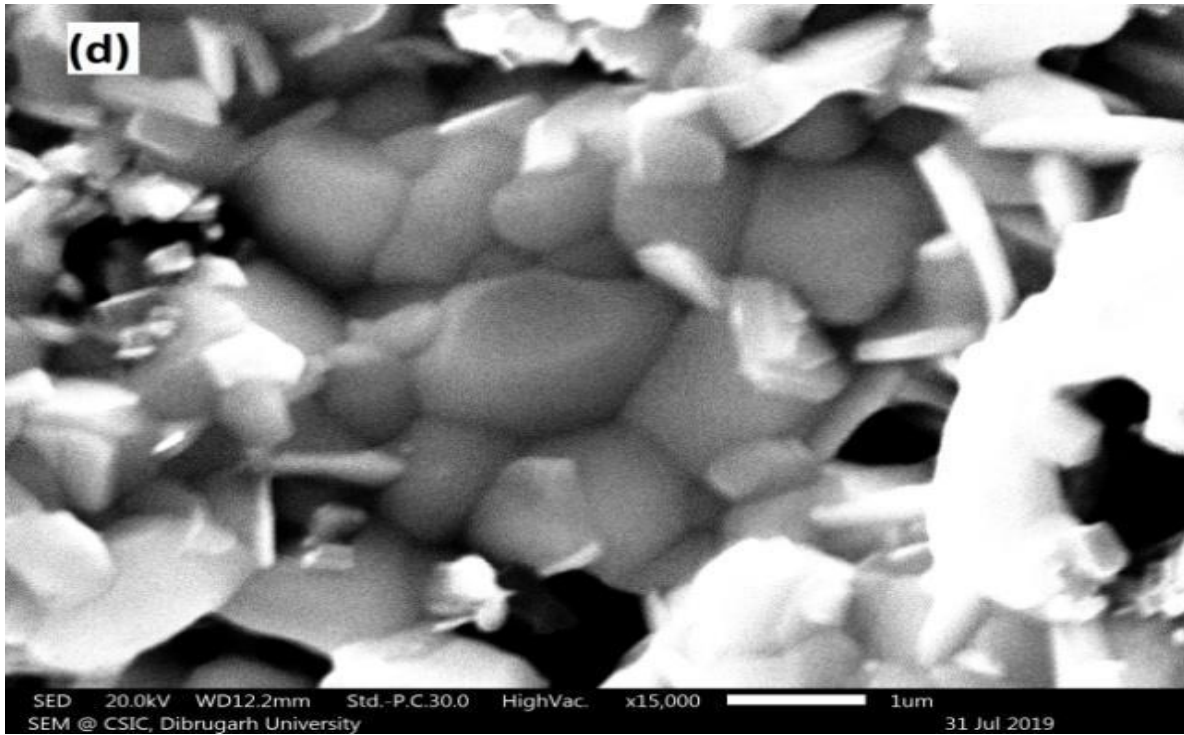
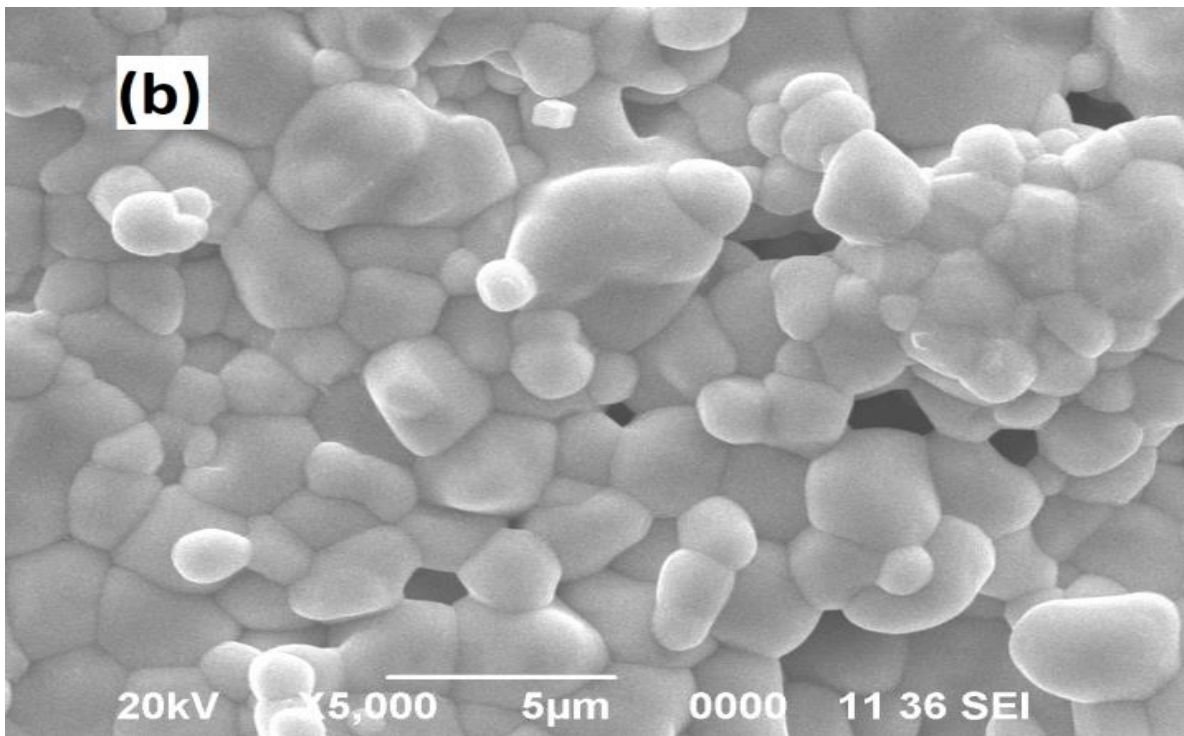
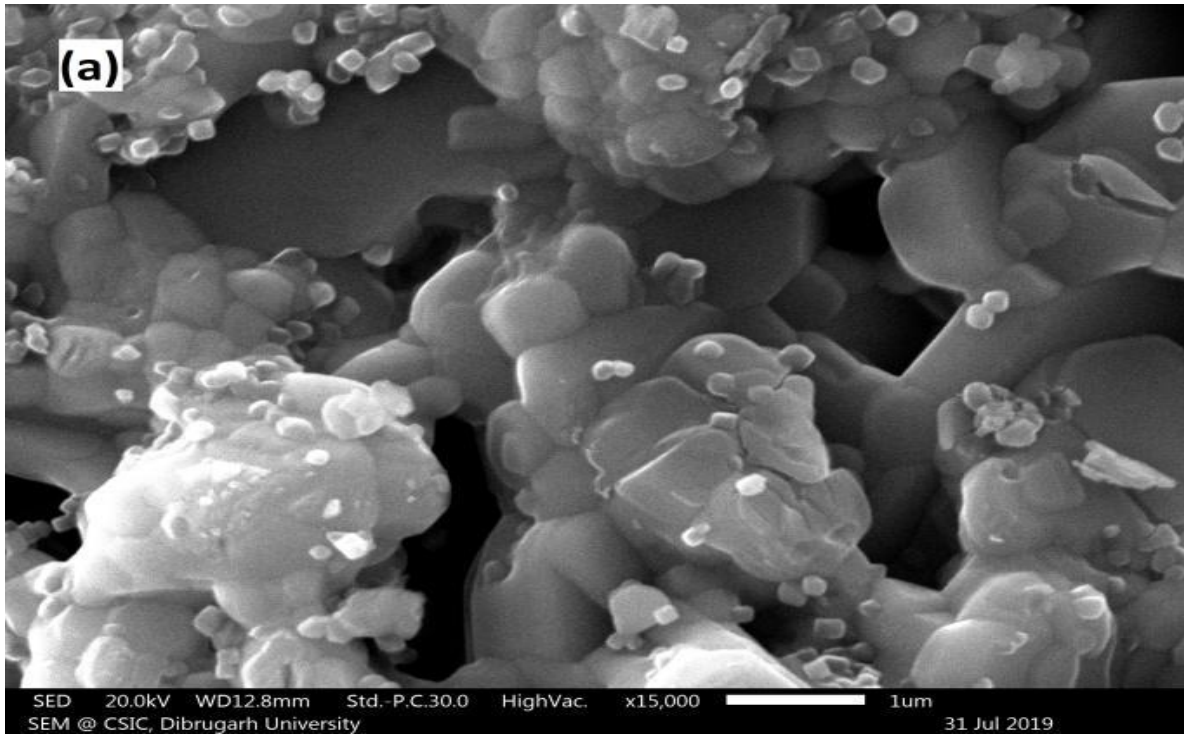


Fig. 3.3. SEM micrographs of $(1-x)\text{Ba}_5\text{TbTi}_3\text{V}_7\text{O}_{30}-x\text{BiFeO}_3$ (a) $x=0$ (b) $x=0.3$ (c) $x=0.5$ (d) $x=0.7$ (e) $x=1$.

- a) For $x=0$: SEM micrograph of $\text{Ba}_5\text{TbTi}_3\text{V}_7\text{O}_{30}$ shows that the average size is around $0.89 \mu\text{m}$, the shape is of oval, elongated and angular shape. There is no secondary recrystallization. There is presence of irregular dimension voids signifying that the composite has a some degree of inhomogeneity and porosity.
- b) For $x=0.3$: SEM micrograph of $0.7\text{Ba}_5\text{TbTi}_3\text{V}_7\text{O}_{30}-0.3\text{BiFeO}_3$ shows that the average size is around $1.13 \mu\text{m}$, as x increases, compactness increases and the grains are most compact for $x= 0.3$.
- c) For $x=0.5$: SEM micrograph of $0.5\text{Ba}_5\text{TbTi}_3\text{V}_7\text{O}_{30}-0.5\text{BiFeO}_3$ shows that the average size is around $1.8 \mu\text{m}$. The shape is spherical and elongated. The presence of porosity is distinctly visible in the compound also there is the appearance of columnar shape grains (it may be due to an increase in the content of BiFeO_3).
- d) For $x=0.7$: SEM micrograph of $0.3\text{Ba}_5\text{TbTi}_3\text{V}_7\text{O}_{30}-0.7\text{BiFeO}_3$ shows that the average size of the grain is $\sim 1.36 \mu\text{m}$. The shape is more cubicle and angular. The size of the grain decreases when BFO is increased but the porosity also increases. The columnar shape grain becomes more distorted.
- e) For $x=1$: SEM micrograph of BiFeO_3 shows that the process of the growth of grain is more or less complete all through the sintering process, and on the whole it becomes dense, but also a small amount of scattered pores are being found, indicating that there is some degree of porosity present in the composites. It can also be observed that the grains are in the form of needles along the axis.

3.3.2.2. Group B: $(1-x)\text{Ba}_5\text{PrTi}_3\text{V}_7\text{O}_{30}-x\text{BiFeO}_3$

Fig 3.4 (a-d) shows the SEM micrographs of which show for $x= 0, 0.3, 0.5$ and 0.7 which shows that the grain growth is more or less complete. From fig 2(a-d) by linear intercept method the average grain size of all the materials are measured.



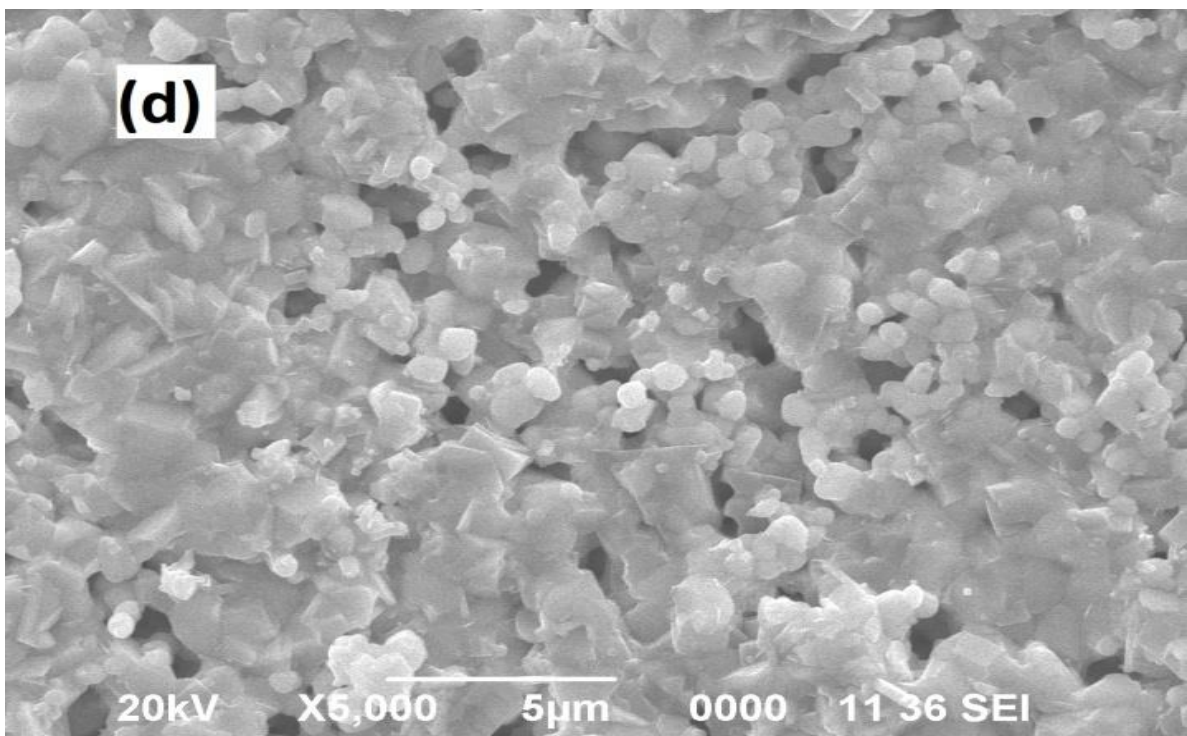
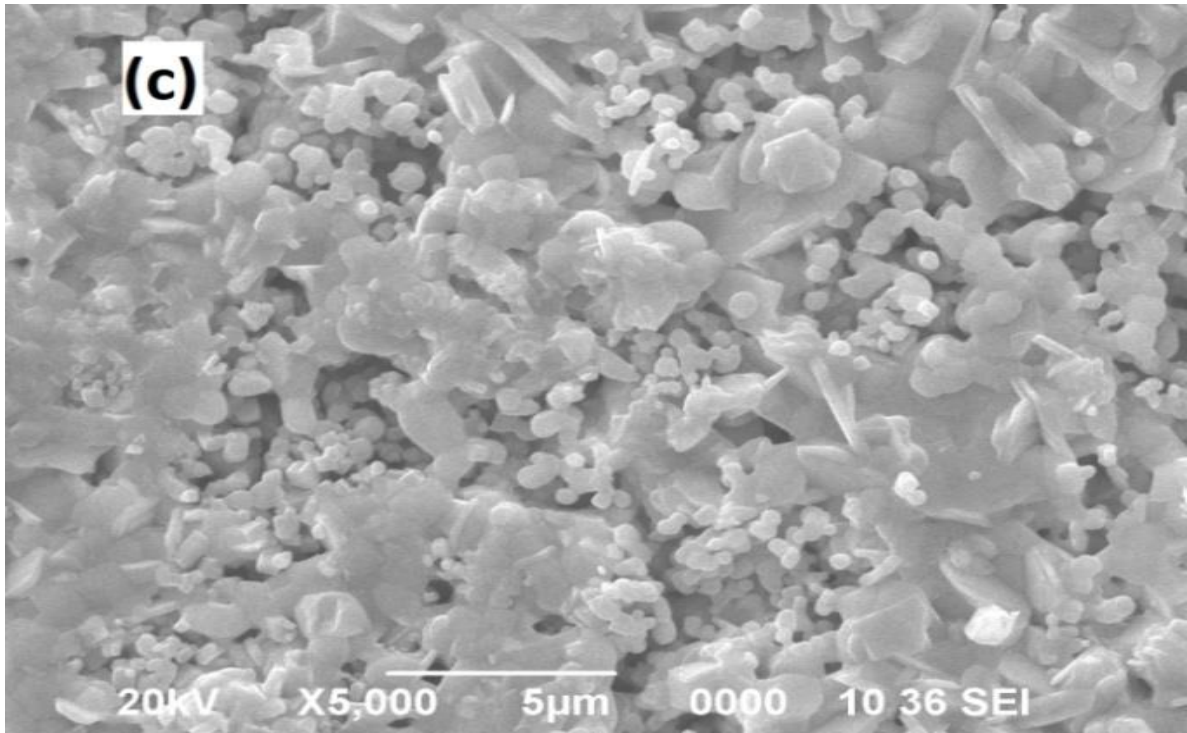


Fig. 3.4. SEM micrographs of $(1-x)\text{Ba}_5\text{PrTi}_3\text{V}_7\text{O}_{30-x}\text{BiFeO}_3$ (a) $x=0$ (b) $x=0.3$ (c) $x=0.5$ (d) $x=0.7$

- (i) For $x=0$: SEM micrograph of $\text{Ba}_5\text{PrTi}_3\text{V}_7\text{O}_{30}$ shows that the average size is around $0.75\ \mu\text{m}$. The shape shows that its granule formed is of cuboid, agglomerate, elongated in feature. There is no secondary recrystallization. There is presence of irregular dimension voids indicating that the sample has certain degree of inhomogeneity and porosity.
- (ii) For $x=0.3$: SEM micrograph of $0.7\text{Ba}_5\text{PrTi}_3\text{V}_7\text{O}_{30}-0.3\text{BiFeO}_3$ shows that the average size is around $3.63\ \mu\text{m}$ as x increases, compactness has increased and the grains are most compact for $x=0.3$. There is an increase in grain size with the addition of BiFeO_3 in the system. The grains are more or less homogeneously distributed. Some of them are spherical in shape. There is no secondary recrystallization. The presence of voids also decreases with addition of BiFeO_3 in the system.
- (iii) For $x=0.5$: SEM micrograph of $0.5\text{Ba}_5\text{PrTi}_3\text{V}_7\text{O}_{30}-0.5\text{BiFeO}_3$ shows that the average size is around $2.27\ \mu\text{m}$. There is presence of some spherical and some columnar-shaped grains with intra- and inter- grain porosity. The grains are inhomogeneously distributed. The presence of voids also increases.
- (iv) For $x=0.7$: SEM micrograph of $0.3\text{Ba}_5\text{PrTi}_3\text{V}_7\text{O}_{30}-0.7\text{BiFeO}_3$ shows that the average size of the grain is $\sim 2.10\ \mu\text{m}$. The shape is more cubicle and angular. The size of the grain decreases when BiFeO_3 is increased and the porosity also decreases. The nature and distribution of microstructure suggests the presence of polycrystalline texture of the composite.

Table 3.5. Comparison of lattice parameters (Å), particle size (P) (in Å) and volume (Å³) of (1-x)Ba₅RTi₃V₇O₃₀-xBiFeO₃ (x= 0 ,0.3, 0.5, 0.7, 1; R = Pr, Tb).

(1-x)Ba ₅ RTi ₃ V ₇ O ₃₀ -xBiFeO ₃		a (in Å)	b (in Å)	c (in Å)	P (in Å)	V (in Å ³)	Structure
R=Tb	x=1	5.6343	5.6343	5.6343	5.5	124.5979	Rhombohedral
	x=0.7	3.9210	3.9210	15.5710	3.5	239.39	Tetragonal
	x=0.5	5.6380	7.7350	24.6470	4.0	1046.63	Monoclinic
	x=0.3	8.5762	8.5762	8.5762	4.2	630.7898	Orthorhombic
	x=0	5.5310	5.5340	25.9840	4.6	795.3327	Orthorhombic
R=Pr	x=0.7	12.5427	6.585	6.585	7.5	1196.2094	Rhombohedral
	x=0.5	12.1070	12.107	11.0911	6.9	1625.7273	Tetragonal
	x=0.3	17.475	4.4120	25.3900	6.7	1957.5613	Orthorhombic
	x=0	8.8140	9.2080	14.2610	4.4	1157.412	Orthorhombic

3.4. Conclusion

Thus following observations are made comparing the micrographs of the composites:

- The growth of the grain is more or less complete through sintering and no secondary recrystallization has been observed.
- The presence of irregular dimensions voids shows that the pellet samples have some degree of inhomogeneity and porosity.
- The distribution and shape of grains in the microstructure show indication of the polycrystalline nature of the composites.
- The grain size average of all the composites has been measured by linear intercept method [14,15], which are compared in Table 3.5.
- The distribution and shape of grains show evidence of the polycrystalline nature of the composites.
- Porosity was found to increase with decrease in ionic radius of the doped rare earth element.
- With the increase of the BiFeO_3 content in the solid solution, there is the appearance of columnar shape grains. There is also increase in porosity which may be due to the loss of Bi_2O_3 during high temperature processing resulting into porosity or may be due to presence of small amount of impurity phases in BiFeO_3 .

CHAPTER IV
DIELECTRIC STUDY

4.1 Introduction

The ceramic materials are well suited for the solid-state electronics because of its various advantages, having better electrical properties, greater resistance to environmental change and nonappearance of deformation under stress at room temperature, etc. Dielectric ceramic materials have capacitive properties which are fundamental in electrical insulation and electronic circuits. Dielectric response is an effect of charge carriers' short range motion under the influence of an external electric field, whereas in electrical conductivity long range motion of charge carriers are involved. Dielectric properties are functions of various factors like frequency of electric field, temperature, crystal structure, humidity, etc. The important characteristic of dielectric material which make it suitable for device applications are:

- i. **Relative dielectric constant (ϵ_r)** it explains the ability of a sample to store electrostatic energy.
- ii. **Loss tangent ($\tan \delta$)** it shows the ability to hold the electrostatic field at the same time as dissipating least energy loss in heat form.
- iii. **Dielectric strength (breakdown)** specifies the maximum voltage which a dielectric material can withstand undamaged.

Among various classes of dielectric ceramic materials, there is a class of materials called ferroelectric materials. Ferroelectric materials have a diversity of properties like piezoelectric, pyroelectric, electro-optic, and electro-mechanical. Due to its range of properties it has application in devices such as display printer, memories, logic circuit, light deflector and modulator, photographic pick up, frequency changer, PTC thermistors, actuators, resonators, microphones, detectors, filters, etc. The properties of ferroelectric ceramics depend in some way to their response to electrical stimuli. Electrical behaviour of these materials is important to their successful applications. Ferroelectrics are in general characterized by:

- a. High dielectric constant (500-4000) than ordinary insulator making them useful as capacitors and energy storage materials,
- b. Low dielectric loss,
- c. High resistivity (10^{11} - $10^{13} \Omega\text{cm}$),
- d. Moderate dielectric breakdown strength and

- e. Non-linear electrical behaviour (Hysteresis loop).

Ferroelectrics possess optical and mechanical effects which are interactive with the electrical properties and have applications as electro-optic and electro-mechanical devices. For characterising and understanding the ferroelectric materials it is important to study electrical properties. Among the various electrical properties, dielectric study is one of the most important properties which provide many information regarding ferroelectrics.

4.2. Principle

For detail perceptive of ferroelectricity in ceramics the primary tool is to analyse the dielectric properties of ferroelectrics over an extensive range of frequency and temperature. The dielectric constant at the given temperature is calculated using the relation:

$$\epsilon = \frac{C}{C_0}, \text{ where } C \text{ is sample capacitance}$$

$$C_0 = \frac{\epsilon_0 A}{t} \text{ geometrical capacitance}$$

$$\epsilon_0 = 8.854 \times 10^{-14} \text{ f/cm, permittivity for free space}$$

$$A = \text{Area of the flat surface}$$

$$t = \text{thickness of the pellet}$$

On application of alternating current, the charges are stored up in a dielectric as imaginary (out of phase) and real (in phase) components, caused either or both by dielectric absorption and resistive leakage. The dielectric loss ($\tan \delta$) is the ratio of the out of phase components to that of in phase components, which is also termed as loss tangent or dissipation factor (D):

$$D \text{ or } \tan \delta = \frac{\epsilon''}{\epsilon'}$$

Where, ϵ' and ϵ'' are the real and imaginary parts of the complex dielectric constant:

$$\epsilon = \epsilon' - j\epsilon''$$

When relative dielectric constant is considered in a zero or constant stress, then it is called as free dielectric constant, ϵ . However, if it is measured in the presence of constant strain then it is known as clamp dielectric constant ϵ^s . In piezoelectric materials, free and clamp dielectric constant may be different and they are correlated by electromechanical coupling factor (K) i.e. $\epsilon^s = K (1 - \epsilon^2)$. For strong piezoelectric materials, K may be as large as 0.7 or more. The relative dielectric constant value for normal substances is low, for organic material it is generally less than 5 and for inorganic solids less than 20. But ferroelectrics materials have a much higher value of relative dielectric constant ranging from several hundred to several thousands.

Ferroelectric materials consist of crystal matrices having grains and pores. Dividing the surface between matrices, and grains and pores on the other, cause additional system energy which influences the physical properties (i.e. dielectric loss, dielectric constant, Curie constant and Curie temperature). Based on the thermodynamically model of ferroelectric ceramics and the experimental measurements carried out by some authors such as by Yurkevich and Rolov [1], the relative features can be summarised as:

1. Under the influence of ceramic micro-structure (density and dimension of pores and grains) and impurities, phase transition may change its character in comparison with phase transition in single crystal.
2. In the transition region, dielectric constant may not change sharply but could show a round peak that spreads over a broad temperature range.
3. The ferroelectric Curie temperature strongly depends upon the micro-volume inhomogeneity and also upon the grains and pores present in the ceramics.
4. The Curie-Weiss constant of ceramics has a higher value than that of the value of a single crystal and depends on the density and dimension of the grains and pores present in the ceramics.
5. The temperature corresponding to $\tan \delta_{\max}$ need not coincide with the temperature of ϵ_{\max} in ceramic materials.

4.3. Experimental

Using HIOKI-IM3536 the dielectric factors i.e. relative dielectric constant (ϵ_r) and dielectric loss ($\tan \delta$), of the sample is done for frequency range 4Hz-8MHz and at temperature are range 250 – 773 K. For dielectric studies, the pellets are polished

thoroughly by fine emery for smooth flat surfaces and painted with excellence conducting silver paste on both sides of the flat surface. The pellet is fired at 423K for 2 hours, to warrant high-quality electrical contact between pellet and silver paste. The signal amplitude for dielectric studies is kept at constant 300mV for the whole temperature range. The flow chart for testing the sample is given in Fig. 4.1.

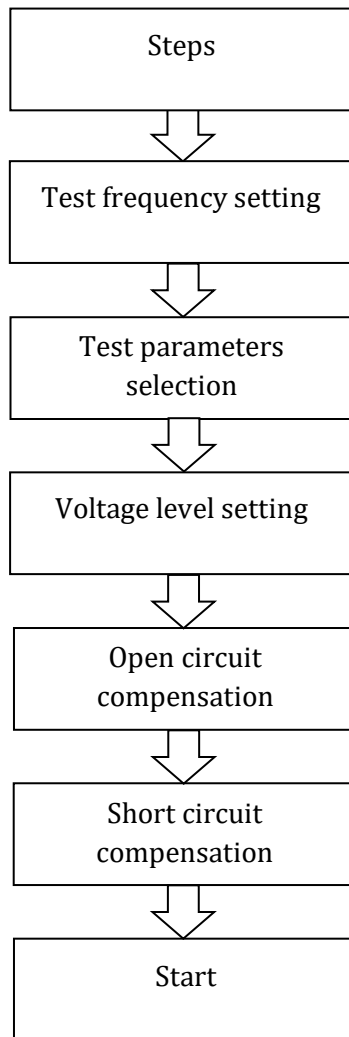
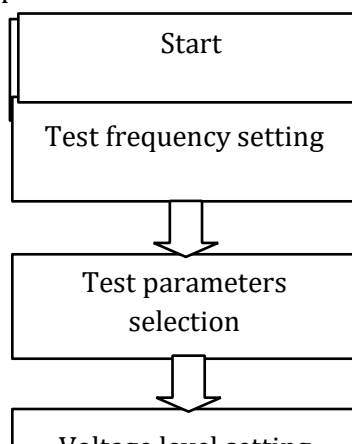


Fig. 4.1. Testing procedure flow chart for in impedance meter



4.4. Result and discussion

4.4 (a) Variation of ϵ_r and $\tan \delta$ with frequency

All kinds of components of polarization (i.e., ionic, electronic, interfacial and dipolar polarization) are there in the audible frequency range [2].

At low frequencies (10^2 Hz to 10^4 Hz) all kinds of polarization exist, of which space charge is predominant due to which the dielectric constant has a large value [3]. This is consistent with the Debye equation [4]. The effect of orientational polarization can be shown by materials sometime even up to 10^{10} Hz. Electronic and ionic polarization can exist even up to 10^{13} Hz. However, above 10^{13} Hz only electronic polarization exists. Due to which as frequency increases, the dielectric constant decreases [5,6]. Unlike electronic and ionic polarization which exists in relatively high frequency, dipolar polarization takes place at lower frequencies, which significantly affect the insulating and capacitive properties of ceramics and glasses. From the character of the variant of dielectric constant with frequency, it is feasible to determine the predominant polarization contributor present in a frequency range [7]. In the given range of frequency, only the polar component contributing to the total dielectric constant goes through dispersion. At temperature below transition temperature, all kinds of spontaneously polarized sections contribute to the dielectric constant. At low frequencies the space charge is predominant and its contribution to the crystal depends upon the perfection and purity of the crystal lattice [8]. The proliferation of space charge polarization enlarges the dielectric loss and relative dielectric constant value.

The dielectric loss in pellets is typically because of the scattering mechanism of defects or charge carriers [8]. The cross section scattering is dependent on the grain boundaries, grain size, and inter-grain spacing. The high value of packing fraction of the pellets is due to the reason that the powder is pressed by high pressure and the pellets are sintered at high temperature. Reduction of the cross section scattering also results in decrease in the inter-grain spacing and the grain boundaries. Due to which dielectric loss also decreases with the increase in frequency because of the high value of packing fraction.

(i) Group A: $(1-x)\text{Ba}_5\text{TbTi}_3\text{V}_7\text{O}_{30}-x\text{BiFeO}_3$

Fig. 4.2. shows the frequency variation of ϵ_r of $(1-x)\text{Ba}_5\text{TbTi}_3\text{V}_7\text{O}_{30}-x\text{BiFeO}_3$ at room temp, it shows that with increase in frequency from 1kHz to 100kHz, the ϵ_r decreases for $x=0$ from ~ 50 to ~ 18 , for $x=0.3$ from ~ 29 to ~ 19 , for $x=0.5$ from ~ 34 to ~ 24 and for $x=0.7$ from ~ 46 to ~ 33 , the trend we got is as expected of the polar dielectric materials i.e. with increase in frequency the dielectric constant decreases. It is seen that with addition of BiFeO_3 the dependency of dielectric constant with frequency decreases.

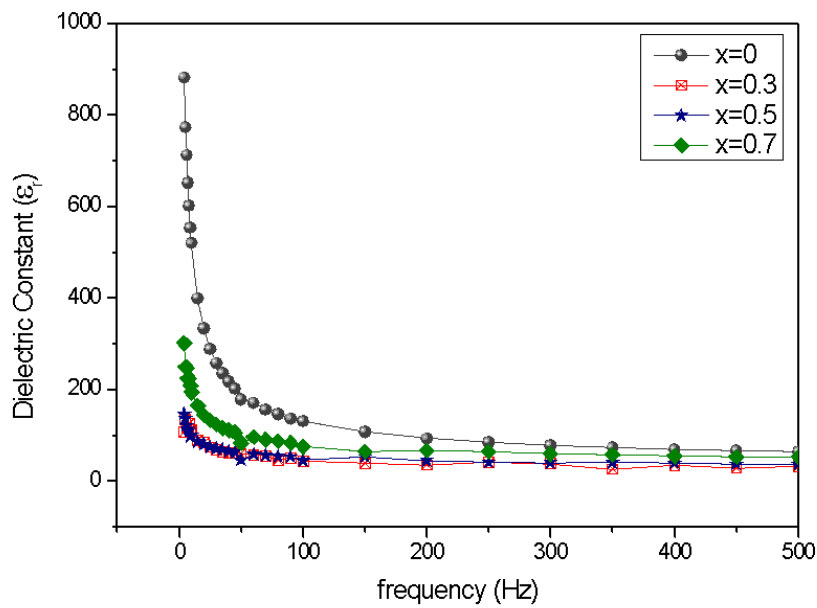


Fig. 4.2. Frequency variation of ϵ_r form $(1-x)\text{Ba}_5\text{TbTi}_3\text{V}_7\text{O}_{30}-x\text{BiFeO}_3$ at room temp.

Fig. 4.3. shows the variation of $\tan\delta$ with frequency for $(1-x)\text{Ba}_5\text{TbTi}_3\text{V}_7\text{O}_{30}-x\text{BiFeO}_3$ at room temp, it shows that with increase in frequency from 4Hz to 1000Hz, the $\tan\delta$ decreases for $x=0$ from ~ 1.25 to ~ 0.18 , for $x=0.3$ from ~ 0.38 to ~ 0.07 , for $x=0.5$ from ~ 0.26 to ~ 0.05 and for $x=0.7$ from ~ 0.36 to ~ 0.045 , the trend is as expected for dielectric materials. It can also be seen from the figure that when BiFeO_3 is increased i.e. from $x= 0.3$ to 0.7 , change in $\tan\delta$ with frequency remains more or less the same.

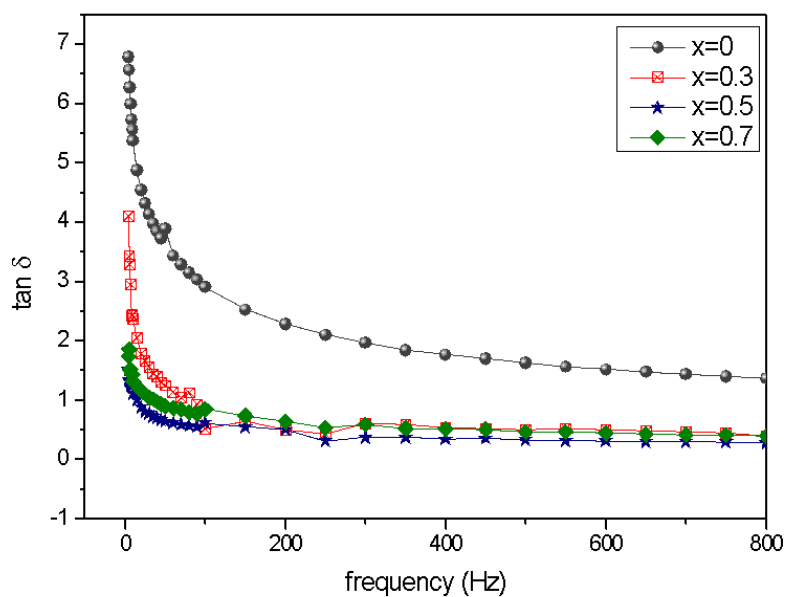


Fig. 4.3. Frequency variation of $\tan\delta$ of $(1-x)\text{Ba}_5\text{TbTi}_3\text{V}_7\text{O}_{30-x}\text{BiFeO}_3$ at room temp.

(ii) Group B: $(1-x)\text{Ba}_5\text{PrTi}_3\text{V}_7\text{O}_{30-x}\text{BiFeO}_3$

Fig. 4.4. shows the frequency variation of ϵ_r of $(1-x)\text{Ba}_5\text{PrTi}_3\text{V}_7\text{O}_{30-x}\text{BiFeO}_3$ at room temp, it shows that with increase in frequency from 4Hz to 1000Hz, the ϵ_r decreases for $x=0$ from ~ 85 to ~ 71 , for $x=0.3$ from ~ 68 to ~ 48 , for $x=0.5$ from ~ 31 to ~ 24 and for $x=0.7$ from ~ 31 to ~ 16 , the trend we got is as expected of the dielectric materials i.e. with increase in frequency the dielectric constant decreases. It is seen that when BiFeO_3 is added the value of dielectric constant decreases.

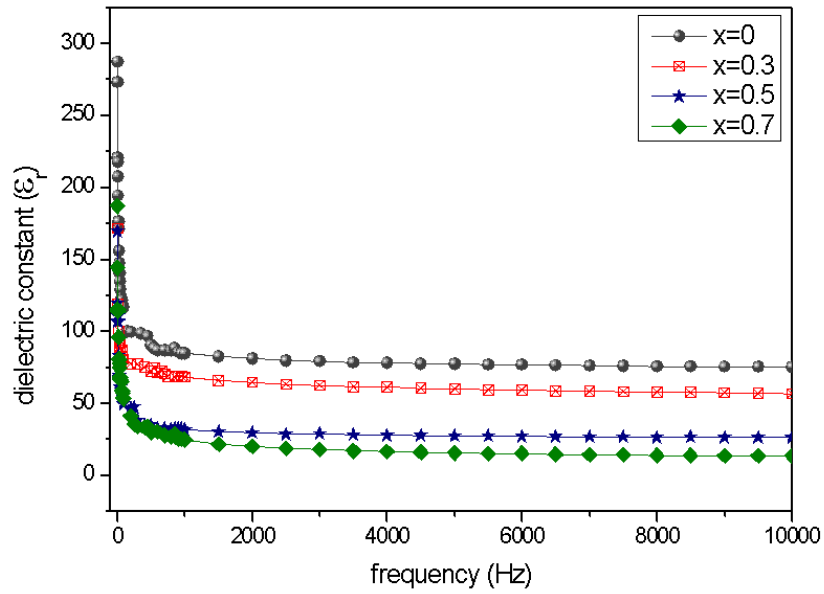


Fig 4.4. Frequency variation of ϵ_r form $(1-x)\text{Ba}_5\text{PrTi}_3\text{V}_7\text{O}_{30-x}\text{BiFeO}_3$ at room temp.

Fig. 4.5. shows the variation of $\tan\delta$ with frequency for $(1-x)\text{Ba}_5\text{PrTi}_3\text{V}_7\text{O}_{30-x}\text{BiFeO}_3$ at room temp, it shows that with increase in frequency from 4Hz to 100kHz, the $\tan\delta$ decreases for $x=0$ from ~ 0.17 to ~ 0.03 , for $x=0.3$ from ~ 0.13 to ~ 0.09 , for $x=0.5$ from ~ 0.25 to ~ 0.04 and for $x=0.7$ from ~ 0.6 to ~ 0.08 , the trend is as expected for dielectric materials. With increase in the content of BiFeO_3 there is an increase in tangent loss which may be due to the semiconducting nature of BiFeO_3 .

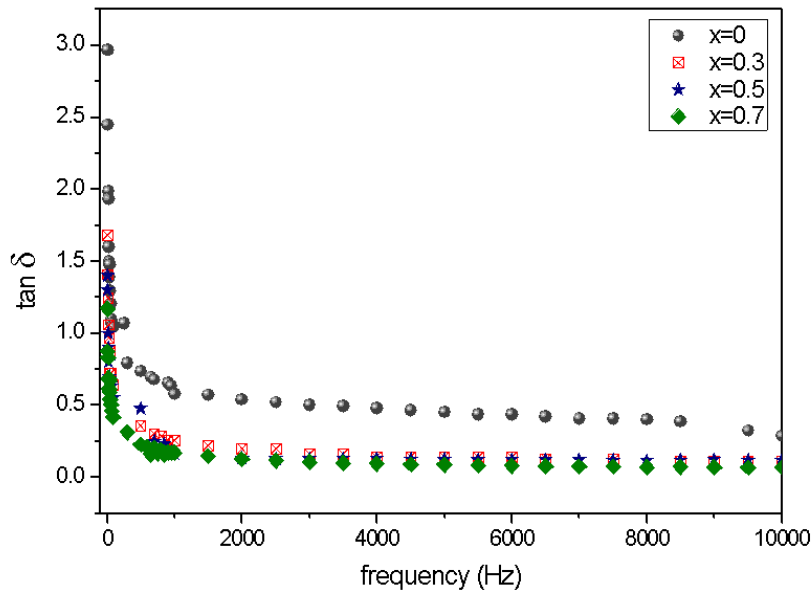


Fig. 4.5. Frequency variation of $\tan\delta$ of $(1-x)\text{Ba}_5\text{PrTi}_3\text{V}_7\text{O}_{30}-x\text{BiFeO}_3$ at room temp.

4.4 (b) Variation of Dielectric constant and loss tangent with temperature

Normally, in ferroelectrics up-to a transition temperature (T_c), the relative dielectric constant first increases with increase in temperature and after that it decreases. And in some cases, when the temperature is further increased then there is a faster rate of increase of dielectric constant. It may be because of the presence of space charge polarization in the sample.

(i) Group A: $(1-x)\text{Ba}_5\text{TbTi}_3\text{V}_7\text{O}_{30}-x\text{BiFeO}_3$

Fig. 4.6. shows variation of dielectric constant ϵ_r with temp in a broad range (RT-500°C) for selected static or low frequency [9-11] at 1000Hz in case of the composite for different values of x. It is being observed that the dielectric constant (ϵ_r) at the beginning rises with temperature and at the transition temperature it reaches to the peak and then it decreases with further temperature rise and after certain temperature the dielectric constant becomes independent of temperature. Which might be because of the interaction of Bismuth ion of BiFeO_3 with diverse lattice site of $\text{Ba}_5\text{TbTi}_3\text{V}_7\text{O}_{30}$ and in the ionic radii mismatch of Fe^{3+} and V^{5+} (as the V^{5+} ionic radii is smaller than

Fe³⁺). The value of dielectric constant become more or less constant ($\epsilon_r \sim 148$). It may be inferred that after a certain temperature the addition of multiferroic BiFeO₃ doesn't change the properties of the solid solution and the material behaves as pure ferroelectric materials. It has been observed that for pure Ba₅TbTi₃V₇O₃₀ the dielectric constant (ϵ_{max}) is ~ 1100 . When $x=0.3$ i.e. 30% BiFeO₃ is added the dielectric constant reduces to the ~ 566 and when $x=0.5$ i.e. 50% BiFeO₃ is added the maximum dielectric constant is ~ 631 which further reduces to ~ 377 when $x=0.7$ i.e. 70% BiFeO₃ is added. It can also be inferred that even at the room temperature pure ferroelectric has higher dielectric constant ($\epsilon_{RT} \sim 671$) than that of maximum dielectrics of either of the composites.

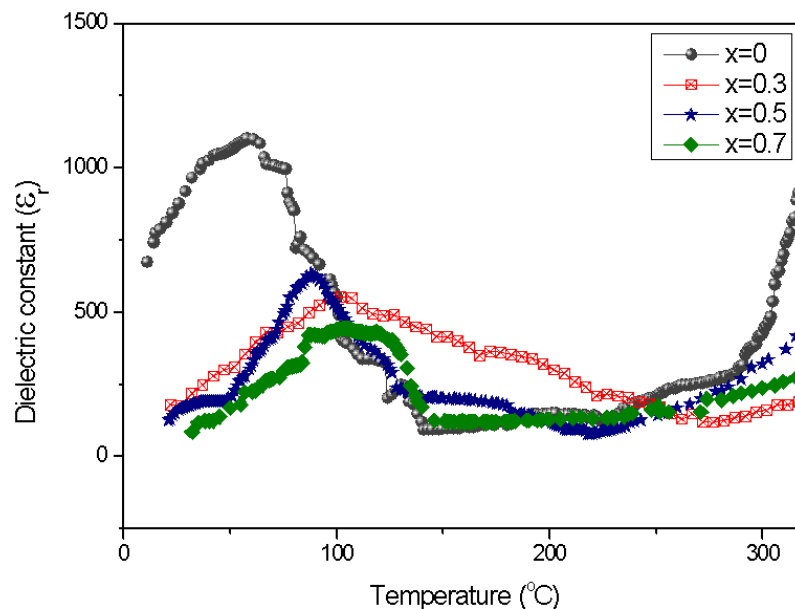


Fig. 4.6. Variation of ϵ_r with temperature for $(1-x)\text{Ba}_5\text{TbTi}_3\text{V}_7\text{O}_{30-x}\text{BiFeO}_3$ at 1 kHz.

The loss tangent ($\tan \delta$) variation with temperature for $(1-x)\text{Ba}_5\text{TbTi}_3\text{V}_7\text{O}_{30-x}\text{BiFeO}_3$ at 1kHz for the temperature range ($RT- 400^\circ\text{C}$) are shown in Fig. 4.7. It can be seen as the BiFeO₃ is introduced in the solid solution there is an increase in the dielectric loss ($\tan \delta$). By further increase in 'x' i.e. increasing BiFeO₃ content, there is an increase in the value of dielectric loss ($\tan \delta$), it may be due to semiconducting nature of BiFeO₃ which leads to high dielectric loss. For $x=0.3$, the dielectric loss is ~ 4.35 and it is maximum for $x=0.5$ i.e. ~ 6.76 . However, there is anomaly for $x=0.7$ i.e. ~ 3.67 , having moderate dielectric loss ($\tan \delta$), indicating dielectric loss also depends on structural change. The

value of $\tan \delta$ increases considerably at high temperature which might be because of the enhanced conductivity and also due to the decline in ferroelectric domain wall's contribution at higher temperatures (paraelectric phase).

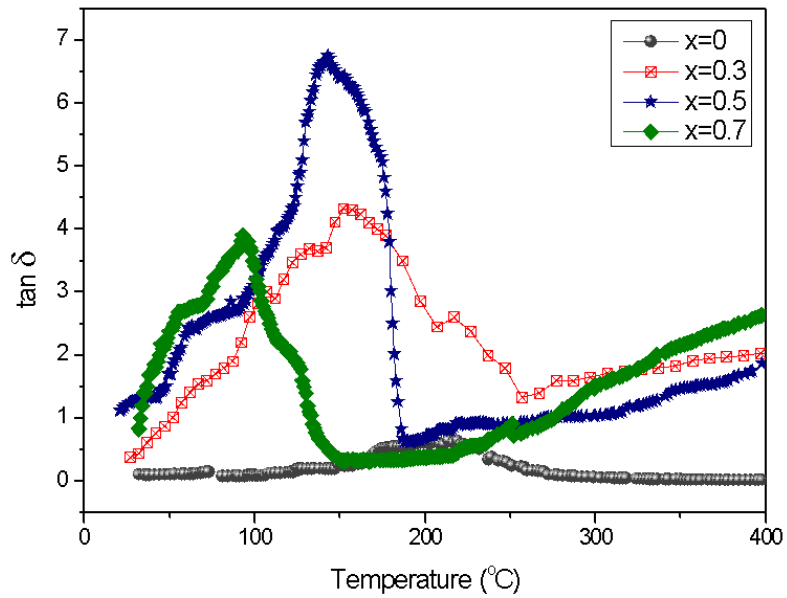


Fig. 4.7. Tangent loss with temperature for $(1-x)\text{Ba}_5\text{TbTi}_3\text{V}_7\text{O}_{30-x}\text{BiFeO}_3$ at 1 kHz.

Table 4.1. The Dielectric properties such as dielectric constant and dielectric loss are analysed for $(1-x)\text{Ba}_5\text{TbTi}_3\text{V}_7\text{O}_{30}-x\text{BiFeO}_3$ at 1kHz.

$(1-x)\text{Ba}_5\text{TbTi}_3\text{V}_7\text{O}_{30}-x\text{BiFeO}_3$	ϵ_{RT}	ϵ_{max}	$\tan \delta_{RT}$	$\tan \delta_{max}$	Transition Temp
$x= 0.7$	84	439	0.796	3.697	105
$x= 0.5$	157	631	1.232	6.762	88
$x=0.3$	172	566	0.52	4.35	103
$x= 0$	671	1100	0.133	0.610	83

(ii) **Group B: $(1-x)\text{Ba}_5\text{PrTi}_3\text{V}_7\text{O}_{30}-x\text{BiFeO}_3$**

Fig. 4.8. shows variation of dielectric constant ϵ_r with temp in a wide range (RT-500°C) for selected static or low frequency at 1000Hz in case of the composite for different values of x. It is seen that there is increase in dielectric constant (ϵ_r) with rise in temperature and reaches peak value at transition temperature, and then decreases. The existence of dielectric anomaly might be because of the contribution from both the long range migration and dipole orientation of charge species. Further, above T_c , after certain duration there is again rapid increase of the relative dielectric constant. This may be due to the reason that at higher temperatures space charge polarization predominates. The dielectric constant value keeps on increasing after a certain temperature, which may be because of the creation of space charge polarization at higher temperature. It has been observed that for pure $\text{Ba}_5\text{PrTi}_3\text{V}_7\text{O}_{30}$ the dielectric constant (ϵ_{max}) is ~ 377 and when BiFeO_3 is added the dielectric constant reduces from ~ 205 for $x= 0.3$ to ~ 121 when $x= 0.7$ i.e. 70% BiFeO_3 is added. It can also be inferred that even at the room temperature pure ferroelectric has higher dielectric constant ($\epsilon_{RT} \sim 194$) than that of maximum dielectrics of either of the composites.

Thus the dielectric property of BiFeO_3 is improved by mixing it with a pure ferroelectric material, $\text{Ba}_5\text{PrTi}_3\text{V}_7\text{O}_{30}$.

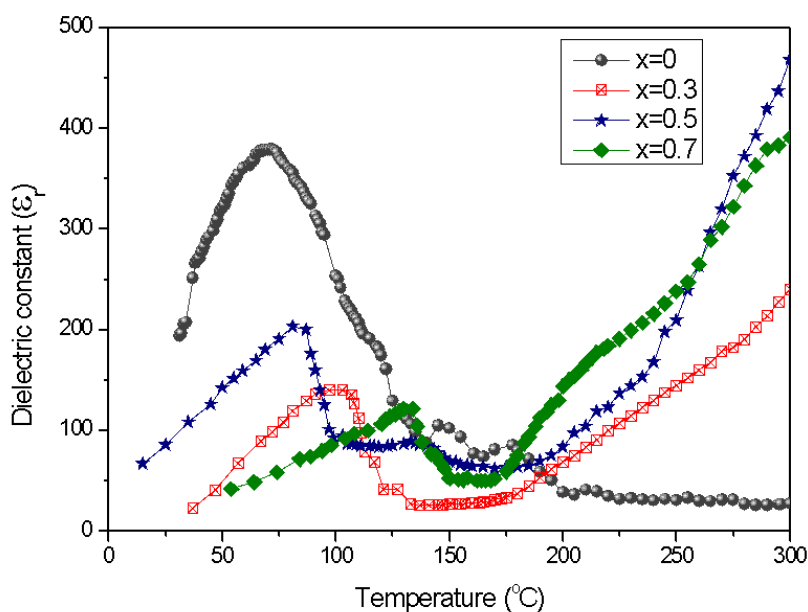


Fig. 4.8. Variation of ϵ_r with temperature for $(1-x)\text{Ba}_5\text{PrTi}_3\text{V}_7\text{O}_{30-x}\text{BiFeO}_3$ at 1 kHz.

The loss tangent ($\tan \delta$) variation with temperature for $(1-x)\text{Ba}_5\text{PrTi}_3\text{V}_7\text{O}_{30-x}\text{BiFeO}_3$ at 1kHz for the temperature range ($RT- 400^\circ\text{C}$) are shown in Fig. 4.9. It can be seen as the BiFeO_3 is introduced in the solid solution there is an increase in the dielectric loss ($\tan \delta$) it may be due it may be due to semiconducting nature of BiFeO_3 which leads to increased dielectric loss. When further 'x' is increased i.e. increasing BiFeO_3 content, there is further increase in the value of dielectric loss ($\tan \delta$). The $\tan \delta$ value of the solid solution was found to be very high at higher temperature, which may be because of the enhanced conductivity due to addition of BiFeO_3 , and indicates loss characteristic of the material.

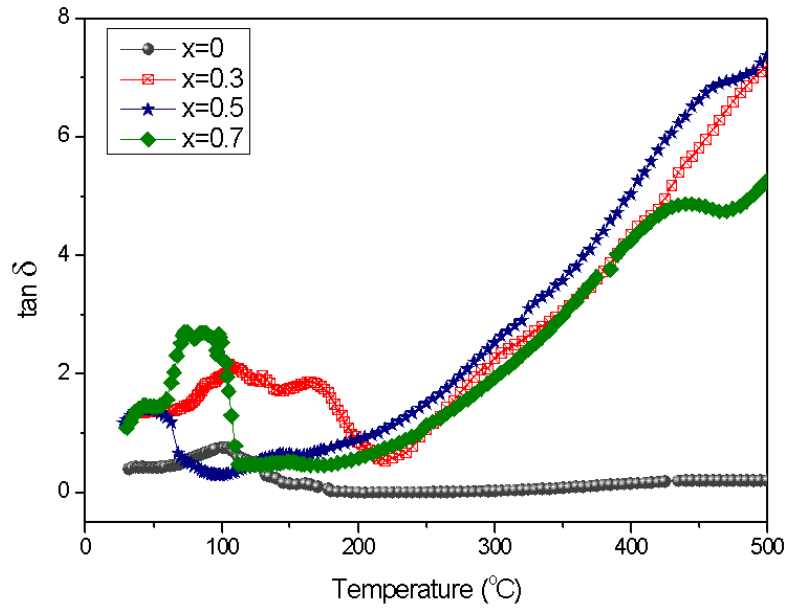


Fig. 4.9. Variation of $\tan \delta$ with temperature for $(1-x)\text{Ba}_5\text{PrTi}_3\text{V}_7\text{O}_{30}-x\text{BiFeO}_3$ at 1 kHz.

Table 4.2. The Dielectric properties such as dielectric constant and dielectric loss for

$(1-x)\text{Ba}_5\text{PrTi}_3\text{V}_7\text{O}_{30}-x\text{BiFeO}_3$ at 1 kHz.

$(1-x)\text{Ba}_5\text{PrTi}_3\text{V}_7\text{O}_{30}-x\text{BiFeO}_3$	ϵ_{RT}	ϵ_{max}	$\tan \delta_{\text{RT}}$	$\tan \delta_{\text{max}}$	T_c (°C)
x= 0.7	31	121	1.02	2.74	129
x= 0.5	22	141	0.59	2.19	99
x=0.3	86	205	1.07	1.39	84
x= 0	194	377	0.38	0.76	70

4.5 Conclusion

On the basis of above discussion on the dielectric and tangent loss of solid solution $(1-x)\text{Ba}_5\text{RTi}_3\text{V}_7\text{O}_{30}-x\text{BiFeO}_3$ for $x = 0, 0.3, 0.5, 0.7$; $R = \text{Pr, Tb}$. Following conclusion can be drawn:

- ❖ It has been found that both $\text{Ba}_5\text{PrTi}_3\text{V}_7\text{O}_{30}$ and $\text{Ba}_5\text{TbTi}_3\text{V}_7\text{O}_{30}$ are ferroelectrics in nature.
- ❖ The transition temperature of $\text{Ba}_5\text{PrTi}_3\text{V}_7\text{O}_{30}$ is less than that of $\text{Ba}_5\text{TbTi}_3\text{V}_7\text{O}_{30}$, also the maximum dielectric constant of $\text{Ba}_5\text{PrTi}_3\text{V}_7\text{O}_{30}$ is considerably lesser than that of $\text{Ba}_5\text{TbTi}_3\text{V}_7\text{O}_{30}$. It may be because of the difference in Ionic radius of the rare earth element. The ionic radius of Praseodymium (Pr) is 1.13 Å and ionic radius of Terbium (Tb) is 1.18 Å. The smaller ionic radius of Pr might increase the mobility of ions which increases the conductivity thus decreasing the dielectric constant.
- ❖ At the lower temperature range $\text{Ba}_5\text{PrTi}_3\text{V}_7\text{O}_{30}$ has more tangent loss than $\text{Ba}_5\text{TbTi}_3\text{V}_7\text{O}_{30}$. It may be because of the more mobility of charge carriers, and there is an increase in cross section collisions, thus more tangent loss.
- ❖ At the higher temperature range the tangent loss of $\text{Ba}_5\text{TbTi}_3\text{V}_7\text{O}_{30}$ is more than $\text{Ba}_5\text{PrTi}_3\text{V}_7\text{O}_{30}$. It may be because of the reason that the heavier charge carrier is more prominent in high temperature, thus increase in tangent loss.
- ❖ $\text{Ba}_5\text{TbTi}_3\text{V}_7\text{O}_{30}$ has been found to be better ferroelectrics than $\text{Ba}_5\text{PrTi}_3\text{V}_7\text{O}_{30}$.
- ❖ The solid solution $(1-x)\text{Ba}_5\text{RTi}_3\text{V}_7\text{O}_{30}-x\text{BiFeO}_3$ (where $R = \text{Pr, Tb}$) for all values of x i.e. $x = 0, 0.3, 0.5, 0.7$; shows ferroelectric properties.
- ❖ In $\text{Ba}_5\text{RTi}_3\text{V}_7\text{O}_{30}$ (where $R = \text{Pr, Tb}$) with the addition of BiFeO_3 content in the solid solution there is reduction in dielectric constant and at the same time increase in tangent loss. It may be due to the reason that addition of different phase results into change in morphotropic phase boundary. With the further increase in the BiFeO_3 in solid solution there is decrease in dielectric constant and increase in the tangent loss. It may be due to the reason that BiFeO_3 is semiconducting in nature, due to which the conduction in the solid solution increases.
- ❖ For $x=0.5$ in solid solution $(1-x)\text{Ba}_5\text{TbTi}_3\text{V}_7\text{O}_{30}-x\text{BiFeO}_3$ the dielectric constant is slightly increased in comparison to its neighbor $x=0.3$. It is due to

transformation of structure from orthorhombic to monoclinic. Again the dielectric constant decreases considerably for $x=0.7$ (which may be due to increase in BiFeO_3 content).

- ❖ The ferroelectric property of BiFeO_3 is improved by the effect of $\text{Ba}_5\text{RTi}_3\text{V}_7\text{O}_{30}$ (where $R = \text{Pr, Tb}$).

CHAPTER V
ELECTRICAL CONDUCTIVITY STUDY

5.1. Introduction

In dielectrics, electrical conduction is because of the ordered movement of weak bound charge species under the influence of an external applied electric field. The electrical conduction in dielectric refers generally to amorphous and polycrystalline materials. The essential factor by which the conduction process is measured is called electrical conductivity. For physical study of ferroelectrics, the study of nature of electrical conductivity becomes imperative. Solid may be categorized chiefly as electronic or ionic conductor depending on which charge carrier is dominant i.e. holes/electrons or anions/cations. The ferroelectric and non-linear dielectric crystals mainly exhibit ionic conduction. Distinct electric polarization is being observed only in crystals of oxygen octahedral, ferroelectrics Barium Titanate (BaTiO_3), it is due to the occurrence of oxygen defects or vacancy in the structure. In ionic crystals, electrical conduction is owing to the movement of ions of the host in the crystal lattice due to the external electric field. Such a category of conduction is known as intrinsic conduction which occurs at high temperature. Ions are responsible for electrical conduction in such ionic crystals. They also include impure ions beside ions at defect sites, which give rise to impurity or extrinsic conduction with high conductivity and low activation energy. In actual crystals, the electrical conductivity is mostly due to intrinsic conduction but at low temperature the main contributor is extrinsic. The relation between conductivity (σ) with temperature can be illustrated as [1]:

$$\sigma = A_1 e^{\frac{-E_g}{kT}} + A_2 e^{\frac{-E_x}{kT}}$$

Where, E_g and E_x are activation energy for intrinsic band gap and extrinsic impurity level conduction respectively. At high temperature, the intrinsic conduction is a major contributor over the extrinsic one. Hence, the above expression trims down to:

$$\sigma = A_1 e^{\frac{-E_g}{kT}}$$

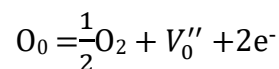
In the restraining case the electrical conductivity is linked with impurities. The electrical conduction robustly increases by introduction of rare-earth ions in TB niobates.

AC conductivity

On the application of an alternating emf(V) across the condenser, a current of alternating nature will flow across it having value; $i=j\omega\epsilon C_0V$ given that the dielectric is ideal[2]. Current having in-phase component will appear in corresponds to the resistive current of the condenser plates. These currents are wholly because of the dielectric medium and are also a property. Such dielectric conductivity is called AC conductivity and it can be inferred from the real part of current density passing through it. AC conductivity can be expressed by using the dielectric data [3] i.e. $\sigma = \omega\epsilon\epsilon_0\tan\delta$.

Activation energy is calculated by using the relation $\sigma = \sigma_0 e^{\frac{-E_a}{kT}}$ [1]. The stated relation is consequential when the main contributor to the loss tangent of crystal is the pure charge transport. In polycrystalline materials, dielectric loss is comparatively high, indicative of the involvement of various kinds of loss mechanism, like the existence of porosity resulting in a parallel conduction. It is not easy to isolate the pure charge transport mechanism from the effect of loss contributed by a diverse loss mechanism. Hence, the conductivity relation given is an approximate at the regions where the dissipation factor is relatively high, and is more realistic at temperature where the loss tangent is substantially low.

In pure state of the specimen, the V ion has 5+ valence and functions as an insulator having little tangent losses. During the calcination and sintering process, charge carriers (holes and electrons) and oxygen vacancies are created, which also contributes to a complex conduction mechanism. Using Kröger-Vink notations, the presence of oxygen vacancies are represented by the thermally activated reaction [4]:



In the reaction when the electron is being liberated, it is captured by the V^{5+} ions leading to formation of V^{4+} according to the reaction $V^{5+} + e^- \rightarrow V^{4+}$. This leads to hopping of electrons between V^{4+} and the V^{5+} ions, and increases the conductivity [4]. Similarly, via oxidation-reduction serial process there is a transport of charge by hopping of an electron between the V ions in the structural chain $V^{4+}-O-V^{5+}$. Thus, V^{4+} acts as donor centres enhancing extrinsic conduction of n-type. Concurrently, the existence of vacancies of oxygen (V_0'') aids the creation of acceptor or holes centres at the A site. The

existence of holes results in p-type conductivity. Two other conduction mechanisms are linked to the ferroelectric materials. First, during the increase of temperature (but below the ferro-paraelectric transition), lattice gets strained which is due to order-disorder changes and induces the conduction of polarons (interaction of hole and/or electron-phonon), where the carrier are being transported by hopping of the charges. Second, an ionic conductivity in ferroelectric materials is intrinsic in nature and usually the conduction mechanism takes place only at high temperature. Mechanism for the electrical conductivity in the above stated are thermally activated and follows Arrhenius behaviour according to the equation: $\sigma_a = \sigma_0 e^{\frac{-E_a}{kT}}$ (symbols having their usual meanings) in a given temperature range [5].

5.2. Experimental

Using HIOKI-IM3536 the dielectric factors i.e. relative dielectric constant (ϵ_r) and dielectric loss ($\tan \delta$), of the sample is measured for frequency range 4Hz-8MHz and at temperature are range 250 – 773 K. Conductivity is measured using the formula $\sigma = \omega \epsilon \epsilon_0 \tan \delta$.

5.3 Result and Discussion

5.3.1. AC conductivity variation with inverse absolute temperature at 1000 Hz

The dielectrics data are used in the given equation to analyse. The variation of ac conductivity ($\ln \sigma$) over a broad temperature range supports that the material has thermally activate transport properties obeying Arrhenius equation. The graph can be divided into different regions having different slopes representing the different conduction mechanisms in correspond to their activation energy values. The abnormal conductivity is observed for the compound in the vicinity of its Curie temperature, which may be type of order-disorder nature and the readjustment of the lattice during the phase transition.

Group A: $(1-x)\text{Ba}_5\text{TbTi}_3\text{V}_7\text{O}_{30}-x\text{BiFeO}_3$

Fig. 5.3.1 shows the variation of ac conductivity ($\ln \sigma$) with temperature ($1/T$) of the solid solution $(1-x)\text{Ba}_5\text{TbTi}_3\text{V}_7\text{O}_{30}-x\text{BiFeO}_3$ for all values of x (i.e. $x=0$, $x=0.3$, $x=0.5$, $x=0.7$) at frequency of 1 kHz. Because of the dielectric phase transition, abnormality in conductivity is observed at above their respective transition temperature (T_c).

For $x=0$, i.e. $\text{Ba}_5\text{TbTi}_3\text{V}_7\text{O}_{30}$, the graph can be divided in two regions I, II with different slopes indicating the presence of one paraelectric region named as II and one ferroelectric region as I. There is a change in slope on both sides of this transition. There is anomaly at higher temperature which may be due to anomalous variation of the loss tangent of the compounds in that region. AC conductivity first increases with increase in temperature, and shows the negative coefficient of resistance (NCRT) behavior then it decreases at the similar region of transition around $T_c \sim 356$ K for $\text{Ba}_5\text{TbTi}_3\text{V}_7\text{O}_{30}$. The change in conductivity may be due to change in phase i.e. from ferro to para and after a certain temperature the conductivity further increases with rise in temperature. It may be concluded that the conduction mechanism is due to the hopping of charge carriers.

For $x=0.3$, i.e. $0.7\text{Ba}_5\text{TbTi}_3\text{V}_7\text{O}_{30}-0.3\text{BiFeO}_3$ the graph can be divided into three regions, one paraelectric region (III) and two ferroelectric regions (I, II) characterized by three different slopes and activation energy. In the ferroelectric region there is an increase in activation energy in comparison to $x=0$, which may be due to increase in BiFeO_3 content, which might increase the conduction in the solid solution which subsequently results in more dielectric loss and low dielectric constant.

For $x=0.5$, i.e. $0.5\text{Ba}_5\text{TbTi}_3\text{V}_7\text{O}_{30}-0.5\text{BiFeO}_3$ the graph can be divided into three regions, one paraelectric region (III) and two ferroelectric regions (I, II) characterized by three different slopes and activation energy. In the region III, the main contribution to the conductivity may be due to space charges.

For $x=0.7$, i.e. $0.3\text{Ba}_5\text{TbTi}_3\text{V}_7\text{O}_{30}-0.7\text{BiFeO}_3$, the graph can be divided into three regions, one paraelectric region (III) and two ferroelectric regions (I, II) characterized by three different slopes and activation energy. As the temperature increases there is onset of an intrinsic conductivity mechanism [6].

In the ferroelectric regions with increase in temperature the ac conductivity also increases and shows the negative temperature coefficient of resistance (NTCR) behaviour which is normal behaviour of ferroelectric materials. It is being observed that average activation energy increases from 0.05eV for pure ferroelectric $\text{Ba}_5\text{TbTi}_3\text{V}_7\text{O}_{30}$ to 0.193eV for $0.5\text{Ba}_5\text{TbTi}_3\text{V}_7\text{O}_{30}-0.5\text{BiFeO}_3$ to 0.629 for $0.3\text{Ba}_5\text{TbTi}_3\text{V}_7\text{O}_{30}-0.7\text{BiFeO}_3$. The increase in the activation energy may be due to increases in BiFeO_3 content which may be due to the increase in the conduction in the solid solution which subsequently results in more dielectric loss and low dielectric constant.

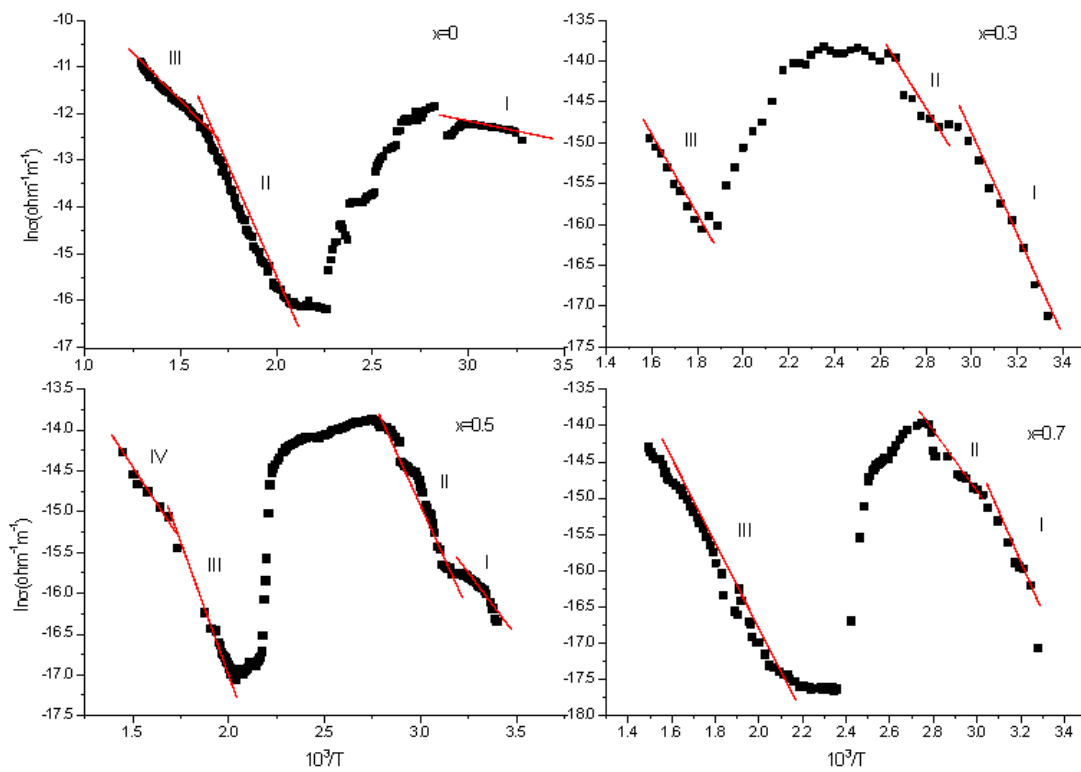


Fig 5.3.1. Variation of $\ln\sigma_{ac}$ with $10^3/T$ of $(1-x)\text{Ba}_5\text{TbTi}_3\text{V}_7\text{O}_{30}-x\text{BiFeO}_3$ ($x= 0, 0.3, 0.5, 0.7$) at 1 kHz.

(i) **Group B: $(1-x)\text{Ba}_5\text{PrTi}_3\text{V}_7\text{O}_{30}-x\text{BiFeO}_3$**

Fig. 5.3.2 shows the variation of ac conductivity ($\ln \sigma$) with temperature ($1/T$) of the solid solution $(1-x)\text{Ba}_5\text{PrTi}_3\text{V}_7\text{O}_{30}-x\text{BiFeO}_3$ for all x (i.e. $x=0$, $x=0.3$, $x=0.5$, $x=0.7$) values at frequency of 1 kHz. Because of dielectric phase transition, abnormality in values of conductivity is being observed equal to or near to their respective transition temperature (T_c).

For $x=0$, i.e. $\text{Ba}_5\text{PrTi}_3\text{V}_7\text{O}_{30}$, the graph can be divided in three regions I, II with different slopes indicating the presence of one paraelectric region named as III and two ferroelectric regions as I and II. There is a change in slope on both sides of this transition. The variation of σ_{ac} over a broad range of temperature shows that the material has thermally activated processes which might be because of the existence of low temperature immobile species, and high temperature defects. The low values of activation energy may be due to reason that the energy of small amount is necessary to activate the electrons/carriers for an electrical conduction. Similar pattern in variation of ac conductivity was found in some material of similar kind [7].

For $x= 0.3$, i.e. $0.7\text{Ba}_5\text{PrTi}_3\text{V}_7\text{O}_{30}-0.3\text{BiFeO}_3$, the graph can be divided into four regions, three paraelectric regions (II, III, IV) and one ferroelectric region (I) characterized by three different slopes and activation energy. The conductivity is high at higher temperature, which is a general behaviour for dielectric ceramics.

For $x= 0.5$, i.e. $0.5\text{Ba}_5\text{PrTi}_3\text{V}_7\text{O}_{30}-0.5\text{BiFeO}_3$, the graph can be divided into three regions, two paraelectric regions (III, IV) and two ferroelectric regions (I, II). The variation of slope in different temperatures indicates that there is a presence of different types of conduction mechanisms. Hence, have different values of activation energy.

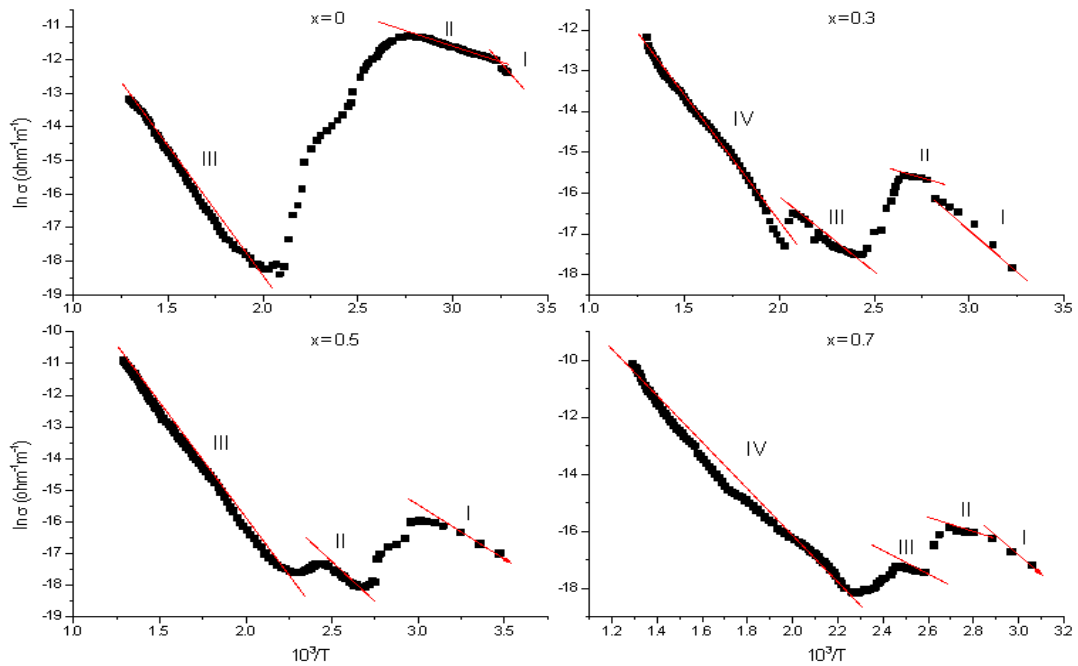


Fig. 5.3.2. Variation of $\ln \sigma_{ac}$ with $10^3/T$ of $(1-x)\text{Ba}_5\text{PrTi}_3\text{V}_7\text{O}_{30-x}\text{BiFeO}_3$ ($x = 0, 0.3, 0.5, 0.7$) at 1 kHz.

For $x = 0.7$, i.e. $0.3\text{Ba}_5\text{TbTi}_3\text{V}_7\text{O}_{30}-0.7\text{BiFeO}_3$, the graph can be divided into four regions, three paraelectric regions (I, II, III) and one ferroelectric region (IV) characterized by three different slopes and activation energy.

The values of E_a in different regions are calculated from Arrhenius equation and summarized in Table 5.1. The conductivity is high at higher temperature, which is a general phenomena for most of the dielectric materials [7,8]. The variation of σ_{ac} over a broad temperature range shows that the material has properties of thermally activated transport which might be because to the existence of low temperature immobile species, and presence of defects at high temperatures. It can be concluded from the activation energy that energy of small amount is essential to activate the electrons/charge carriers for conduction. Pattern of Similar kind was observed in some other materials of same kind [7].

Table 5.1 Comparison of Activation energy E_a (eV) of $(1-x)\text{Ba}_5\text{RTi}_3\text{V}_7\text{O}_{30}-x\text{BiFeO}_3$ multiferroics at 1000kHz, where $x = 0,0.3,0.5,0.7$ and $R= \text{Tb, Pr}$ calculated for $\ln\sigma_{ac}$ vs. $1/T$ graphs.

R	X	Compounds	E_a (eV)			
			I	II	III	IV
Tb	0	$\text{Ba}_5\text{TbTi}_3\text{V}_7\text{O}_{30}$	0.05	0.713	0.337	-
	0.3	$0.7\text{Ba}_5\text{TbTi}_3\text{V}_7\text{O}_{30}-0.3\text{BiFeO}_3$	0.472	0.341	0.434	-
	0.5	$0.5\text{Ba}_5\text{TbTi}_3\text{V}_7\text{O}_{30}-0.5\text{BiFeO}_3$	0.193	0.476	0.451	0.315
	0.7	$0.3\text{Ba}_5\text{TbTi}_3\text{V}_7\text{O}_{30}-0.7\text{BiFeO}_3$	0.629	0.308	0.421	-
Pr	0	$\text{Ba}_5\text{PrTi}_3\text{V}_7\text{O}_{30}$	0.480	0.149	0.638	-
	0.3	$0.7\text{Ba}_5\text{PrTi}_3\text{V}_7\text{O}_{30}-0.3\text{BiFeO}_3$	0.361	0.058	0.286	0.424
	0.5	$0.5\text{Ba}_5\text{PrTi}_3\text{V}_7\text{O}_{30}-0.5\text{BiFeO}_3$	0.214	0.267	0.617	-
	0.7	$0.3\text{Ba}_5\text{PrTi}_3\text{V}_7\text{O}_{30}-0.7\text{BiFeO}_3$	0.463	0.138	0.159	0.666

5.4. Conclusions

- The slopes of the graph ($\ln\sigma$ vs $10^3/T$) indicate the occurrence of diverse types of conduction mechanism which is related to the corresponding activation energy values.
- A linear variation of σ_{ac} over an extensive range of temperature suggests the transport properties are thermally activated obeying Arrhenius behaviour.
- The conductivity was observed in the vicinity of its transition (Curie) temperature, which may be due to type of order-disorder nature and could be accredited to the rearrangement of the lattice in the ferro-paraelectric phase transition.
- The increase in the values of E_a may be due to the hopping charge mechanism mainly associated with oxidation-reduction route through the chain and its combinations is consistent with the behaviour at low temperature and the degree of structural ordering.

- The ac conductivity plot shows that when temperature is increased, the conductivity values also increases. Thus, shows a negative temperature coefficient of resistance (NTCR) like semiconductors.
- In lower temperature ferroelectric regions with the increase in temperature there is increase in the activation energy which can be ascribed to the creation of polarons prompted by the interaction of hole and/or electron-phonon which is increased by deformation of structure during the phase transition.
- The occurrence of polarons in these regions is ascribed to the diffusive nature of the system. Whereas at higher temperature ($>T_c$), nano and micro regions are present in ferroelectric regions.
- At higher temperature, Vanadium (i.e., V^{4+} - V^{5+}) variable valence state may results into creation of oxygen ion vacancy which might add to the process of conduction. The conductivity is of mixed type (i.e., space charge and ionic-polaronic) [7,8].
- BiFeO_3 has a semiconducting property which increases the conduction in the solid solutions.
- The activation energy of the solid solution increases with the increase in the content of BiFeO_3 in solid solution.
- The ferroelectric properties of BiFeO_3 has been improved by the effect of $\text{Ba}_5\text{TbTi}_3\text{V}_7\text{O}_{30}$

CHAPTER VI
MAGNETIC STUDY

6.1. Introduction

Ferromagnetic materials have a domain structure, similar to that of the domain structure of ferroelectric materials. In each domain the spins are aligned parallel but unless the material is in the saturation condition, different domains have different spin orientation.

The response of ferromagnetic materials to an applied magnetic field is analogous to that of ferroelectric in an applied electric field. A hysteresis loop occurs in the plot of magnetization, M , or induction, B , against the applied field, H . At significantly high fields the saturation magnetization condition is achieved when the spins of all the domains are parallel. During the process of magnetization and demagnetization in all alternative magnetic fields, energy is dissipated, usually as heat. During one full cycle the amount of energy (i.e. hysteresis loss) is in proportion to the area of the hysteresis loop. For certain applications, low loss materials are required, one essential condition for which is that the area encompassed by the hysteresis should be as small as possible. Magnetically soft materials have a low coercivity, H_c . The coercivity is the strength of reverse field required to have demagnetization. Soft materials also have high permeability and hence a hysteresis loop has a small area and has a narrow waist. Magnetically hard materials have a high coercivity and high remanent magnetization, M_r . Remanent magnetization is the residue of magnetization that remains when the applied external magnetic field is turned off. Since magnetically hard materials cannot be easily demagnetized, therefore they could be used as permanent magnet.

In ferromagnetic materials the exchange interaction forces neighbouring spins to be parallel resulting in ferromagnet. There are also certain cases where depending on how the atom interacts in the magnetic material; it is also possible that the spins of each magnetic atom may also prefer the opposite of the neighbours. The exchange interaction favours antiparallel alignment and, in this occasion, the material becomes antiferromagnetic, where neighbouring spins are arranged antiparallel to each other. In the 1930s the French physicist Louis Neel first suggested the idea and the configuration are also referred to as the Neel state.

There is a new family of material which combines the electric and magnetic properties. This family of material is called as multiferroics because it combines different types of 'ferro' order: ferroelectricity (alignment of electric dipoles), ferromagnetism (alignment of magnetic moments) and possibly ferroelasticity (alignment of elastic deformation). The prefix 'ferro' even though is derived from Latin *ferrum* for iron; it does not describe the spontaneous alignment of various physical properties, which is reminiscent of the spontaneous alignment of magnetic moments in Fe (iron).

The different properties of the multiferroics often interact with each other. It is possible to switch the magnetic order state using electric fields and electrically order states using magnetic fields. The magnetically ordered state is good for storing information, but in application magnetic fields are more complicated to control those states. However, electric voltage is relatively easy to apply at microscopic level; therefore an electrically controlled magnetic state is very useful. Electrical control can be achieved because the electric voltages can switch the ferroelectric state which interacts with the magnetic state and thus causing it to switch on too.

Since the discovery of multiferroic material BiFeO_3 [1], many such materials have been studied which show both ferroelectricity and ferromagnetism in single phase. An electric polarization can be induced by applying an external magnetic field and magnetization can be induced by an external electric field in this material [2]. Due to this unique property these materials have potential applications in magnetic as well as ferroelectric devices [3] such as dual storage devices, ferromagnetic resonance devices controlled by an electric field and transducers with magnetically modulated Piezoelectrics [4].

Mahesh *et. al.* have reported phase pure BiFeO_3 ceramics [5] with the frequency independent Neel temperature (T_N) at around 653K [6]. It has a rhombohedral distorted perovskites structure with the space group $R3c$ [7, 8]. There are reports on the modification of magnetic (Neel temperature, T_N) properties of BiFeO_3 by addition of niobate ferroelectrics [9, 10]. It has also been observed that the magnetic order parameters in BiFeO_3 can be improved by employing the solid solution technique with ferroelectric compounds [11]. $\text{Ba}_5\text{RTi}_3\text{V}_7\text{O}_{30}$ is one such kind of ferroelectrics compound with high dielectric constant and low dielectric loss [12].

This work focuses on the modulation of the magnetic properties of BiFeO_3 by mixing with the ferroelectric materials $\text{Ba}_5\text{TbTi}_3\text{V}_7\text{O}_{30}$. The final composite $(1-x)\text{Ba}_5\text{RTi}_3\text{V}_7\text{O}_{30}-x\text{BiFeO}_3$ ($x = 0, 0.3, 0.5, 0.7$ and 1.0 : where $R = \text{Tb, Pr}$) are synthesized and systematically studied their magnetic properties to achieve better magnetic properties in these material for certain value of x .

6.2. Experimental

The Magnetic measurement of the solid solution is done by using a Physical Property Measurement System (PPMS: Quantum Design, San Diego, USA) Vibrating Sample Magnetometer (VSM) at a wide temperature range of (10-350 K) which is already described in the Methodology. Hysteresis (M-H) loops are reported at room temperature (300 K).

6.3. Magnetization studies

Group A: $(1-x)\text{Ba}_5\text{TbTi}_3\text{V}_7\text{O}_{30-x}\text{BiFeO}_3$ for $x = 0, 0.3, 0.5, 0.7$ and 1.0

The relation between magnetic moment M (emu/g) vs. temperature for $x = 0.3, 0.5, 0.7$ are depicted in Fig.6.3.1. It is being observed that the magnetic moment decreases as the temperature increases, which is as per an expected trend. Magnetization increases with the decrease in the content of BiFeO_3 in the composite. Also, at around ~ 230 K there is a kink, indicating development of local weak ferromagnetism.

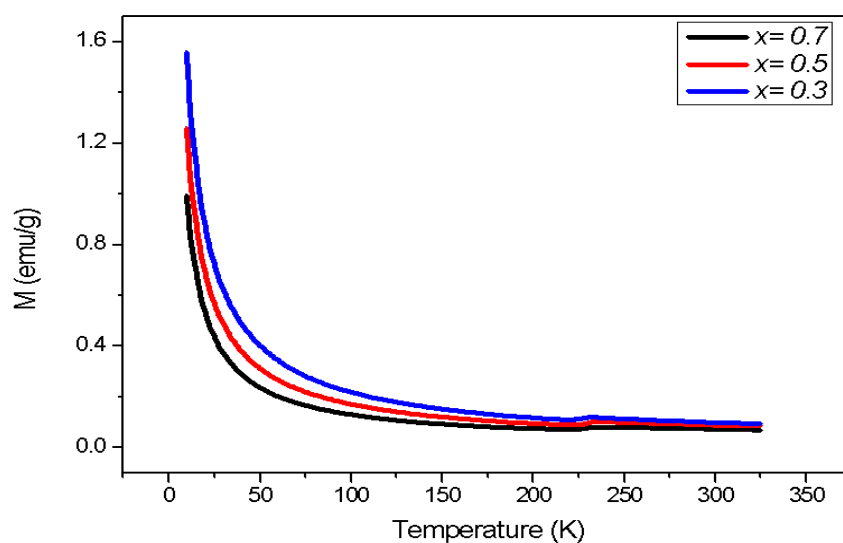


Fig. 6.3.1 Variation of Magnetization, M (emu/g) w.r.t. Temp of $(1-x)\text{Ba}_5\text{TbTi}_3\text{V}_7\text{O}_{30-x}\text{BiFeO}_3$.

Fig. 6.3.2 is plot between the inverse of susceptibility ($1/\chi$) and temperature which shows that the extrapolation of the straight line makes an almost zero intercept on the x- axis (temperature axis) which indicates the samples have nearly perfect antiferromagnetic order. However, there is sharp change of slope after ~ 222 K (the slope makes positive intercept in x-axis and after about ~ 239 K, it makes negative intercept) which indicates that there is development of local ferromagnetism and canted antiferromagnetism[14].

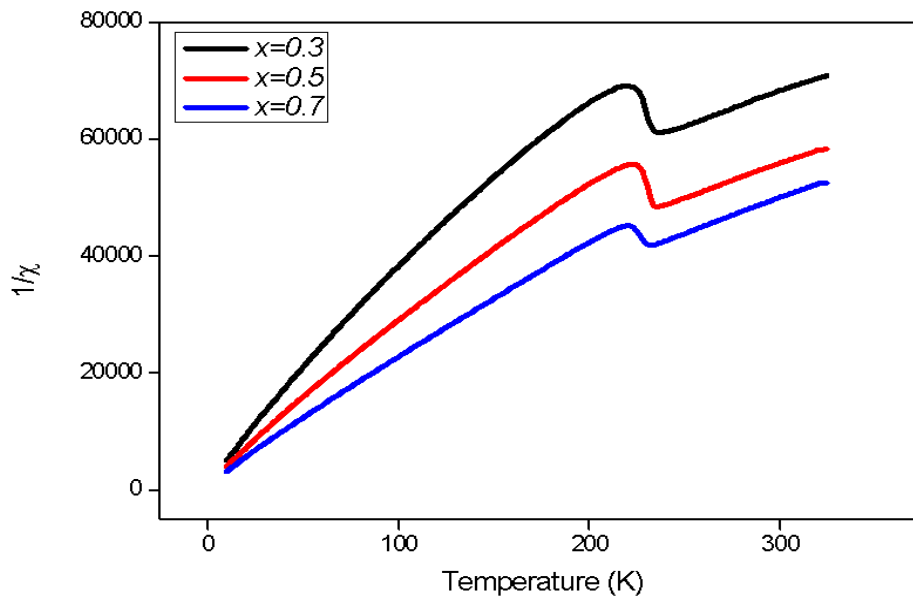


Fig. 6.3.2 Variation of Susceptibility with Temperature for $(1-x)\text{Ba}_5\text{TbTi}_3\text{V}_7\text{O}_{30-x}\text{BiFeO}_3$.

Fig. 6.3.3 shows the hysteresis curves for pure BiFeO_3 (i.e. $x=1$ in the composite). The curve does not saturate which indicates typical anti-ferromagnetic behaviour [15]. There is appearance of hysteresis loop in pure BiFeO_3 having low value of $H_c \sim -65$ Oe and $M_r \sim 8.5068 \cdot 10^{-4}$ emu/g suggesting that it is a weak ferromagnetic in nature [13]. The appearance of hysteresis loops may be because of canting of an antiferromagnetic order of Fe-O-Fe chains of spins results into weak spontaneous magnetic moments. The low values of magnetization and non-saturation even at high magnetic fields may be due to uncompensated antiferromagnetism.

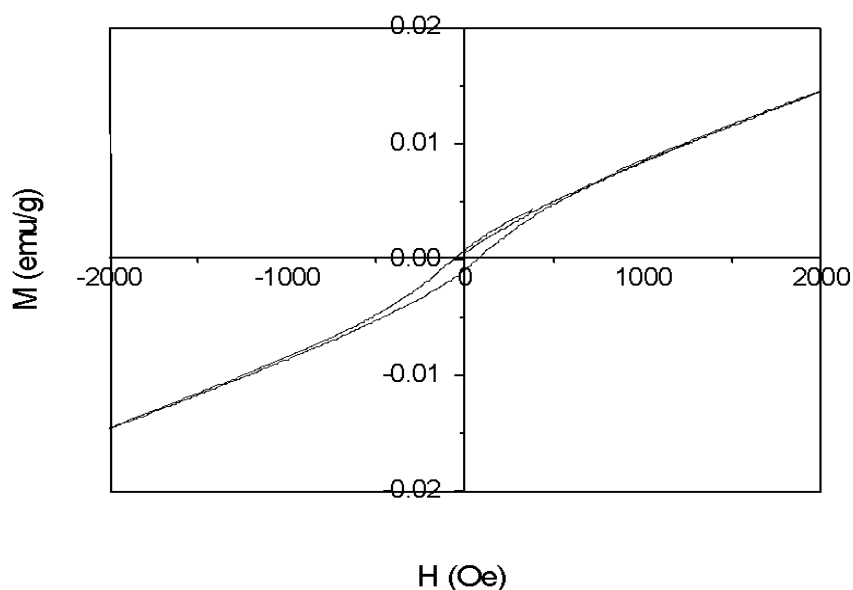


Fig. 6.3.3 M-H hysteresis loops for BiFeO₃ at 300 K.

Fig. 6.3.4 shows the M-H curves for the composite $(1-x)\text{Ba}_5\text{TbTi}_3\text{V}_7\text{O}_{30} - x\text{BiFeO}_3$ at 300 K (for $x = 0.7, 0.5, 0.3$ and 0). From table I, it can be seen that addition of $\text{Ba}_5\text{TbTi}_3\text{V}_7\text{O}_{30}$ in pure BiFeO_3 ; there is an increase in the spontaneous magnetic moment and hence there is the appearance of hysteresis loop. It shows that there is development of parallel spin clusters or canting spins in an antiferromagnetic material. It may be due to distortion in the perovskite layers of superstructure of pure BiFeO_3 which results in magnetic anisotropy and canting of spin structure of the compound. As a result local ferromagnetism or weak antiferromagnetism is developed increasing ferromagnetic order. For $x = 0.7$ (70% BiFeO_3 and 30% $\text{Ba}_5\text{TbTi}_3\text{V}_7\text{O}_{30}$) there is maximum magnetization i.e. $M_r = 180.57 \cdot 10^{-4}$ emu/g and $H_c = -1206$ Oe. Thus the Hysteresis loop is most developed. However, with further decrease in BiFeO_3 , magnetization decreases. Finally, for $x=0$ (pure $\text{Ba}_5\text{TbTi}_3\text{V}_7\text{O}_{30}$) the graph is linear with $M_r = 0$ and $H_c = 0$. It is because pure $\text{Ba}_5\text{TbTi}_3\text{V}_7\text{O}_{30}$ is paramagnetic in nature.

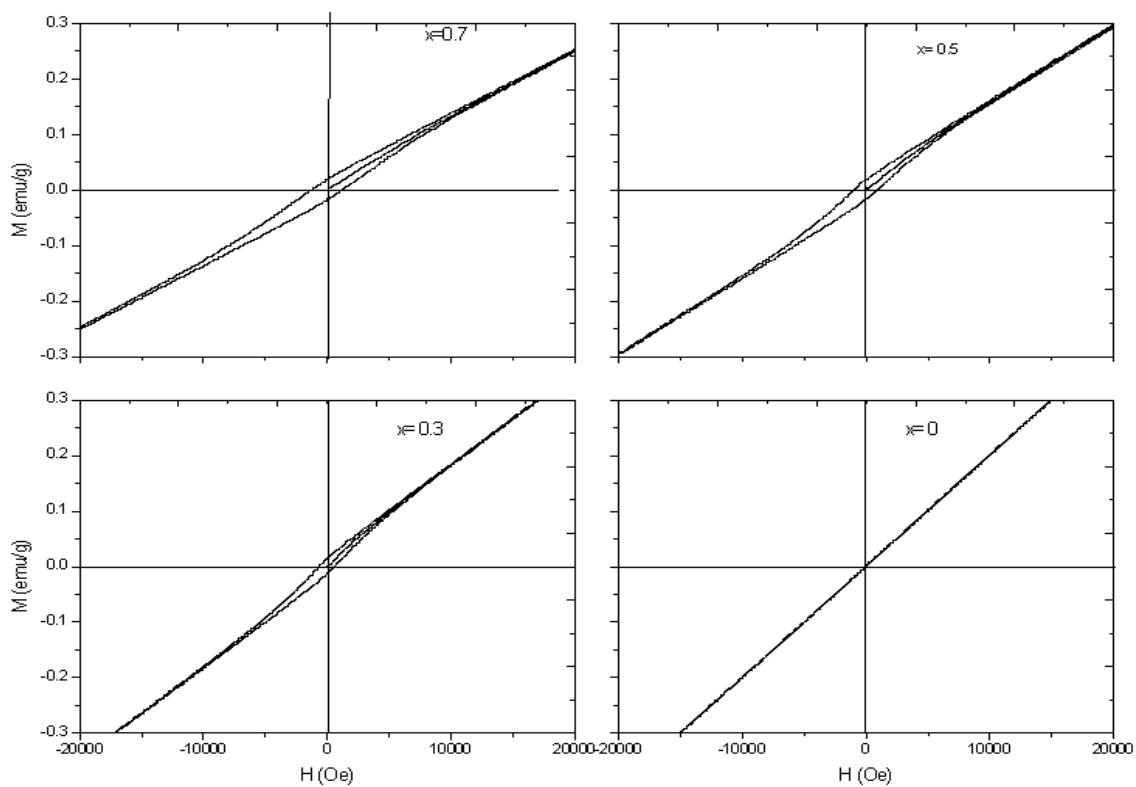


Fig. 6.3.4: M-H hysteresis loops for $(1-x)\text{Ba}_5\text{TbTi}_3\text{V}_7\text{O}_{30-x}\text{BiFeO}_3$ at 300 K.

Group B: $(1-x)\text{Ba}_5\text{PrTi}_3\text{V}_7\text{O}_{30}-x\text{BiFeO}_3$ for $x = 0, 0.3, 0.5,$ and 0.7 .

Fig. 6.3.5 shows the Hysteresis loop of $(1-x)\text{Ba}_5\text{PrTi}_3\text{V}_7\text{O}_{30}-x\text{BiFeO}_3$ for $x = 0, 0.3, 0.5$ and 0.7 at the room temperature (300 K). It can be seen that as the BiFeO_3 content in the solid solution is increased the loop starts appearing. From Table 6.1 it can be seen that the Remanence ($M_r = 118.4 \cdot 10^{-4}$ emu/g) is maximum for $x=0.3$ i.e. $0.7\text{Ba}_5\text{PrTi}_3\text{V}_7\text{O}_{30}-0.3\text{BiFeO}_3$ and Coercivity ($H_c = -1206$ Oe) is maximum for $x=0.7$ i.e. $0.3\text{Ba}_5\text{PrTi}_3\text{V}_7\text{O}_{30}-0.7\text{BiFeO}_3$.

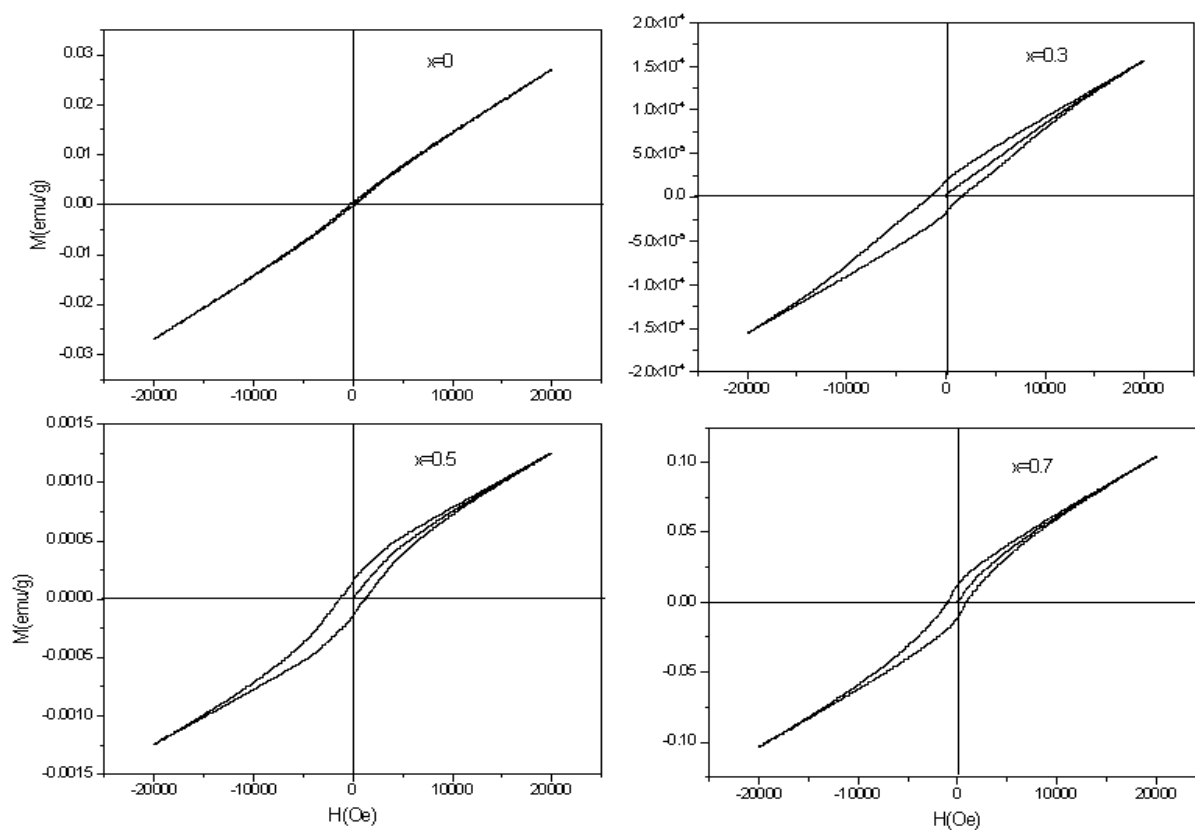


Fig. 6.3.5. M-H hysteresis loops for $x\text{BiFeO}_3-(1-x)\text{Ba}_5\text{PrTi}_3\text{V}_7\text{O}_{30}$ at 300 K.

Table 6.1 The values of the parameters obtained for $(1-x)\text{Ba}_5\text{RTi}_3\text{V}_7\text{O}_{30}-x\text{BiFeO}_3$ at 300 K.

$(1-x)\text{Ba}_5\text{RTi}_3\text{V}_7\text{O}_{30}-x\text{BiFeO}_3$		H_c (Oe)	$M_r(10^{-4}\text{emu/g})$
R=Tb	$x=1$	-65	8.5068
	$x=0.7$	-1206	180.57
	$x=0.5$	-966	173.94
	$x=0.3$	-612	139.99
	$x=0$	0	0
R=Pr	$x=1$	-65	8.5068
	$x=0.7$	-1527	18.00
	$x=0.5$	-1223.92	1.4918
	$x=0.3$	-964.596	118.4
	$x=0$	0	0

Conclusion:

- The composite $(1-x)\text{Ba}_5\text{TbTi}_3\text{V}_7\text{O}_{30}-x\text{BiFeO}_3$ has been formed in a composite phase which is confirmed from XRD analysis.
- For $x=1$, i.e. for pure BiFeO_3 it is antiferromagnetic with weak ferromagnetism.
- The addition of $\text{Ba}_5\text{TbTi}_3\text{V}_7\text{O}_{30}$ increases spontaneous magnetization (in comparison to BiFeO_3)
- However, with decrease in BiFeO_3 , there is a decrease in spontaneous magnetization.
- At $x= 0.7$ (i.e. 70% of $\text{Ba}_5\text{TbTi}_3\text{V}_7\text{O}_{30}$ and 30% of BiFeO_3), magnetization is maximum. Thus the magneto-electric coupling is more effective for $x=0.7$ in this composite. So the composite $(1-x)\text{Ba}_5\text{TbTi}_3\text{V}_7\text{O}_{30}-x\text{BiFeO}_3$ for $x=0.3$ is a better multiferroic material.
- Pure $\text{Ba}_5\text{TbTi}_3\text{V}_7\text{O}_{30}$ and $\text{Ba}_5\text{PrTi}_3\text{V}_7\text{O}_{30}$ are paramagnetic in nature.
- The material could be suitable for construction of the non volatile magnetic storage memory device.

REFERENCES

- [1] J. Valasek, Phys. Rev. **15**(1920)357.
- [2] B.Wull, L.M.Goldmann, C.R.Acad. Sci. USSR. **46**(1945)139.
- [3] W. G. Cady, "*Piezoelectricity*", McGraw Hill, New York (1946).
- [4] S.B.Lang, Ferroelectrics, **53**(1984)189.
- [5] J.F.Nye, "*Physical properties of Crystals*", Oxford, U.K. (1957).
- [6] S. Bhagavantam, "*Crystal Symmetry and Physical Properties*", Acad. Press, London, New York(1966).
- [7] A.R.Von Hippel, "*Dielectrics Materials and Applications*", Technology Press, MIT and Wiley, New York(1971).
- [8] A.R.Von Hippel, Rev. Mod. Phys., **22**(1950)228.
- [9] I.S. Zheludev, "*Physics of Crystalline Dielectric*", Plenum, New York, London(1971).
- [10] H.D.Megaw, "*Ferroelectrics in Crystals*", Methuen and Co., London(1957).
- [11] A.F.Devonshire, Phil. Mag., **40**, (1949)1040.
- [12] M. E.Lines, A.M. Glass, "*Principles and Application of Ferroelectrics and Related Materials*" Oxford University Press(1977).
- [13] A.J. Burggraaf, Proc. 9th Int. Cong. On Sci. Of Ceramics, Noordwijkerhout, Netherlands(1977).
- [14] W. Kanzig, Helv. Phys. Acta. **24** (1951)175.
- [15] W. Kanzig, "*Ferroelectrics and Antiferroelectrics*," Academic Press, New York,(1957).
- [16] J.Fritesburg, Proc. 4th Int. Meeting of Ferroelectricity, Leningrad 1977.
- [17] A.G. Smolensky, J. Phys. Soc. Japan, **18** (1970)26.
- [18] B.N.Rolov, Soviet Phys. Solid State, **6** (1965)1676.
- [19] A.G. Smolensky, J. Ferroelectricity, **53** (1984)129.
- [20] V.S. Tiwari and D. Pandey, J. Am. Ceram. Soc. II, **77**(1994)1819.
- [21] V.V. Kirolov and V.A. Isupov, Ferroelectrics, **5**(1973)3.
- [22] L.E. Cross, Ferroelectrics, **76**(1987)241.
- [23] A.J.Bell, Proc.1994 Int. Symp. Appl. Ferroelectrics, 1994.
- [24] A.Von. Hippel, Revs. Mod. Phy. **22**(1950)221.
- [25] K.M. Rittenmyer and R.Y. Ting, Ferroelectrics, **110** (1990)171.

- [26] R.B. Atkin, R. L. Holman, and R.M. Fularth, *J. Am. Ceram. Soc.*, **54**(1971)113.
- [27] G.H. Haertling, *Ferroelectrics*, **75**(1987)25.
- [28] M.H. Francombe and B. Lewis, *Acta Cryst.*, **11**(1958)696.
- [29] S.L. Swartz, W.A. Schulze, and J.V. Biggers, *Ferroelectrics*, **38**(1981)765.
- [30] K.Nassau, H.J. Levinstein, and G.M. Loiacona, *J. Phys. Chem. Solids*, **27** (1966)983.
- [31] F.W. Aiger, "*Modern Oxide Materials-Preparation, properties and device applications*", Academic Press. Inc. London(1972).
- [32] A. Magneli, *Ark. Kem*, **1**(1949)213.
- [33] P.B. Jamieson, S.C. Abrahams, J.L.Bernstein, *J.Chem. Phys.* **48**(1965)5048.
- [34] G.Goodman, *J. Am. Ceram. Soc.* **36**(1953)368.
- [35] M.H.Francombe, B. Lewis, *Acta Crystallogr.* **11**(1958)696.
- [36] H. Schmid, *Ferroelectrics* **62**, 317(1994).
- [37] Schmid H. *Ferroelectrics* 1994; **221**,9.
- [38] K.S. Nalwa, A. Garg, A. Upadhaya, *Mater. Lett.* **62** (2008)878.
- [39] V. E. Wood, A. E. Austin, *Int. J. Magn.* **5**(1974)303.
- [40] W. Eerenstein, N. D. Mathur, and J. F. Scott, *Nature* 442,759(2006)
- [41] S. W. Chong and M. Mostovoy, *Nat. Mater.* **6**, 13(2007).
- [42] T. Kimura, T. Goto, H. Shintani, K. Ishizaka, T. Arima & Y. Tokura, *Nature*, **426** (2003)55-58.
- [43] N. A. Spaldin & M. Fiebig, *Science*, **309**(2005)391-392.
- [44] N. A. Hill, *J. Phys. Chem. B*, **104**(2000)6694-6709.
- [45] M. Mostovoy, *Phys. Rev. Lett.*, **96**(2006) 067601.
- [46] N. A. Hill, *J. Phys. Chem. B*, **104** (2004)6694.
- [47] J. Wei, D. Xue, C. Wu, Z. Lai, *J. Alloys Compd.* **453**(2008)20.
- [48] X. Zhang, Y. Sui, X. Wang, Y. Wang, Z. Wang, *J. Alloys Compd.* **507**(2010)157.
- [49] V. R. Reddy, D. Kothari, A. Gupta, S. M. Gupta, *Appl. Phys. Lett.*, **94**(2009)082505.
- [50] A. Z. Simões, E. C. Aguiar, A. H. M. Gonzalez, J. Andrés, E. Longo, J. A. Varela, *J. App. Phys.*, **104**(2008)104115-1.
- [51] F.Kubel and H. Schimd, *Acta Crystallogr. B* **46**(1990)698.
- [52] C. Michel, J. M. Moreau, G. D. Achenbach, R. Gerson, and W. J. James, *Solid State Commun.* **7**(1969)701.

- [53] D. I. Khomskii, *J. Magn. Magn. Mater.* **6** (2007)1.
- [54] S. V. Kiselev, R. P. Ozerov, and G. S. Zhdanov, *Sov. Phys. Dokl.* **7**, 742 (1963).
- [55] I. Sosnowska, T. Peterlin-Neumaier, and E. Steichele, *J. Phys. C* **15**, 4835 (1982).
- [56] I. E. Dzyaloshinskii, *Sov. Phys. JETP* **5**, 1259 (1957).
- [57] T. Moriya, *Phys. Rev.* **120**, 91 (1960).
- [58] C. Ederer, and N. A. Spaldin, *Phys. Rev. B* **71**, 060401(R) (2005).
- [59] J. Wang, J. B. Neaton, H. Zheng, V. Nagarajan, S. B. Ogale, B. Liu, D. Viehland, V. Vaithyanathan, D. G. Schlom, U. V. Waghmare, N. A. Spaldin, K. M. Rabe, M. Wuttig, and R. Ramesh, *Science* **299**, 1719 (2003).
- [60] J. B. Neaton, C. Ederer, U. V. Waghmare, N. A. Spaldin, and K. M. Rabe, *Phys. Rev. B* **71**, 014113 (2005).
- [61] W.-M. Zhu and Z.-G. Ye, *Appl. Phys. Lett.* **89**, 232904 (2006).
- [62] Schmid H. Multi- ferroic magnetoelectrics, *Ferroelectrics* 1994; **162**: 317-38
- [63] Schmid H. Multi- ferroic magnetoelectrics, *Ferroelectrics* 1994; **221**: 9
- [64] N. A. Hill, *J. Phys. Chem. B* **104**,6694 (2000).
- [65] G.A.Smolenskii, A.I. Agranovskaya, S. N. Popov, and V.A.Isupov, *Zh. Tekh. Fez.* **28**, 2152 (1958) [*Sov. Phys. Tech. Phys.* **3**, 1981(1958)]
- [66] G.A.Smolenskii, and I.E. Chupis, *Ups. Fiz. Nauk.* **137**, 415 (1982) [*Sov. Phys. Usp.* **25**, 1982
- [67] N. N. Krainik, N. P. Khuchua, V. V. Zhdanova, and V. A. Evseev, *Sov. Phys. Solid State* **8**, 654 (1966).
- [68] Y. Y. Tomas Polski and Y. N. Venevtsev, *Sov. Phys. Crystallogr.* **12**, 18 (1967).
- [69] Y. Y. Tomashpolskii, Y. N. Venevtsev, and G. S. Zhdanov, *Sov. Phys. Crystallogr.* **12**, 209,(1967).
- [70] I. G. Ismailzade, *Sov. Phys. Dokl.* **11**, 747 (1967).
- [71] C. Michel, J. M. Moreau, G. D. Achenbach, R. Gerson, and W. J. James, *Solid State Commun.* **7**, 701 (1969).
- [72] J. R. Teague, R. Gerson, and W. J. James, *Solid State Commun.* **8**, 1073 (1970).
- [73] J. M. Moreau, C. Michel, R. Gerson, and W. J. James, *J. Phys. Chem. Solids* **32**, 1315 (1971).
- [74] C. Blaauw and F. van der Woude, *J. Phys. C* **6**, 1422 (1973).
- [75] A. J. Jacobson and B. E. F. Fender, *J. Phys. C* **8**, 844 (1975).

- [76] P. Fischer, M. Połomska, I. Sosnowska, and M. Szymański, *J. Phys. C* **13**, 1931 (1980).
- [77] S. A. Fedulov, *Sov. Phys. Dokl.* **6**, 726 (1962).
- [78] C. Ederer, and N. A. Spaldin, *Phys. Rev. B* **71**, 060401(R) (2005).
- [79] Y. F. Popov, A. K. Zvezdin, G. P. Vorob'ev, A. M. Kadomtseva, V. A. Murashev, and D.N. Rakov, *JETP Lett.* **57**, 69 (1993).
- [80] J. K. Kim, S. Su, and K. W. Kim, *Mater. Lett.* **59**, 4006(2005).
- [81] M. M. Kumar, V. R. Palkar, K. Srinivas, and S. V. Suryanarayana, *Appl. Phys. Lett.* **76**, 2764(2000).
- [82] R. T. Smith, G. D. Achenbach, R. Gerson, and W. J. James, *J. Appl. Phys.* **39**,70 (1998).
- [83] M. M. Kumar, A. Srinivas, and S. V. Suryanarayana, *J. Appl. Phys.* **87**, 855(2000).
- [84] Y. P. Wang, L. Zhou, M. F. Zhang , X. Y. Chen, J. M. Liu, and Z. G. Liu, *Appl. Phys. Lett.* **84**, 1731(2004).
- [85] C. Tabares-Minoz, J. P. Rivera, A. Bezinges, A Monnier, H Schmid, *Jap. Journ. App. Phys.* **24(B)** (1985)1051.
- [86] J. R. Teague, R. Gerson, and W. J. James, *Solid State Commun.* **8**, (1970)1073.
- [87] A.S. Borovik, M. Polomska, I. Sosnowska, M. Szymanski, *Sov. Phys.-JETP* **12** (1960).
- [88] N.N. Krainik, N.P. Khuchua, V.V. Zhdanova, V.A.Evseev, *Sovt. Phys. Solid States, USSR* **8**,(1966)816.
- [89] R.T. Smith, G. D. Achenbach, R. Gerson, and W.J. James. *J. Appl. Phys.* **39** (1968)70.
- [90] K. Kato, S. Lida, K. Yanai, and K. Mizushima, *J. Magn. Magn. Mater.* **31-34**, 783(1983).
- [91] E. Ascher, H. Rieder, H. Schmid, and H. Stossel, *J. Appl. Phys.* **37**, 1404(1966).
- [92] A.R. James, G.S. Kumar, M. Kumar, S.V. Suryanarayana, T. Bhimasankaram, *Mod. Phys. Lett.(B)*, **11** (1997)633.
- [93] A.R. James, G.S. Kumar, M. Kumar, S.V. Suryanarayana, T. Bhimasankaram, *Ferroelectrics*, **216** (1998)11.
- [94] A.R. James, G.S. Kumar, M. Kumar, S.V. Suryanarayana, T. Bhimasankaram, *Mat. Res. Bull.*, **34** (1999)989.

- [95] M. M. Kumar, A. Srinivas, S.V. Suryanarayana, G.S. Kumar, and T. Bhimasankaram, *Bull. Mater. Sci.*, **21(3)**,(1998)251.
- [96] M. M. Kumar, A. Srinivas, S.V. Suryanarayana, and T. Bhimasankaram, *phys. stat. sol.(a)*, **165**,(1998)317.
- [97] M. M. Kumar, S. Srinath, G.S. Kumar, and S.V. Suryanarayana, *J. Mag. And Mag. Matt.*, **188**,(1998)203.
- [98] M. M. Kumar, A. Srinivas and S.V. Suryanarayana, *J. of App. Phys.*, **87(2)**, (2000)855.
- [99] M. M. Kumar, V.R. Palkar, A. Srinivas and S.V. Suryanarayana, *App. Phys. Letts.*, **76**,(2000)2764.
- [100] W. M. Zhu, Z. G. Ye, *Ceram. Inter.*, **30**(2004)1435.
- [101] W. M. Zhu, H. Y. Guo, Z. G. Ye, *Phys. Rew.*, **78**(2008)014401.
- [102] J. K. Kim, S. S. Kim, and W. J. Kim, *Matt. Letts.* **59**(2005)4006.
- [103] D. H. Wang, W.C. Goh, M. Ning, and C.K. Ong, *App. Phys. Letts.*, **88**(2006) 212907-1.
- [104] M. Kumar and K. L. Yadav, *J. of Appl. Phys.*, **100**(2006)074111.
- [105] K. S. Nalwa, A. Garg, A. Upadhyaya, *Matt. Letts.* **62** (2008)878.
- [106] A. Z. Simões, E. C. Aguiar, A. H. M. Gonzalez, P. Anres, E. Longo, and J. A. Varela, *J. of App. Phys.*, **104** (2008)104115-1.
- [107] S. Chandarak, A. Ngamjarurojana, S. Srilomsak, P. Laoratankul, S. Rujirawat, and R. Yimnirun, *Ferroelectrics*, **410** (2011)75.
- [108] A. Huang, S. R. Shannigrahi, *Thin Solid Films*, **519**(2011) 4793.
- [109] Y. A. Chaudhari, A. Singh, E. M. Abuassaj, R. Chatterjee, and S. T. Bendre, *J. of Alloys and Comps.*, **518** (2012)51.
- [110] J. Rout, R. N. P. Choudhary, S. R. Shannigrahi, and H. B. Sharma, *J. of Elec. Mats.*, (2015). doi: 10.1007/s11664-015-3843-0.
- [111] J. Schneck, J. C. Toledano, C. Joffrin, J. Aubree, B. Joukoff, and A. Gabelotaud, *Phys. Rev. B* **25(3)**, (1982)1766.
- [112] C. Filipic, Z. Kutnjak, R. Lortz, A. Torres-Pardo, M. Dawber and J. F. Scott, *J. Phys.: Condens. Matter* **19**(2007)236206.
- [113] M. H. Fracombe, *Acta. Cryst.* **13**(1960) 131.
- [114] E.C. Subba Rao and G. Shirone, *J. Chem. Phy.* **32**(1960)1846.
- [115] E. A. Giess, B. A. Scolt, G. Burns, D.F.O. Kenne, *J. A. Ceram. Soc.* **52** (1969)276.

- [116] A. A. Ballman, H. Brown, J. Cryst. Growth **1**(1967)311.
- [117] G. Burns, E.A. Giess, G. Burns, D.F.O'Kane, B.A. Scott, Bull. Am. Phys. Soc. **12**(1967)1078.
- [118] D.F.O'Kane, E.A. Giess, G. Burns, B.A. Scott, Ibid. **12**(1967)1079.
- [119] J.E. Geusic, H. J. Levinstein, J.J. Rubin, S. Singh, L. G. Van Ultert, Appl. Phys. Lett. **11** (1967)269.
- [120] J.J. Rubin, L. G. Van Ultert, and H. J. Levinstein J. Cryst. Growth **1**(1967)315.
- [121] J. Burgeat and J.C. Toledano, Solid State Commun. **20** (1976)281.
- [122] R. Sati, K.S. Singh, R.N.P. Choudhary, J. Mats. Sc. Letts. **11**(1992)788.
- [123] K. Umakantham, S. Narayana Murthy, A. Bhanumathi, Ferroelectrics **94** (1989)291.
- [124] S. Bu, D. Chum, G. Park, Jpn. J. Appl. Phys. **36**(1997)4351.
- [125] N. Wakiya, J. K. Wang, A. Saiki, K. Shinozaki, N. Mizutani, J. Eur. Ceram. Soc. **19** (1999)1071.
- [126] A. Panigrahi, N.K. Singh, R.N.P. Choudhary, J. Mats. Sc. Letts. **18**(1999)1579.
- [127] A. Panigrahi, N.K. Singh, R.N.P. Choudhary, J. Phys. Chem. Solids **63**(2002)213.
- [128] Y.Wu Et al., J. Am. Ceram. Soc. **84**(12),(2001)2882.
- [129] S. Shannigrahi, R. N. P. Choudhary, Atul Kumar and H. N. Acharya, J. Phys. Chem. Solid **59**(1998)737.
- [130] A. Panigrahi, R. N. P. Choudhary and B. N. Das, Ind. J. phys. **74A**(2000)147.
- [131] P.S. Sahoo, A. Panigrahi, S.K. Patri, R. N. P. Choudhary, Central Euro. J. of Phys. **6**(4)(2008)843.
- [132] K. Kathayat, A. Panigrahi, A. Pandey, S. Kar, Int. Ferroelectrics, **118**(1)(2010)8.
- [133] K. Kathayat, A. Panigrahi, A. Pandey, S. Kar, Physica B: Cond. Matt.,**407**(18) (2012)3753.
- [134] B. J. Kalaiselvi, R. Sridarane, and R. Murugan, Ceram. Int. **32**(4), (2006)467.
- [135] A. Srinivas, D. W. Kim, K. S. Hong, S. V. Suryanarayana, Appl. Phys. Lett. **83**(2003)2217.
- [136] W. M. Zhu, H. Y. Guo and Z. G. Ye, Phys. Rev. B **78**(2008)014401.
- [137] M. Kumar, K.L.Kumar, "Study of room temperature magnetoelectric coupling in Ti substituted bismuth ferrite system," J. Appl. Phys., **100** (2006) 074111- 4

- [138] R-Ramesh and Nicola A. Spaldin “Multiferroics: progress and prospects in thin films,” *Nature Materials*, **6** (2007) 21-29.
- [139] S.R. Shannigrahi, A. Huang, N. Chandrasekhar, “Sc modified multiferroic BiFeO₃ thin films prepared through a sol-gel process,” *Appl. Phys. Letts.*, **90** (2007) 022901- 3.
- [140] A.S. Borovik, M. Polomska, I. Sosnowska, M. Szymanski, *Sov. Phys.-JETP* **12** (1960).
- [141] M. Fiebig, *Phys. Rev. Letter.*, **96**, 123 (2005).
- [142] R.T.Smith, G.D.Achenbach, R.Gerson, W.J.James, *J. Appl. Phys.***39**, 70 (1968).
- [143] A. Huang, S.R. Shannigrahi, *Thin Solid Films*, **519**, 4793 (2011).
- [144] M.M. Kumar, A. Srinivas and S.V. Suryanarayana, Structural property relations in BiFeO₃/BaTiO₃ solid solutions, *J of app. Physics*. 87(2), 855(2000)
- [145] A. Magneli, *Ark. Kem.* **1**, 213 (1949).
- [146] R.R. Neurgaonkar, J.G. Nelson, J.R. Oliver, *Mater. Res. Bull.* **25**, 959 (1990)
- [147] P.B. Jamieson, S.C. Abrahams, L. Bernstein, *J. Chem. Phys.* **48**, 5048 (1968)
- [148] S. R. Shannigrahi, R. N. P. Choudhary, Atul Kumar, and H. N. Acharya, Phase transition in Ba₅R_{Ti}3Nb₇O₃₀ (R=Dy, Sm) ferroelectric ceramics. *J. Phys. Chem. Solids* **59**, 737 (1998).
- [149] A.Srinivas, F.Boey, T. Sritharan, D.W. Kim, *Ceram. International*, **30**, 1427(2004).
- [150] M.M. Kumar, A.Srinivas, S.V.Suryanarayana, *Phys. Stat. Sol. (a)*, **165**, 317 (1998).
- [151] J. C. Burfoot, W. Taylor, “*Polar Dielectrics and Their Applications*”, MacMillan Press Ltd. London and Basingstoke, (1971).
- [152] T. Tsukamoto, *Jpn. J. Appl. Phys.*, **23** (1984)424.
- [153] S.E. Cummins, *Ferroelectrics*, **1** (1970) 11.
- [154] A. Kumada, *Ferroelectrics*, **3** (1972) 115.
- [155] James S Reed, “*Introduction to Ceramics Processing*”, John Wiley and Sons, New York (1988).
- [156] L.N. Johnson, *J. Dert, Res.* **51** (1972) 789.
- [157] G. Greskovich and K. W. Lay, *J. Amer. Ceram. Soc.* **55** (1972) 142
- [158] D.W. Johnson, B. B. Ghate, *Advances in Ceramics*, Ed. F. Y. Wang (Am. Ceram. Soc, Columbus OH) **15** (1985) 27.

- [159] S. T. Aruna, M. Muthuraman, K. C. Patil, Solid State Ionics **111** (1998) 45.
- [160] G. H. Haertling, C. E. Land, J. Am. Ceram. Soc. **54** (1965) 289.
- [161] S. S. Chandratreya, R. M. Fulrath, J. A. Pask, J. Am. Ceram. Soc. **64**(1981) 422.
- [162] T. Matsuo, H. Sasaki, J. Am. Ceram. Soc. **54**(1965) 289.
- [163] A. K. Jordan and D. Swallow, Proc. Brit. Ceram. Soc. **2** (1964).
- [164] H. P. Klug and L. E. Alexander "X-ray Diffraction Procedure" 2nd Ed. Wiley, New York (1974).
- [165] P.E.D. Morgan, "*Processing of Crystalline Ceramics*", Eds. Plenum, New York (1978).
- [166] B. D. Cullity, "*Elements of X-Ray Diffraction*," Addison-Wesley Publishing Co. Inc., (1978).
- [167] Saul Wischnitzer, "*Introduction to Electron Microscope*", Pergamon Press, New York (1987).
- [168] M.E. Lines, A. M. Glass, "*Principles and Applications of Ferroelectric and related materials*", Oxford University Press, London, (1977).
- [169] V.E. Yukevich, B. N. Rolov, Ferroelectrics **68** (1986)265.
- [170] J.C.Anderson, "*Dielectrics*" Chapman and Hall, London (1964)16.
- [171] Anthony R. West, Basic Solid State Chemistry, 2nd edition, J. Wiley and Sons, Inc. (1996).
- [172] M.C.Morris, Joint Committee on Powder Diffraction Standards, 1st Edition, Swarthmore, Pa(1976)
- [173] V.K. Perchasky and P.V. Zavalij, fundamentals of Powder Diffraction and Structural characterization of materials, Kluwer Academic Publishers, Boston (2003).
- [174] H.P.Klug, L.E. Alexander, "X-ray diffraction Procedure for polycrystalline and amorphous materials", Wiley-Interscience, New York (1974).
- [175] NBS Monograph standard X-ray Diffraction Powder Patterns, 3, Washington, D.C., U.S. Govt. printing office (1971).
- [176] F.J.Heinrich, C.S. Barrelet, J.B. Newkirk, Eds. Advances in X-ray analysis plenum, New York. Vol **5** (1972)
- [177] B.E. Warren and B.L.Averbach, J. Appl. Phys. **21** (1950) 595
- [178] A.J.C. Wilson, Nature **193** (1962) 568

- [179] P. Scherrer, Goltin, Nactricht**2** (1918) 98
- [180] P.B.Jamieson, S.C. Abrahams, L. Bernstein, J. Chem. Phys., **48**, 5048(1968).
- [181] R.R. Neurgaonkar, J.G. Nelson, J.R. Oliver, Mater. Res. Bull., **25**, 959(1990).
- [182] M.Valant, A.K. Axelsson, and N.Alford, Chem. Mater. **19**, 5431(2007).
- [183] P.Kumar and M. Kar, AIP Conf. Proc. **1536**,1041(2013).
- [184] Banarji Behera, P. Nayak, R.N.P. Choudhary, Materials Letters **59**(2005)3489.
- [185] V.E. Yukevich, B. N. Rolov, Ferroelectrics **68** (1986)265.
- [186] C.J.F. Bottcher, "*Theory of Electric Polarizations*", (Elsevier, Amsterdam), 1962.
- [187] M.E. Lines, A.M.Glass, "*Principles and Applications of Ferroelectrics and Related Materials*", Oxford University press, Oxford,1977.
- [188] P. Debye, Polar Molecules, Dover, New York, 1945.
- [189] C. Kittel, "*Introduction to Solid State Physics*", Wiley, 5th Edition, New York (1976).
- [190] A.J. Dekker, "Solid State Physics", Prentice Hall, New Jersey (1957).
- [191] K. Chi Kao, "*Dielectric Phenomena in Solids*", Elsevier, New York(2004).
- [192] R.N.P. Choudhary, B.K. Choudhary, *J. Mats. Sc. Letts.* **9** (1990)394.
- [193] M. Ali Omar, Elementary Solid State Physics (Pearson Education).
- [194] S. O. Pillai, Solid State Physics (New Age International Publication).
- [195] R. K. Puri, Solid State Physics (S. Chand).
- [196] V.M. Gurevich, "*Electronic Conductivity of Ferroelectrics*", Israel Translation, Jerusalem (1971).
- [197] D.P. Button, R.P. Tandon, H.L. Tuller and D. R. Uhlman, J. Non-Cryst. Solid **42** (1980)297.
- [198] W.D.Kingery, Introduction to Ceramics, (Wiley, New York, 1960).
- [199] S.B.Lee, K.H. Lee and H.Kim, Jpn. J. Appl. Phys., **41** (2002)5266.
- [200] K. Sambasiva Raoa, P. Murali Krishna, D. Madhava Prasad, Joon-Hyung Lee, Physica B **408** (2008)2079.
- [201] O.Raymond, R. Font, N. Suárez-Almodóvar, and J. Portelles, J.M. Siqueriors; J. Appl. Phy. **97**(2005)084107.
- [202] R.N.P. Choudhary, K.S.Singh, R. Sati. Pramana, **38(3)**(1992)161.
- [203] S. Rao, P.S.V. Rao, K. Sambasiva Rao, A. Bhanumathi, Mater. Sci. Engg. B **98(3)** (2003)279.

- [204] M. Kumar, K.L.Kumar, "Study of room temperature magnetoelectric coupling in Ti substituted bismuth ferrite system," *J. App. Phys.*, **100** (2006) 074111- 4.
- [205] R-Ramesh and Nicola A. Spaldin "Multiferroics: progress and prospects in thin films," *Nature Materials*, **6** (2007) 21-29.
- [206] S.R. Shannigrahi, A. Huang, N. Chandrasekhar, "Sc modified multiferroic BiFeO₃ thin films prepared through a sol-gel process," *Appl. Phys. Letts.*, **90** (2007) 022901- 3.
- [207] A.Z.Simões, E.C. Aguiar, A.H. Gonzalez, J.Andreas, "Strain behaviour of lanthanum modified BiFeO₃ thin films prepared via soft chemical method," *J. App. Phys.*, **104** (2008) 104115-6.
- [208] M.M. Kumar, A.Srinivas, S.V.Suryanarayana, *App. Phys.Lett.*, "Ferroelectricity in pure BiFeO₃ ceramic," **76** (2000) 2764- 2766.
- [209] Y.A. Chaudhari, C.M.Mahajan, E.M. Abuassab, "Ferroelectric and dielectric properties of nanocrystalline BiFeO₃ multiferroic ceramics synthesized by solution combustion method (SCM)," *Mat. Sci.-Poland*, **31(2)** (2013) 221-225.
- [210] J.M. Moreau, C. Michel, R. Gerson, W.J. James, "Ferroelectric BiFeO₃ X-ray and neutron diffraction study," *J. Phys. Chem. Solids*, **32** (1971) 1315-1320.
- [211] N.A.Spaldin, S.W.Cheong, R.Ramesh, "Multiferroics: Past, present, and future," *Physics Today*, **63(10)** (2010) 38-43.
- [212] A.Srinivas, F.Boey, T. Srithatan, D.W. Kim, "Processing and study of dielectric and ferroelectric nature of BiFeO₃ modified SrBi₂Nb₂O₉," *Ceram. International*, **30** (2004) 1427-30.
- [213] K.Kathayat, A.Panigrahi, A.Pandey, S.Kar, "Structural and electrical studies of Ba₅RTi₃V₇O₃₀ (R=Ho,Gd,La)compounds," *Physica B*, **407** (2012)3753-3759.
- [214] H.Doley, A. Panigrahi, P. Chakraborty, "Study of Electrical and Magnetic properties of the composite (BiFeO₃)_x(Ba₅RTi₃V₇O₃₀)_{1-x}," *Adv. Int. Sys. Comp.*, **862** (2019) 451-459.
- [215] H.Doley, P.K.Swain, A.Panigrahi, G.T.Tado, "Study of structural and ferroelectric properties of the composite Ba₅RTi₃V₇O₃₀(R=Pr, Tb)," *Bull. Pur. & App. Sci.*, **38-D** (2019) 65-72.

- [216] H.Doley, P.K.Swain, A.Panigrahi, G.T.Tado, "Structural and ferroelectric properties in the solid solution $(\text{BiFeO}_3)_x(\text{Ba}_5\text{RTi}_3\text{V}_7\text{O}_{30})_{1-x}$ " *Ferroelectrics* **658** (2020) 104-111.
- [217] M.M.Kumar, S.Srinath, G.S. Kumar, S.V. Suryanarayan, *J. Magn. Magn. Mater.*,**188**(1998)203-212.
- [218] J. Rout, R. N. P. Choudhary, H. B. Sharma, S.R. Shannigrahi, *Ceram. Int.*, **41**(2015) 9078-9080.
- [219] J. Rout, R. N. P. Choudhary, S.R. Shannigrahi, *J. Electron. Mater.*, **44**(2015) 3811-3818.

List of Publications

1. *Structural and Ferroelectric properties in the Solid solution $(\text{Ba}_5\text{TbTi}_3\text{V}_7\text{O}_{30})_x(\text{BiFeO}_3)_{1-x}$,
Hage Doley, P.K.Swain, A. Panigrahi, G. T. Tado
Ferroelectrics, **568** (2020)104-111.
<https://doi.org/10.1080/00150193.2020.1811034>
2. *Modulating the magnetic properties of BiFeO_3 by addition of $\text{Ba}_5\text{TbTi}_3\text{V}_7\text{O}_{30}$
Hage Doley, P.K.Swain, A. Panigrahi
Processing and Application of Ceramics,**14[4]**(2020) 277-281.
<https://doi.org/10.2298/PAC2004277D>
3. Study of Electrical and Magnetic Properties of Multiferroic Composite $(\text{BiFeO}_3)_x(\text{Ba}_5\text{RTi}_3\text{V}_7\text{O}_{30})_{1-x}$.
Hage Doley, Anuradha Panigrahi and Pinaki Chakraborty
“*Information Systems Design and Intelligent Applications*”, Advances in Intelligent Systems and Computing **862** (2019)451-459,
https://doi.org/10.1007/978-981-13-3329-3_42
4. *Study of structural and ferroelectric properties of the composite $\text{Ba}_5\text{RTi}_3\text{V}_7\text{O}_{30}$ (R=Pr, Tb).
Hage Doley, P.K.Swain, A.Panigrahi, G.T.Tado
Bulletin of Pure and Applied Sciences, **38D(2)**, (2019),65-72.
<https://doi.org/10.5958/2320-3218.2019.00011.3>

Conferences and Proceedings

1. Effect of $\text{Ba}_5\text{RTi}_3\text{V}_7\text{O}_{30}$ (R=Ce, Pr) in the magnetic properties of BiFeO_3 .
Hage Doley, Pinaki Chakraborty, Pratap Kumar Swain
Proceedings of National Conference on Recent Trends in Engineering, Science, Technology & Management (NCRTESTM 2017) **SH-201**(2017)146-153.
1. *Study of Electrical and Magnetic properties of Multiferroic composite $(\text{BiFeO}_3)_x(\text{Ba}_5\text{TbTi}_3\text{V}_7\text{O}_{30})_{1-x}$.
Hage Doley, P.K.Swain, A.Panigrahi, G.T.Tado
XI Biennial National Conference of Physics Academy of North East (PANE), Nov. 21-23, 2018, Assam University, Diphu.
2. *National Conference on materials, condensed matter and theoretical physics (NCMCTP-2018), Dec. 20-21 (2018).

(*) Papers and conferences on which the present thesis is based

CHAPTER VII
SUMMARY, CONCLUSIONS AND FUTURE SCOPES

7.1. Summary

Multiferroic BiFeO_3 has a structure of rhombohedrally distorted perovskite and Ferroelectrics $\text{Ba}_5\text{RTi}_3\text{V}_7\text{O}_{30}$ is of Tungsten Bronze structure. The TB structure has complex array of distorted BO_6 octahedra which shares interstices corner of three different types (A, B and C) for existing cation substitutions having common formula $(\text{A}_1)_2(\text{A}_2)_4(\text{C}_4)(\text{B}_1)_2(\text{B}_2)_8\text{O}_{30}$. Cations of mono or divalent could be accommodated at A1 and A2 sites and cations of tri or pentavalent at B1 and B2 octahedral sites, whereas C interstice (smallest site) generally remain empty; thus the common formula for TB structure is $\text{A}_6\text{B}_{10}\text{O}_{30}$. Range of cations substitution at the A and B sites changes the electrical properties of material significantly.

We have mixed BiFeO_3 of perovskite structure with $\text{Ba}_5\text{RTi}_3\text{Nb}_7\text{O}_{30}$ of different structural family (TB-structure). The open nature of the TB structure as compared to the perovskite provides a room for a wide range of cation and anion substitutions thus improving the ferroelectric and magnetic properties of BiFeO_3 .

In the current work, we have analysed the structural, electrical, and magnetic properties of the solid solution $(1-x)\text{Ba}_5\text{RTi}_3\text{V}_7\text{O}_{30}-x\text{BiFeO}_3$ for all values of x ($x=1$, $x=0.7$, $x=0.5$, $x=0.3$), where R=Pr, Tb. The ten prepared solid solution sample of can be classified into two groups, i.e.

Group A: $(1-x)\text{Ba}_5\text{TbTi}_3\text{V}_7\text{O}_{30}-x\text{BiFeO}_3$

Group B: $(1-x)\text{Ba}_5\text{PrTi}_3\text{V}_7\text{O}_{30}-x\text{BiFeO}_3$

- All the solid solution samples are prepared by high temperature solid-state reaction techniques and the structural, dielectric, conductivity and magnetic characteristics were examined.
- X-ray diffractogram (Rigaku, Miniflex) with CuK_α radiation of wavelength; $\lambda = 1.5405 \text{ \AA}$ is used to (i) determine the configuration of the compounds (ii) recognize the basic crystal system and (iii) find out the lattice parameters, and crystallite size.

- The calcined powders were palletized (1-2 mm thickness and 12-13 mm diameter) by cold pressing (~7 tons) and sintered at an optimized temperature and time.
- Scanning Electron Microscope (SEM: JEOL-IT300) is used to analyse the surface morphology of the sintered pellets from which diverge grain size is determined.
- To comprehend the nature of phase transition, dielectric properties of the sample are scrutinized.
- To find the activation energy and types of conduction, Conductivity studies of the sample were done from the dielectric data.
- Vibrating Sample Magnetometer (VSM) at a temperature range of (10-350 K) is used to study the Magnetization properties of the sample and to study Hysteresis (M-H) loops at room temperature (300 K).

7.2. Conclusions

Following conclusions can be drawn from the current analysis.

- With the addition of BiFeO_3 to $\text{Ba}_5\text{TbTi}_3\text{V}_7\text{O}_{30}$, we did not find any reaction between these two compounds (as confirmed by XRD), therefore, it can be concluded that it is a solid solution
- The grain size is found to be in the nanoscale. Hence, the materials we are dealing with are nanomaterials.
- Voids of irregular dimension are observed which points out that the pellet samples have some degree of porosity and homogeneity due to the low sintering temperature. It is also establish that the grains have platelet like morphology in above base compounds.
- All the above compounds show dielectric anomaly of diffused nature.
- Anomaly in $\tan\delta$ is also observed for all above compounds, near the transition temperature. The change in the values is significantly less at low temperature and at high temperature it increases.
- The plot of conductivity shows that with increase in temperature, there is also increase in values in conductivity. Thus, it has a negative temperature coefficient of resistance (NTCR) properties like semiconductors.

- It was found that both $\text{Ba}_5\text{PrTi}_3\text{V}_7\text{O}_{30}$ and $\text{Ba}_5\text{TbTi}_3\text{V}_7\text{O}_{30}$ are ferroelectrics in nature.
- The transition temperature of $\text{Ba}_5\text{PrTi}_3\text{V}_7\text{O}_{30}$ is less than that of $\text{Ba}_5\text{TbTi}_3\text{V}_7\text{O}_{30}$
- The maximum dielectric constant of $\text{Ba}_5\text{PrTi}_3\text{V}_7\text{O}_{30}$ is considerably lesser than that of $\text{Ba}_5\text{TbTi}_3\text{V}_7\text{O}_{30}$. The explanation for the observed phenomenon may be due to difference in the Ionic radius of the rare earth element. The Ionic radius of Praseodymium (Pr) is 1.13 Å and Ionic radius of Terbium (Tb) is 1.18 Å. The smaller Ionic radius of Pr might increase the mobility of ions which increases in conductivity thus decreasing the dielectric constant.
- Due to more mobility of charge carriers there is an increase in the cross section collisions thus increase in the tangent loss. But at higher temperature the heavier charge carrier is more prominent hence the tangent loss is more for $\text{Ba}_5\text{TbTi}_3\text{V}_7\text{O}_{30}$ in comparison to $\text{Ba}_5\text{PrTi}_3\text{V}_7\text{O}_{30}$.
- $\text{Ba}_5\text{TbTi}_3\text{V}_7\text{O}_{30}$ is better ferroelectrics than $\text{Ba}_5\text{PrTi}_3\text{V}_7\text{O}_{30}$.
- It has been observed that the T_c changes considerably by addition of BiFeO_3 in the different proportion to the base compounds.
- The solid solution $(1-x)\text{Ba}_5\text{TbTi}_3\text{V}_7\text{O}_{30}-x\text{BiFeO}_3$ for all values of x ($x = 0, x = 0.3, x = 0.5, x = 0.7$) shows ferroelectric transition (showing ferroelectric property). By increasing the BiFeO_3 , dielectric constant is reduced considerably and at the same time the loss (tangent) increases, which is as per the expected line. BiFeO_3 having semiconducting properties increases the conduction in the solid solution. This is also reflected in the conductivity study i.e. activation energy increases by increasing BiFeO_3 concentration. At the same time the ferroelectric properties of BiFeO_3 have been improved by the effect of $\text{Ba}_5\text{TbTi}_3\text{V}_7\text{O}_{30}$.
- The formation of a structure consisting of BiFeO_3 and $\text{Ba}_5\text{TbTi}_3\text{V}_7\text{O}_{30}$ was confirmed by XRD analysis. Comparative of SEM micrograph confirms that there is increase in sinterability and in average grain size by increasing BiFeO_3 concentration. Detailed magnetization study shows that for $x=1$ (pure BiFeO_3), it is antiferromagnetic with weak ferromagnetism. Magnetization changes by changing the value of x in this system. The addition of $\text{Ba}_5\text{TbTi}_3\text{V}_7\text{O}_{30}$ increases spontaneous magnetization,
- At $x = 0.7$ (i.e. 70% of BiFeO_3 and 30% of $\text{Ba}_5\text{TbTi}_3\text{V}_7\text{O}_{30}$), magnetization is maximum and hysteresis loop is most developed with $B_r = 180.57 \times 10^{-4}$ emu/g

and $H_c = -1206$ Oe. Thus the magneto-electric coupling is most effective for $x = 0.7$ in this composite. So the composite $(1-x)\text{Ba}_5\text{TbTi}_3\text{V}_7\text{O}_{30}-x\text{BiFeO}_3$ for $x = 0.7$ is a better multiferroic material.

- The material $0.3\text{Ba}_5\text{TbTi}_3\text{V}_7\text{O}_{30}-0.7\text{BiFeO}_3$ could be suitable for construction of the non-volatile magnetic storage memory devices.

7.3. Future Scopes

Multiferroic materials have magnetic as well as ferroelectric properties due to which it has a wide range of applications such as dual storage devices, ferromagnetic resonance devices controlled by electric field, magnetically modulated transducers, Piezoelectrics, etc. We have studied the ferroelectrics properties of $\text{Ba}_5\text{RTi}_3\text{V}_7\text{O}_{30}$ and the ferroelectrics and magnetic properties of solid solution $(1-x)\text{Ba}_5\text{TbTi}_3\text{V}_7\text{O}_{30}-x\text{BiFeO}_3$ for all values of x ($x = 1, x = 0.7, x = 0.5, x = 0.3$), where $R = \text{Pr, Tb}$. Following are a numeral plans that can be act upon in the future for auxiliary studies:

- By doping with other rare earth oxide like $\text{Nd}_2\text{O}_3, \text{Eu}_2\text{O}_3, \text{Sm}_2\text{O}_3$, etc. to form ferroelectrics compound $\text{Ba}_5\text{RTi}_3\text{V}_7\text{O}_{30}$ the properties of the materials can be altered.
- Instead of BiFeO_3 other multiferroic materials such as $\text{BiMnO}_3, \text{YMnO}_3, \text{TbMnO}_3, \text{HoMnO}_3$, etc could be mixed to form solid solution with the base compound $\text{Ba}_5\text{RTi}_3\text{V}_7\text{O}_{30}$ or other ferroelectric compound.
- In our present work we have mixed Perovskite structure with TB structure, but in future Perovskite type structure could also be mixed with other structure groups such as with Layer structure oxides.
- The pyroelectric, piezoelectric property and DC resistivity studies of the ferroelectric material can also be planned (which could not be calculated due to unavailability of experimental infrastructure in the present work).
- The Impedance analysis of the sample could also be performed.
- We have measured the coupling of Magneto-electricity of the multiferroic material, in future Magneto-elasticity and the Piezo-electricity of the material also could be explored.

- Most of the multiferroics are antiferromagnetic, but some Boracites and Magnetite are exceptions. In future, they could be mixed with ferroelectric materials for further analysis.

ABSTRACT

Samples of $Ba_5RTi_3V_7O_{30}$ (R= Pr, Tb), members of tungsten bronze family were prepared by high temperature Solid State Reaction Technique with AR (Analytical Reagent) grade precursors (i.e., oxides and carbonates). Preliminary X-ray analysis of the material to ensure the single phase formation are done at room temperature, X-ray diffraction patterns were taken over a wide range of Bragg's angles ($10^\circ \leq 2\theta \leq 80^\circ$) using CuK_α ($\lambda=1.5405 \text{ \AA}$) radiation. The reflection peaks of the composite are indexed and the lattice parameters are determined by observed d values (interplanar spacing). Surface morphology was studied by Scanning electron microscope (SEM: JOEL-IT300). Dielectric characterization is done for frequency upto 1 MHz at various temperatures by Impedance Analyser (HIOKI-IM3536). Further, The solid solution of $(1-x)Ba_5RTi_3V_7O_{30}-xBiFeO_3$ where R=Tb, Pr; has been synthesized By mixing the tungsten bronze ferroelectric family, $Ba_5RTi_3V_7O_{30}$ with the perovskite structured multiferroic, $BiFeO_3$. For fabrication the Solid State Reaction technique with different x values are employed. XRD (X-ray Diffractogram) shows certain peaks of $BiFeO_3$ are also visible in the XRD pattern of the sample with $x= 0.3, 0.5,$ and 0.7 . Thus it seems that the samples with $x=0.3, 0.5,$ and 0.7 are composite sample in which one phase is of $BiFeO_3$ which confirms the formation of composite phase compound. Grain morphology has been studied by Scanning electron microscope (SEM: JOEL-IT300). Surface morphology shows that average grain size increases by increasing x i.e. by increasing $BiFeO_3$ in the system. By Impedance Analyser (HIOKI-IM3536) dielectric properties such as dielectric constant and loss tangent has been measured in a wide temperature range (RT-500 °C) and also at wide range of frequency which confirms the Ferroelectric nature of all the samples with increasing content of $BiFeO_3$ in these composite the dielectric constant decreases. Magnetic measurement is done in a wide temperature range i.e.10 K to 350 K by vibrating sample magnetometer (VSM) which shows that the magnetization changes by changing the value of x in the composite. $BiFeO_3$ is antiferromagnetic in nature with weak ferromagnetism. By increasing $Ba_5RTi_3V_7O_{30}$ content i.e. by decreasing x value, magnetization increases enhancing magnetic property of the composite. For $x = 0.7$ (70% $BiFeO_3$ and 30% $Ba_5RTi_3V_7O_{30}$) magnetization is maximum. So there's good electro-magnetic coupling for $x = 0.7$ in the composite.